University of Rhode Island

## DigitalCommons@URI

2018

# PHOTONIC METAMATERIALS: SPECTRAL CONTROL AND MODULATION OF NANOSCALE THERMAL RADIATIVE TRANSPORT

Alok Ghanekar
*University of Rhode Island*, alokghanekar@gmail.com

PHOTONIC METAMATERIALS: SPECTRAL CONTROL AND

MODULATION OF NANOSCALE THERMAL RADIATIVE TRANSPORT

BY

ALOK GHANEKAR

A DISSERTATION SUBMITTED IN PARTIAL FULFILLMENT OF THE

REQUIREMENTS FOR THE DEGREE OF

DOCTOR OF PHILOSOPHY

IN

MECHANICAL, INDUSTRIAL AND SYSTEMS ENGINEERING

UNIVERSITY OF RHODE ISLAND

2018

DOCTOR OF PHILOSOPHY DISSERTATION

OF

ALOK GHANEKAR

APPROVED:

Dissertation Committee:

Major Professor   Yi Zheng

Mohammed Faghri

Geoffrey Bothun

Nasser H. Zawia
DEAN OF THE GRADUATE SCHOOL

UNIVERSITY OF RHODE ISLAND

2018

## ABSTRACT

Micro/nano scale radiative transport phenomena present new opportunities to design spectrally selective radiative surfaces and configurations that enable an active control of radiative transfer. Several applications such as thermophotovoltaic energy technology, local thermal management and sensing can benefit from fundamental research in the field. An investigation into photonic metamaterials and near-field thermal radiation was conducted to explore various ways to achieve spectral control and modulation of radiative heat transfer. This was followed by designing novel metamaterials and configurations to consider their feasibility for specific applications of thermophotovoltaics (TPV) and nanoscale thermal management.

An experimental investigation was conducted to estimate optical and radiative properties of SU-8 thin films for various film thicknesses. Samples consisted SU-8 films of thickness ranging from 10 $\mu$m to 157 $\mu$m deposited on gold coated silicon substrates and were prepared using spin coating. Thickness dependent reflective properties were confirmed using Fourier Transform Infrared Spectrometer measurements. Dielectric function of SU-8 in the range 2 $\mu$m to 15 $\mu$m was calculated using the reflectance spectra of the samples. Optical properties of SU-8 in mid-infrared (mid-IR) region were reported before and after UV treatment. Measurements imply a change in optical properties of SU-8 upon exposure to UV and heat treatment.

Using microscopic thin films is one of the simplest ways to achieve a change in emission spectra. A methodology was proposed to shift the wavelength selectivity in the desired location using thin films embedded with nanoparticles. For the media doped with nanoparticles, an effective dielectric function using the Maxwell-Garnett-Mie theory is employed to calculate emissivity and radiative heat transfer.

Influence of parameters such as particle size and volume fraction was studied. It was also shown that wavelength selective behavior of such nanocomposite thin films can be related to their effective refractive indices.

A theoretical study to explore Mie-resonance metamaterials (nanocomposites) for possible use in TPV technology was conducted. Metamaterials were designed to achieve spectral matching of thermal emitter and photovoltaic (PV) cell. The emitter consists of a thin film of $SiO_2$ on the top of tungsten layer deposited on a substrate. Both near-field and far-field configurations were considered. The methodology followed Maxwell-Garnett-Mie theory discussed earlier. The results showed that the proposed Mie-metamaterial thermal emitter can significantly improve the efficiency of TPV system. It was shown that, by changing volume fraction of nanoparticles and thickness of $SiO_2$ it is possible to tune the near-field thermal radiation to obtain enhanced output power and high thermal efficiency.

Methods to achieve dynamic control of radiative heat transfer and thermal rectification characteristics were investigated using a phase-change material called vanadium dioxide ($VO_2$). For a far-field configuration, a tri-layer structure consisting a thin film of KBr sandwiched between a thin film of $VO_2$ and a reflecting layer of gold was proposed. The structure is highly reflective when $VO_2$ is in insulating state (below 68 °C), while it is highly absorbing when $VO_2$ is in its metallic state. Thermal rectification achieved by such a structure is greater than 11 a temperature bias of 20 K, which is the highest rectification ever predicted for far-field radiative diode configurations. A near-field thermal diode configuration was also considered. Possible configurations using bulk, thin film and gratings of $VO_2$ were studied. It was shown that using 1-D rectangular or triangular grating of $VO_2$, a high degree of contrast can be achieved in the tunneling of surface waves across the two interface of thermal diode. For minimal temperature difference of 20 K, rectification

ratio as high as 16 was obtained and it is maximum in existing literature to date for comparable operating temperatures and separation.

# ACKNOWLEDGMENTS

# DEDICATION

This dissertation is dedicated to my mother, Vasundhara Ghanekar.

# PREFACE

Thermal radiation is one of the fundamental modes of heat transfer. Our textbook understanding of thermal radiation is based on Planck's law and Stefan-Boltzmann law. Thermal motion of atoms and molecules lead to fluctuating charges and currents in a material. This in turn leads to a fluctuating electromagnetic field that travels in space and it is what we call thermal radiation. In the infrared and visible part of spectrum, majority of radiation comes from molecular or vibrational motion and the motion of conduction electrons. As this covers a wide range of energy levels, thermal radiation is broadband, incoherent and unpolarized. Meaning, its electromagnetic nature can be ignored and it can be treated as heat rays. However, recent advances in the field of radiative heat transfer have defied the common generalizations observed in the macroscopic world.

When the dimensions of an object or surface features of a material become comparable to the wavelength of radiation, electromagnetic nature of thermal radiation gives rise to two interesting phenomena that cannot be ignored. Micro/nanoscale radiative transfer refers to scenarios where at least one of the two conditions are satisfied: (i) features or dimensions of micro/nanostructured materials are comparable to the characteristic thermal wavelength $\lambda_{th}$ and (ii) Separation between bodies is smaller or comparable to the thermal wavelength. In the first case, features of a material are comparable to the wavelength of electromagnetic radiation and effects like interference, diffraction, partial coherence and surface scattering come into picture. These nanostructures could be a stack of thin films, nanocomposites, diffraction gratings, 2-D surface patterns or photonics crystals. As a result, radiative properties of such a nanostructured material can be substantially different than those of a flat surface of the same material(s). This can give rise to unusual properties such as spectrally selective absorption/emission,

coherent thermal radiation, linearly or circularly polarized thermal radiation, negative refraction and so on. Materials with such unusual properties are known as metamaterials. The second case is known as near-field thermal radiation. When separation between two objects at different temperatures is comparable or smaller than the wavelength of thermal radiation, radiative heat transfer can exceeds what is predicted by Planck's law (the blackbody limit). Derivation of Planck's law is based on the assumption that all dimensions involved in a problem are much larger than the thermal wavelength $\lambda_{th}$. Therefore, Planck's law is unable to explain radiative heat transfer between closely spaced bodies as surface waves dominate the radiative heat transfer.

These novel phenomena allow us to spectrally control and modulate overall radiative heat transfer. Spectral control refers to 'tuning' the spectral response of a radiating surface, while modulation of radiative heat transfer refers to attaining an active control of radiative heat transfer coefficient. Spectral control and modulation of nanoscale heat transfer are the two central themes of this dissertation. Metamaterials and micro/nanoscale thermal radiation in general, have great applications in advanced energy conversion systems, thermal management, thermal cloaking and sensing. Therefore, major goals of this dissertation are:

1. Explore various ways to achieve spectral control and modulation of nanoscale radiative transfer (manuscripts 1 and 2).

2. Investigate feasible applications of various metamaterials in thermophotovoltaic technology (manuscripts 3 and 4) and local thermal management (manuscripts 5 and 6).

This dissertation is prepared using the manuscript format. Sequence of the manuscripts is according to their chief themes rather than chronological.

In manuscript 1, optical and radiative properties of a polymer SU-8 in its bulk form and thin-film form are investigated. Reflectivity of SU-8 samples was experimentally measured using fourier transform infrared spectrometer. Thickness-dependent reflectivity (or emissivity) was observed as expected. Reflectivity spectra of samples were used to calculate refractive indices of the polymer in infrared region. As SU-8 is sensitive to UV exposure, its properties before and after UV exposure were reported. The manuscript follows the formatting guidelines specified by Optical Materials Express.

Manuscript 2 investigates a possible way to attain spectral tuning of radiative transfer by using nanoparticle embedded thin films. The Calculations of emission spectra were performed using the Fresnel equations in the far-field limit, while the dyadic Green's function formalism was used to calculate for transmissivity between the closely spaced objects in the near-field regime. Media containing nanoparticle inclusions were modeled using Maxwell-Garnett-Mie theory. It was shown that the spectral selectivity in the emission spectra can be influenced by varying the size and/or the volume fraction of nanoparticles. Characteristic features of the spectra were linked to refractive indices of the composite. Influence of metallic and dielectric inclusions are separately investigated.

Manuscript 3 deals with design of a novel, efficient and cost effective thermal emitter for thermophotovoltaic (TPV) applications. A Mie-resonance metamaterial based on nanoparticle-embedded thin film was used to attain desired spectral response. The emitter consists of a thin film of $SiO_2$ on the top of tungsten layer deposited on a substrate. Effective dielectric properties are calculated using Maxwell-Garnett-Mie theory. It was shown that, this would significantly improve the efficiency of TPV cells. A new parameter to gauge the efficacy of thermal emitters was also introduced and it was used to compare different emitter designs.

In manuscript 4, the idea of Mie-metamaterial thermal emitter was implemented to a near-field TPV system. Performance characteristics of a near-field thermophotovoltaic system consisting a Mie-metamaterial emitter and GaSb based photovoltaic cell at separations less than the thermal wavelength were theoretically analyzed. Numerical results were obtained using formulae derived from dyadic Green's function formalism and Maxwell-Garnett-Mie theory. It was shown that, by changing the volume fraction of nanoparticles and thickness of $SiO_2$ it is possible to tune the near-field thermal radiation to obtain enhanced output power and high thermal efficiency. Materials considered can withstand high temperatures and are suitable for thermal emitter. Improvement in spectral selectivity as well as overall heat transfer was accounted for an increased power output and efficiency.

In manuscript 5, a concept of a far-field radiative thermal rectification device was proposed. The device uses a phase change material to achieve a high degree of asymmetry in radiative heat transfer. The proposed device has a tri-layer structure on one side and a blackbody on other side. The tri-layer structure consists of a thin film of KBr sandwiched between a thin film of $VO_2$ and a reflecting layer of gold. When $VO_2$ is in its insulating phase, the structure acts as an infrared mirror due to the two transparent layers on highly reflective gold. When $VO_2$ is in the metallic phase, Fabry-Perot type of resonance occurs and the tri-layer structure acts like a highly absorbing surface achieved by destructive interference of partially reflected waves making it highly absorptive for majority of spectral range of thermal radiation. The proposed structure forms the active part of configuration that acts like a far-field radiative thermal diode. Thermal rectification greater than 11 was obtained for a temperature bias of 20 K, which is the highest rectification ever predicted for far-field radiative diode configurations.

Manuscript 6 investigates a near-field radiative thermal diode that uses a phase

change material to achieve asymmetry in radiative heat transfer. The temperature dependent dielectric properties of $VO_2$ were exploited due to its metal-insulator transition near 341 K. Analogous to an electrical diode, heat transfer coefficient is high in one direction while it is considerably small when the polarity of temperature gradient is reversed. It was shown thermal rectification can be greatly enhanced by using 1-D rectangular and triangular surface gratings of $VO_2$. Enhanced rectification in the near-field was accounted to reduced tunneling of surface waves across the interfaces for negative polarity. It was predicted that for minimal temperature difference of 20 K, rectification ratio as high as 16 can be obtained and it is maximum in existing literature to date for comparable operating temperatures and separation.

# TABLE OF CONTENTS

# LIST OF FIGURES

# LIST OF TABLES

# Dynamic Optical Response of SU-8 upon UV Treatment

by

Alok Ghanekar[1], Matthew Ricci[2], Yanpei Tian[1], Otto Gregory[2] and Yi Zheng[1]

[1] Department of Mechanical, Industrial and Systems Engineering, University of Rhode Island,

Kingston, RI 02881

[2] Department of Chemical Engineering, University of Rhode Island, Kingston, RI 02881

Corresponding Author: Yi Zheng

Department of Mechanical, Industrial and Systems Engineering

University of Rhode Island

Kingston, RI 02881, USA

Phone: +1 401-874-5184

Email Address: zheng@uri.edu

**Abstract**

We report the optical properties of SU-8 in mid-infrared (mid-IR) region before and after UV treatment. Samples consisted SU-8 films of thickness ranging from 10 um to 157 um deposited on gold coated silicon substrates and were prepared using spin coating. Mid-IR diffuse reflectance measurements were conducted using Fourier Transform Infrared Spectroscopy. Spectra measurements imply a change in optical properties of SU-8 upon exposure to UV and heat treatment. A gradual change in optical properties is seen after each step of UV treatment and baking process. Reflectance spectra of thin-films were also observed to be thickness dependent. We calculate dielectric function of SU-8 in the range 2 um to 15 um using the reflectance spectra of the samples.

## 1.1 Introduction

Continuous development in lithography and micromachining has led to invention of a photoresist known as SU-8 by IBM$^{®}$ research [1, 2]. SU-8 is a photosensitive epoxy polymer that is now commonly used as negative photoresist for optical lithography, especially for high-aspect ratio lithography [3]. SU-8 has been shown compatible with other nanoscale lithography techniques, such as electron beam lithography and x-ray lithography [4]. SU-8 is of prime importance in fabrication of semiconductor devices, micro-electromechanical systems (MEMS) and microfluidics [5]. Due to its bio-compatibility, SU-8 is also used for bio-MEMS applications [6]. Owing to its good thermal stability and young's modulus, SU-8 can be potentially used for nanoimprint lithography [7]. When exposed to ultraviolet (UV) light, SU-8 undergoes cross-linking leading to polymerization, making it insoluble in solvents such as Acetone, Methyl Ethyl Ketone (MEK) or N-Methyl Pyrrolidinone [2]. While optical properties of SU-8 in visible and UV range have been characterized [8], infrared refractive indices of SU-8 were not estimated until

2

recently [9]. Fourier Transform Infrared Spectroscopy (FTIR) measurements using attenuated total reflectance (ATR) method have also been documented before and various IR absorption bands have been assigned to several different functional groups [10, 11, 12]. Mid-IR dielectric function of SU-8 was first reported by Mota-harifar et al. [9] using reflection and transmission spectra of a free-standing SU-8 sample. Here, we calculate dielectric function of SU-8 using reflectance data for various thickness of SU-8 films. We also observe its reflectance spectra before and after UV treatment.

Polymers in general have been investigated for possible selective thermal emission properties [13]. They can also be embedded with nanoparticles furthering spectral control of thermal emission [14, 15, 16, 17]. Infrared spectral response of polydimethylsiloxane (PDMS) [13], poly(vinyl chloride) (PVC) [18], poly(vinyl fluoride) (PVF) [19] and poly(4-methyl-1-pentene) (PMP) [20] have been studied before. It would be crucial to study spectral response of SU-8 thin films in the infrared region, especially given its sensitivity to UV treatment. We report the optical response of SU-8 in mid-infrared (mid-IR) region: 2 $\mu$m to 15 $\mu$m. Here, mid-IR optical response of SU-8 thin films have been reported before and after UV treatment. Based on the reflectance spectra of thin films of various thicknesses of SU-8, we have calculated its dielectric function using extended Lorentz model.

The main constituents of the SU-8 photoresists are the EPON$^{\circledR}$ Resin SU-8 (Shell Chemical) and triarylsulfonium hexafluoroantimonate salt (CYRACURE$^{\circledR}$ UVI, Union Carbide) photoacid generator that makes it photosensitive to UV light at 310 and 230 nm [21]. UV exposure causes hexafluoroantimonate salt to decompose to form hexafluoroantimonic acid that in turn protonates the EPON$^{\circledR}$ oligomer. These protonated ions react with epoxides in cross-linking reactions upon heating (baking) [21]. Therefore, UV exposure of SU-8 pattern is usually followed by a few
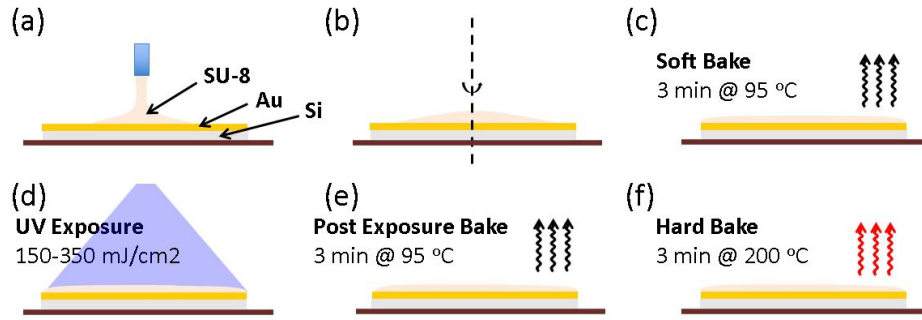
Figure 1.1: Schematic of sample preparation, UV exposure and heat treatment steps.

baking steps during optical photolithography. In this work, we prepared several samples of SU-8 thin films of various thickness coated on a reflecting layer of gold over silicon wafers and recorded the reflectance spectra of the samples after each step that would normally be undertaken during optical lithography. Reflectance spectra of samples with various thicknesses are used to estimate refractive indices of the polymer in the mid-IR region.

## 1.2 Sample Preparation

Silicon (Si) wafers were cleaned using successive washes of acetone, methanol and deionized water and dried using nitrogen gas. The wafers were then heated to 120 °C on a hot plate to release adsorbed gases. 2 $\mu$m of 4N gold were deposited on the smooth side of the Si wafer using RF sputtering via an MRC$^{\circledR}$ 8667 RF Sputtering Machine in 9 mTorr argon gas. Various thicknesses of SU-8 3005 were spin coated onto the gold coated substrates using a Laurell Technologies$^{\circledR}$ WS-400 Spin Coater. Soft baking, exposure, post exposure baking and hard baking were performed according to procedures suggested by the manufacturer and heated using a Fischer Scientific$^{\circledR}$ Isotemp hotplate (see Fig. 1.1 for schematic). UV Exposure was performed using an OAI$^{\circledR}$ UV Exposure and Aligner$^{\circledR}$ workstation. Photoresist thicknesses were confirmed using a Dektak II stylus profilometer.

## 1.3 Reflectance Measurements

Reflection spectra of the prepared samples were measured using Jasco® 6600 FTIR spectrometer equipped with PIKE®'s diffuse reflectance accessory known as mid-IR integrated sphere. The spectrometer has a ceramic source that radiates IR light while the integrated sphere uses its own dedicated mercury cadmium telluride (MCT) detector. The source and the detector allow measurements in the range 2 $\mu$m to 15 $\mu$m with sufficient accuracy. Sample is placed on the the top of the accessory facing downwards. The accessory has a spherical shell coated with a highly reflective layer of gold. The IR light from the interferometer falls on the sample via a gold mirror. Light scattered by the sample is collected by the gold sphere and is eventually captured by the MCT detector. The central mirror can be turned to point at the sphere to take reference measurement of gold (assumed to be 100% reflecting). Angle of incidence on the sample is fixed to 12 °. Nearly 96% of the reflection is specular while about 4% is diffuse. This highlights the quality of the samples. As all scattered light is collected, measured reflectance ($r$) can be directly related to absorbance ($a$) by $a = 1 - r$. Each measurement consists of a background measurement and a sample measurement. Scan rate was set to 64 scans per measurement with a resolution of 0.4 cm$^{-1}$. Three measurements were taken for each sample from different location on the sample. Repeated measurements at different locations were found to be essentially same; this also confirms the quality of the samples.

## 1.4 Results and Discussion
### 1.4.1 Reflectance Spectra

Four samples of SU-8 thin films of thicknesses 10 $\mu$m, 20 $\mu$m, 50 $\mu$m and 157 $\mu$m coated on a gold substrate were prepared (hereafter we will refer to samples as thin films). This was followed by standard processing steps during optical lithog-

raphy: soft baking (Stage I), UV exposure (Stage II), post-exposure bake (Stage III) and hard bake (Stage IV). For the 10 $\mu$m sample, reflectance measurement were recorded at each stage as shown Fig. 1.2(a). As the thickness of the gold layer is much larger than the penetration depth ($\lambda/4\pi\kappa$) of mid-IR radiation, it is thick enough to be opaque. The layer of gold is also highly reflecting (>98%) for the range of wavelengths considered here. Therefore, the spectra show optical properties of SU-8. Reflectance spectrum shows several absorption bands. Each of the absorption bands relate to a specific chemical bond. FTIR spectroscopy using attenuated total reflection (ATR) mode is often performed to identify different chemical bonds in the samples [12]. Here, we have conducted diffuse reflectance measurements instead. While diffuse reflectance spectroscopy is more quantitative than ATR method, the spectrum does not necessarily display all the distinct absorption bands. However, some typical absorptions peaks are clearly visible in the thin-film reflectance spectrum that we briefly discuss. The most notable peaks are due to O-H stretch around 3200-3500 cm$^{-1}$ ($\sim$ 3 $\mu$m), aromatic C-H stretch at 3050 cm$^{-1}$($\sim$ 3.3 $\mu$m ) and aliphatic C-H stretch around 2960-2870 cm$^{-1}$($\sim$ 3.45 $\mu$m). In addition, peaks corresponding to aliphatic CH$_3$ bending ( $\sim$1390 cm$^{-1}$; 7.2 $\mu$m), CH$_2$ bending ($\sim$1540 cm$^{-1}$; 6.5 $\mu$m), and aromatic C-C stretching ($\sim$1724 cm$^{-1}$; 5.8 $\mu$m are also observed. This denotes presence of alkyl and aryl groups present in SU-8.

A change in reflectance spectrum is seen after each stage of treatment, more prominent changes are seen at specific wavelength bands, while some parts of spectrum are unchanged. The UV exposure step induces the greatest change in the reflectance spectrum. Absorption band near 3 $\mu$m shows prominent increase in absorption upon UV exposure. This is the band corresponding to O-H stretch. Increase in absorption in this region suggests an increased number of hydroxyl (O-
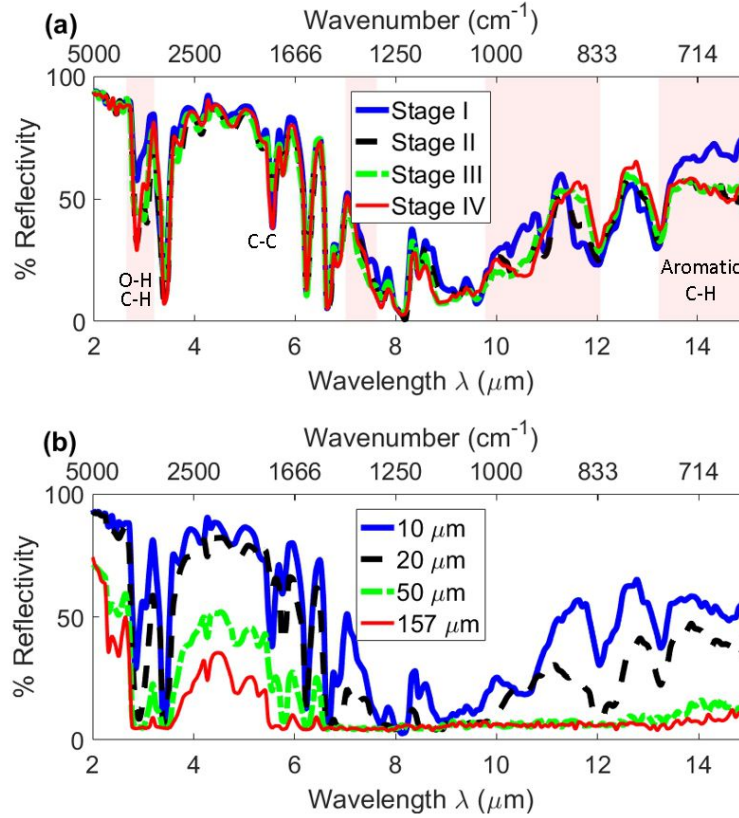
Figure 1.2: (a) Effect on reflectance spectrum after each treatment step on the 10 $\mu$m sample of SU-8; stage I: soft baking, stage II: UV exposure, stage III: post-exposure bake and stage IV: hard bake. Shaded region highlights wavelengths at which a significant change in reflectance is seen. (b) Measured reflectance of UV and heat treated SU-8 samples with various film thicknesses.

H) groups through crosslinking of epoxy groups in SU-8. At longer wavelengths (10 to 15 $\mu$m), it is difficult to assign the change in spectrum to particular bonds. However, this is the region where absorption bands corresponding to aromatic C-H bends lie [10]. Being an epoxy, SU-8 layers are sticky, especially for thicker films. Hence it was not possible to conduct reflectance measurements for the thicker films before UV exposure (as they tend to stick to the apparatus). However, after UV exposure and baking stages, SU-8 becomes completely dry and measurements can be taken.

Figure 1.2 (b) shows reflectance spectra of UV exposed and baked samples of
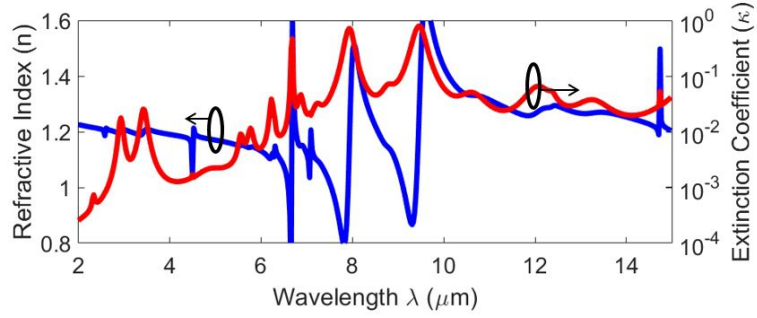
Figure 1.3: Estimated refractive indices of UV treated SU-8
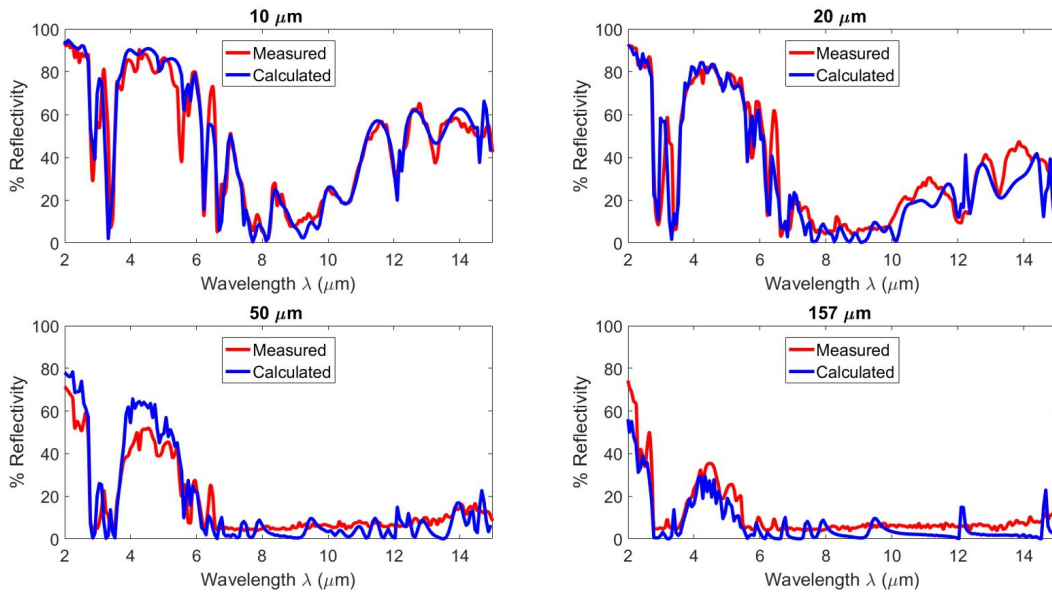


Figure 1.4: Comparison of measured and calculated reflectance of UV treated SU-8 samples with different thickness.

SU-8 of various thicknesses: 10 $\mu$m, 20 $\mu$m, 50 $\mu$m and 157 $\mu$m, respectively. A gradual reduction in reflectance was observed as the thickness of the films increases. While thinner films show absorption at several bands, thicker samples display a broader absorption throughout the infrared region. Appearance of several sharp peaks in the thin film spectra is due to surface phonon modes [22] corresponding various modes of vibrations. Absorption peaks in thin-film spectra can be related to refractive indices of the material[22].

### 1.4.2  Estimation of Dielectric Function

To estimate the dielectric function of SU-8, we use the method outlined by Verleur et al. [23]. Inspired by Srinivasan's [13] approach to calculate dielectric function of PDMS, we employ a similar process to calculate dielectric function of SU-8. We picked reflectance measurements of all samples to extract the dielectric function. Dielectric function $\varepsilon(\omega)$ of a polymer can be assumed to be of Lorentz-Drude oscillator form given by [23],

$$\varepsilon(\omega) = \varepsilon_\infty + \sum_{k=1}^{N} \frac{s_k}{1 - (\frac{\omega}{\omega_k})^2 - j\Gamma_k(\frac{\omega}{\omega_k})}. \tag{1.1}$$

Here, $s_k$, $\omega_k$, $\Gamma_k$ and $j$ are the strength, resonant frequency, damping factor of $k$th Lorentz-Drude oscillator and the imaginary unit, respectively. $N$ such oscillators are assumed. $\varepsilon_\infty$ is the contribution from higher frequencies. Since the angle of incidence in the measurements is 12°, reflectance values were calculated for that angle of incidence. $\omega_k$ correspond to several of the vibrational bond resonances inside the material. High absorption and strong dispersion exist around these resonance frequencies.

For an unpolarized incident beam of light, reflectance $r_c$ for any angle of incidence is related to polarized reflection coefficients by [24]

$$r_c = \frac{1}{2}[|R^{TE}|^2 + |R^{TM}|^2] \tag{1.2}$$

Here, $R^{TE}$ and $R^{TM}$ are effective reflection coefficients at the given angle of incidence for transverse electric (TE) and transverse magnetic (TM) polarization, respectively.

Consider a structure having 3-layer media: air, SU-8 and gold, respectively. Substrate below the gold layer can be ignored as gold is assumed to be 100% reflective. By solving the boundary conditions at the interfaces, one can obtain the expression for the generalized (or effective) reflection coefficient at the air-SU-8 interface

which is given by [24],

$$R^{(\mu)} = \frac{R_{12}^{(\mu)} + R_{23}^{(\mu)} e^{2jk_{2z}L}}{1 + R_{12}^{(\mu)} R_{23}^{(\mu)} e^{2jk_{2z}L}} \qquad (1.3)$$

where $R_{12}^{(\mu)}$ is the Fresnel reflection coefficient at the interface between the layer 1 and 2, and $R_{23}^{(\mu)}$ is the Fresnel reflection coefficient at the interface between the layer 2 and 3, $\mu = s$ (or $p$) refers to TE (or TM) polarization, $L$ is the thickness of SU-8 layer. Since we are dealing with an oblique angle of incidence ($12\,°$), $k_{2z} = \sqrt{\varepsilon(\omega)\omega^2/c^2 - k_\rho^2}$ is the normal component of the wave vector in SU-8 wherein $\varepsilon(\omega)$ is the relative permittivity of SU-8 as a function of angular frequency $\omega$, $c$ is the speed of light in vacuum and $k_\rho = \sin(12°)\omega/c$ is the magnitude of the in-plane wave vector. The above expression accounts for multiple reflections and inventual absorption within the SU-8 layer and it is valid for thin as well as bulk SU-8 coated on gold.

Dielectric function of SU-8 was obtained by tuning several oscillator parameters by matching reflectance spectra of both thin films and bulk samples. This involved an optimization procedure that aims to minimize the error between calculated and measured spectra. The error between the spectra is given by

$$\delta = \sum_{i=1}^{M} [r_m - r_c]^2 \Bigg|_{10\ \mu m} + \sum_{i=1}^{M} [r_m - r_c]^2 \Bigg|_{20\ \mu m} + \sum_{i=1}^{M} [r_m - r_c]^2 \Bigg|_{50\ \mu m} + \sum_{i=1}^{M} [r_m - r_c]^2 \Bigg|_{157\ \mu m}$$
$$(1.4)$$

Here, $r_m$ and $r_c$ are measured and calculated values of reflectance, respectively. Index $i$ refers to $M$ different frequencies over which the measurements are taken. One may use reduced Chi-Squared function instead of using absolute error squared as an objective function. One of the issues with reduced Chi-Squared function is that, it produces large values for low reflectance points. This gives higher weightage to thicker samples (because they have very low reflectance on an average). As a result, it produces a good fit for thick samples but not for films. This method is not practical when dealing with samples of various thicknesses. Therefore, absolute

error squared was used as objective function.

The minimization was done in two steps. In the first step, we used Matlab$^{\circledR}$ based genetic algorithm to arrive at an initial guess of oscillator parameters. This brings us closer to the global optimum of the objective function, providing a reasonable fit. This is further improved by using constrained optimization function *fmincon*. It was found that eighteen such resonant frequencies are needed to achieve a good fit with the experimental data. As observed by Verleur [23], at least one oscillator mode is needed to be outside the spectral range of measurement to achieve a good fit. In our case, this is located at 15.4 $\mu$m. The oscillator parameters for the UV exposed and heat treated SU-8 are provided in Table 1.1. Infrared refractive indices calculated using reflectance measurements of UV exposed and heat treated SU-8 samples are shown in Fig. 1.3. Comparison of measured and calculated reflectance of UV treated SU-8 samples are shown in Fig. 1.4. Although thicker samples of unexposed SU-8 could not be used for measurements, thin film measurements of unexposed SU-8 samples (10 $\mu$m) and measurements of exposed SU-8 samples with 50 $\mu$m and 157 $\mu$m thickness were used to estimate dielectric function of SU-8 pre-exposure are tabulated in Table 1.1. While resonant frequencies of the dielectric function of SU-8 are very similar before and after exposure, values of oscillator strength parameters and damping factors are different. Some of the resonant frequencies can be related to well-known IR absorption bands that are associated with typical chemical bonds in organic materials. Those are also listed in the tables for the reader's convenience. In the recent work, Motaharifar et al.[9] estimated dielectric function of UV and heat treated SU-8. Their model identifies only six resonance frequencies that are also similar to the frequencies identified in this work. These frequencies are 24.3 (24.7), 30.6 (32), 33.4 (32), 35.3 (36.8), 36.7 (36.8) and 45.0 (44.4) THz. Here, the numbers in the bracket denote

11

Table 1.1: Lorentz-Drude oscillator parameters of SU-8 after UV and heat treatment

| k | $\omega_k$ (cm$^{-1}$) | $\lambda_k$ ($\mu$m) | $s_k$ | $\Gamma_k$ | Vibrational Bond |
|---|---|---|---|---|---|
| - | - | - | - | - | |
| 1 | 3469 | 2.9 | 5.379E-04 | 1.198E-02 | O-H |
| 2 | 2955 | 3.4 | 1.474E-02 | 2.654E-03 | Aliphatic C-H |
| 3 | 1768 | 5.7 | 1.345E-03 | 2.151E-04 | |
| 4 | 1702 | 5.9 | 4.714E-03 | 2.520E-05 | Aromatic C-C |
| 5 | 1610 | 6.2 | 2.330E-03 | 2.242E-04 | |
| 6 | 1599 | 6.3 | 1.138E-03 | 1.100E-01 | |
| 7 | 1479 | 6.8 | 6.422E-03 | 1.928E-03 | |
| 8 | 1344 | 7.4 | 3.731E-04 | 4.898E-05 | |
| 9 | 1339 | 7.5 | 9.896E-03 | 8.090E-05 | |
| 10 | 1265 | 7.9 | 2.033E-02 | 1.242E-02 | |
| 11 | 1227 | 8.2 | 1.944E-03 | 2.234E-02 | |
| 12 | 1067 | 9.4 | 3.227E-02 | 1.668E-02 | |
| 13 | 947 | 10.6 | 3.071E-03 | 3.863E-02 | |
| 14 | 831 | 12.0 | 3.412E-03 | 4.090E-02 | |
| 15 | 823 | 12.1 | 5.759E-03 | 3.790E-05 | |
| 16 | 757 | 13.2 | 3.073E-03 | 3.831E-02 | Aromatic C-H (out of plane) |
| 17 | 682 | 14.7 | 5.168E-03 | 5.400E-05 | |
| 18 | 648 | 15.4 | 6.622E-03 | 2.668E-02 | Aromatic C-C (out of plane) |

$$\epsilon_\infty = 1.4$$

Table 1.2: Lorentz-Drude oscillator parameters of SU-8 before UV exposure

| k | $\omega_k$ (cm$^{-1}$) | $\lambda_k$ ($\mu$m) | $s_k$ | $\Gamma_k$ | Vibrational Bond |
|---|---|---|---|---|---|
| - | - | - | - | - | |
| 1 | 3459 | 2.9 | 5.288E-04 | 1.633E-02 | O-H |
| 2 | 2963 | 3.4 | 1.615E-02 | 2.009E-03 | Aliphatic C-H |
| 3 | 1766 | 5.7 | 1.101E-03 | 1.195E-04 | |
| 6 | 1727 | 5.8 | 9.321E-04 | 1.500E-01 | Aromatic C-C |
| 4 | 1702 | 5.9 | 4.727E-03 | 1.630E-05 | |
| 5 | 1611 | 6.2 | 2.569E-03 | 3.018E-04 | |
| 7 | 1480 | 6.8 | 7.252E-03 | 2.295E-03 | |
| 8 | 1344 | 7.4 | 2.120E-04 | 3.086E-05 | |
| 9 | 1338 | 7.5 | 9.496E-03 | 3.953E-05 | |
| 10 | 1267 | 7.9 | 2.267E-02 | 1.143E-02 | |
| 11 | 1180 | 8.5 | 9.107E-04 | 1.241E-02 | |
| 12 | 1055 | 9.5 | 2.862E-02 | 1.448E-02 | |
| 13 | 938 | 10.7 | 1.886E-03 | 4.126E-02 | |
| 14 | 836 | 12.0 | 4.794E-03 | 3.526E-02 | |
| 15 | 823 | 12.1 | 5.726E-03 | 4.452E-05 | |
| 16 | 760 | 13.2 | 2.895E-03 | 2.617E-02 | Aromatic C-H (out of plane) |
| 17 | 682 | 14.7 | 5.220E-03 | 3.001E-05 | |
| 18 | 642 | 15.6 | 6.403E-03 | 3.637E-02 | Aromatic C-C (out of plane) |

$$\epsilon_\infty = 1.4$$

resonance frequencies estimated in the present work.

Average error between calculated and reflected spectra is about 5%. Given that the estimated dielectric function allows us to calculate and match reflectance curves for four different film thicknesses, such an error is reasonable. In Fig. 1.4, we observe that reflectance curves of thickers samples of SU-8 show flat regions. Such a response cannot be a result of Lorentzian model as clearly seen from the deviations in spectrum for thicker films, e.g. 157 $\mu$m sample. However, it does not mean that Lorentz-Drude model is invalid for SU-8. We account for such differences to the errors in reflectance measurements for thicker samples. Uncertainties in reflectivity measurements for thick samples can be larger due to their low reflectance. As the reference standard is 100% reflectance, measured signal for highly absorbing (weakly reflecting) samples is small and contains more noise. As a results, some features of the reflectance spectra are lost. However, the reflectance data from these thicker samples is necessary for correct estimation of $\varepsilon_\infty$. We also observed that thicker samples tend to have non-uniformity issues. Moreover, there are difficulties in fabricating bulk samples that do not crank or display wrinkling on the surface. For this reason, we did not include bulk samples measurements of SU-8 for estimation of dielectric function.

## 1.5 Conclusion

In summary, we have reported optical properties of SU-8 using FTIR diffuse reflectance spectroscopy. Observations were made before and after UV treatment of the samples. Reflectance spectra clearly show change standard steps of UV exposure and heat treatment are followed. Reflectance spectra of the polymer is thickness-dependent. Reflectance spectra of various thicknesses can be used to estimate dielectric function of the polymer that obeys Lorentz-Drude oscillator model. The oscillator parameters for the dielectric function were identified using

a curve fitting optimization routine between predicted and simulated reflectance spectra.

**List of References**

[1] N. C. LaBianca and J. D. Gelorme, "High-aspect-ratio resist for thick-film applications," in *SPIE's 1995 Symposium on Microlithography.* International Society for Optics and Photonics, 1995, pp. 846–852.

[2] H. Lorenz, M. Laudon, and P. Renaud, "Mechanical characterization of a new high-aspect-ratio near uv-photoresist," *Microelectronic Engineering*, vol. 41, pp. 371–374, 1998.

[3] "http://www.microchem.com/prod-su8.htm."

[4] A. del Campo and C. Greiner, "Su-8: a photoresist for high-aspect-ratio and 3d submicron lithography," *Journal of Micromechanics and Microengineering*, vol. 17, no. 6, p. R81, 2007.

[5] J. Zhang, K. Tan, G. Hong, L. Yang, and H. Gong, "Polymerization optimization of su-8 photoresist and its applications in microfluidic systems and mems," *Journal of Micromechanics and Microengineering*, vol. 11, no. 1, p. 20, 2001.

[6] K. V. Nemani, K. L. Moodie, J. B. Brennick, A. Su, and B. Gimi, "In vitro and in vivo evaluation of su-8 biocompatibility," *Materials Science and Engineering: C*, vol. 33, no. 7, pp. 4453–4459, 2013.

[7] J. Sua, F. Gaob, Z. Gub, W. Daic, G. Cernigliaroc, and H. Sun, "Fabrication of su-8 based nanopatterns and their use as a nanoimprint mold," in *Proc. of SPIE Vol*, vol. 8974, 2014, pp. 897 409–1.

[8] O. P. Parida and N. Bhat, "Characterization of optical properties of su-8 and fabrication of optical components," in *Int. Conf. on Opt. and Photon.(CSIO)*, 2009, pp. 4–7.

[9] E. Motaharifar, R. Pierce, R. Islam, R. Henderson, J. Hsu, and M. Lee, "Broadband terahertz refraction index dispersion and loss of polymeric dielectric substrate and packaging materials," *Journal of Infrared, Millimeter, and Terahertz Waves*, vol. 39, no. 1, pp. 93–104, 2018.

[10] T. Tan, D. Wong, P. Lee, R. Rawat, and A. Patran, "Study of a chemically amplified resist for x-ray lithography by fourier transform infrared spectroscopy," *Applied spectroscopy*, vol. 58, no. 11, pp. 1288–1294, 2004.

[11] B. C. Smith, *Infrared spectral interpretation: a systematic approach*. CRC press, 1998.

[12] X.-B. Wang, J. Sun, C.-M. Chen, X.-Q. Sun, F. Wang, and D.-M. Zhang, "Thermal uv treatment on su-8 polymer for integrated optics," *Optical Materials Express*, vol. 4, no. 3, pp. 509–517, 2014.

[13] A. Srinivasan, B. Czapla, J. Mayo, and A. Narayanaswamy, "Infrared dielectric function of polydimethylsiloxane and selective emission behavior," *Applied Physics Letters*, vol. 109, no. 6, p. 061905, 2016.

[14] A. R. Gentle and G. B. Smith, "Radiative heat pumping from the earth using surface phonon resonant nanoparticles," *Nano letters*, vol. 10, no. 2, pp. 373–379, 2010.

[15] G. Smith, C. Deller, P. Swift, A. Gentle, P. Garrett, and W. Fisher, "Nanoparticle-doped polymer foils for use in solar control glazing," *Journal of Nanoparticle Research*, vol. 4, no. 1, pp. 157–165, 2002.

[16] A. Heilmann, *Polymer films with embedded metal nanoparticles*. Springer Science & Business Media, 2013, vol. 52.

[17] A. Ghanekar, L. Lin, J. Su, H. Sun, and Y. Zheng, "Role of nanoparticles in wavelength selectivity of multilayered structures in the far-field and near-field regimes," *Optics Express*, vol. 23, no. 19, pp. A1129–A1139, 2015.

[18] T. Felix, "Devices for lowering the temperature of a body by heat radiation therefrom," Mar. 21 1967, uS Patent 3,310,102.

[19] B. Bartoli, S. Catalanotti, B. Coluzzi, V. Cuomo, V. Silvestrini, and G. Troise, "Nocturnal and diurnal performances of selective radiators," *Applied Energy*, vol. 3, no. 4, pp. 267–286, 1977.

[20] P. Grenier, "Radiative cooling-inverse greenhouse effect," *Revue de Physique Appliquee*, vol. 14, pp. 87–90, 1979.

[21] W. Teh, U. Dürig, U. Drechsler, C. Smith, and H.-J. Güntherodt, "Effect of low numerical-aperture femtosecond two-photon absorption on (su-8) resist for ultrahigh-aspect-ratio microstereolithography," *Journal of applied physics*, vol. 97, no. 5, p. 054907, 2005.

[22] A. Narayanaswamy, J. Mayo, and C. Canetta, "Infrared selective emitters with thin films of polar materials," *Applied Physics Letters*, vol. 104, no. 18, p. 183107, 2014.

[23] H. W. Verleur, "Determination of optical constants from reflectance or transmittance measurements on bulk crystals or thin films," *JOSA*, vol. 58, no. 10, pp. 1356–1364, 1968.

[24] W. C. Chew, *Waves and fields in inhomogeneous media*. IEEE press, 1995.

# MANUSCRIPT 2

# Role of Nanoparticles in Wavelength Selectivity of Multilayered Structures in the Far-field and Near-field Regimes

by

Alok Ghanekar[1], Laura Lin[1,2], Junwei Su[3], Hongwei Sun[3], Yi Zheng[1]

[1]Department of Mechanical, Industrial and Systems Engineering, University of Rhode Island, Kingston, RI 02881, USA

[2]Department of Mechanical Engineering, Technische Universität Braunschweig, 38106 Braunschweig, Germany

[3]Department of Mechanical Engineering, University of Massachusetts Lowell, Lowell, MA 01854, USA

Corresponding Author: Yi Zheng

Department of Mechanical, Industrial and Systems Engineering

University of Rhode Island

Kingston, RI 02881, USA

Phone: +1 401-874-5184

Email Address: zheng@uri.edu

**Abstract**

Microscopic thin films have shown wavelength selectivity in the context of radiative heat transfer. We propose a methodology to shift the wavelength selectivity in the desired location. This work deals with the far-field and near-field radiation from thin films embedded with nanoparticles. The calculations of emission spectra are performed using the Fresnel equations in the far-field limit, and using the dyadic Green's function formalism for transmissivity between the closely spaced objects in the near-field regime. For the media doped with nanoparticles, an effective dielectric function using the Maxwell-Garnett-Mie theory is used to calculate emissivity and radiative heat transfer. It has been shown that the wavelength selectivity in the emission spectra can be influenced by varying the size and/or the volume fraction of nanoparticles. We characterize the wavelength selectivity using real and imaginary parts of the effective refractive index. We show that the influence of nanoparticles on wavelength selectivity is different depending on whether the particles are of polar materials or are metallic.

## 2.1 Introduction

Most naturally occurring materials exhibit a broad range of emission spectrum. However, thermal and optical properties of nanomaterials and nanostructures are significantly different than that of bulk materials. They are the basis of development of selective thermal emitters and absorbers that are crucial for development of solar cells and thermophotovoltaics (TPV) [1]. Wavelength selective emitters also have a wide range of potential applications such as biosensors, chemical sensors [2, 3], thermal cooling and thermal detectors [4]. It has been shown that one dimensional (1-D) metallo-dielectric periodic structures display great selective emission properties in the infrared and visible region [5]. Multi-layered structures of thin films (1-D photonic crystals) of polar materials can also be used to develop selec-

tive emitters [6]. The property of multi-layered structures to exhibit wavelength selectivity can be explained by presence of surface phonon polaritons (SPhPs) for polar materials and surface plasmon polaritons (SPPs) for metals [5, 7]. It has also been demonstrated that two dimensional (2-D) or three dimensional (3-D) photonic crystals can be used to develop selective emitters [8, 9]. However, thin-film layered structures are easy to design and fabricate. Calculation of their emission spectra is also relatively simple.

Wavelength selectivity of 1-D photonic crystals is a far-field phenomenon. When the distance between two objects is of the order of the dominant thermal wavelength, the radiative heat transfer is enhanced to many orders of magnitude due to the coupling of surface waves and is referred to as near-field thermal radiation [10]. If the materials support SPhPs or SPPs, the near-field radiative flux can be shown to be inversely proportional to the square of the distance. The enhancement of heat transfer does not take place at all wavelengths but only at specific wavelengths [10]. This wavelengths selectivity in the near-field is exhibited by thin films as well as bulk materials. Wavelength selectivity in the near-field limit is due to the coupling of SPPs or SPhPs across the two surfaces [10].

While many articles dedicated to design and fabrication of selective emitters can be found in the literature, use of nanoparticles specifically for the application of selective emitters is relatively sparse [11]. Optical properties of materials doped with nanoparticles have been investigated before [12, 13]. Experimental and analytical study of thermal coatings doped with nanoparticles such as Gonome et al. [14, 15] can also be found in literature. However, emissive properties of nanoparticles embedded thin films have not been studied in detail to the best of our knowledge. This paper presents the multi-layered structures which contain nanoparticles (NPs) doped into the thin films which are suitable for any of the potential applications

in both far-field and near-field. In this paper, we investigate a methodology which can be used to develop selective thermal emitters for a desired wavelength band. Ideally, one may want to develop a selective emitter for specific wavelength band as per the requirements. As the emission spectrum displays peaks at the wavelengths which are characteristics of the refractive index of the material, changing the thickness of the film allows control over only a narrow spectral band. We propose to dope the top layer (thin film) with nanoparticles to change the dielectric properties of the material. The usual Maxwell-Garnett equation for effective medium approximation is often employed for such an analysis disregarding the sizes of doped materials [16]. Here, we apply the Maxwell-Garnett-Mie formulation [17] for effective medium approximation to calculate the dielectric function of a composite that consists of a host material embedded with nanoparticles of various sizes and volume fractions, and extend the same approach to calculate radiative heat transfer for thin-films doped with nanoparticles. Thin film structure with nano-particles would be easy to fabricate as submicron thin films embedded with nanoparticles have been fabricated before [18, 19]. We aim to study the effect on the wavelength selectivity of thin films due to combination of surface polaritons of the films and the nanoparticles and their effects in near-field radiative heat transfer and spectral heat flux. We consider hypothetical cases of thin-film embedded with nanoparticles although fabrication of these particular NPs embedded films discussed here is relatively unknown. We choose SiC and Polystyrene as the host materials (for thin films). SiC is chosen as a host because it has high permittivity in the infrared region and supports SPhP. Polystyrene is chosen because it does not support either SPPs or SPhPs. BN which supports SPhP and Au which supports SPPs are picked for the material of inclusion (NPs).

The structure of the paper is as follows. In section 2.2 we present the theoretical

background and analytical expressions used for calculation of emissivity of thin film structures, calculation of heat transfer between closely placed half spaces and the application of Maxwell-Garnett-Mie theory. In section 2.3 we discuss the results of our calculations obtained using the formulations outlined in section 2.2. Subsequently, the ideas and conclusions of the paper are narrated in section 2.4.

## 2.2 Theoretical Fundamentals

Consider a structure having $N$-layer media having $(N-1)$ interfaces. By solving the boundary conditions at the interfaces, one can obtain the expression for the generalized reflection coefficient at the interface between region $i$ and region $i+1$ and is given by [20],

$$\widetilde{R}_{i,i+1}^{(\mu)} = \frac{R_{i,i+1}^{(\mu)} + \widetilde{R}_{i+1,i+2}^{(\mu)} e^{2jk_{i+1,z}(d_{i+1}-d_i)}}{1 + R_{i,i+1}^{(\mu)} \widetilde{R}_{i+1,i+2}^{(\mu)} e^{2jk_{i+1,z}(d_{i+1}-d_i)}} \tag{2.1}$$

where $R_{i,i+1}^{(\mu)}$ is the Fresnel reflection coefficient at the interface between the layer $i$ and $i+1$, and $\widetilde{R}_{i+1,i+2}^{(\mu)}$ is the generalized reflection coefficient at the interface between the layer $i+1$ and $i+2$, $\mu = s$ (or $p$) refers to transverse electric (or magnetic) polarization, $z = -d_i$ is the location of the $i$th interface. $k_{i,z} = \sqrt{\varepsilon_i(\omega)\omega^2/c^2 - k_\rho^2}$ is the normal $z$-component of the wave vector in medium $i$ wherein $\varepsilon_i(\omega)$ is the relative permittivity of the medium $i$ as a function of angular frequency $\omega$, $c$ is the speed of light in vacuum and $k_\rho$ is the magnitude of the in-plane wave vector. With $\widetilde{R}_{N,N+1}^{(\mu)} = 0$, the above equation provides a recursive relation to calculate the reflection coefficients $\widetilde{R}_{i,i+1}^{(\mu)}$ in all regions. The generalized transmission coefficient for the layered slab is given by

$$\widetilde{T}_{1,N}^{(\mu)} = \prod_{i=1}^{N-1} e^{jk_{iz}(d_i-d_{i-1})} S_{i,i+1}^{(\mu)} \tag{2.2}$$

where $S_{i,i+1}^{(\mu)} = T_{i,i+1}^{(\mu)}/(1 - R_{i,i+1}^{(\mu)} \widetilde{R}_{i+1,i+2}^{(\mu)} e^{2jk_{i+1,z}(d_{i+1}-d_i)})$ and $j = \sqrt{-1}$. Alternatively, the generalized reflection and transmission coefficients can also be calcu-
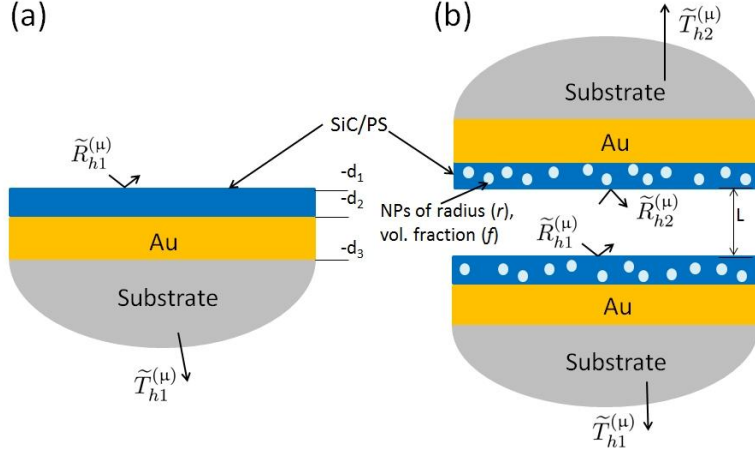
Figure 2.1: Configurations of thin-film structures embedded with nanoparticles. (a) A thin film of SiC (or Polystyrene) on top of gold film of 1 $\mu$m placed on a substrate, and (b) two multi-layered half-spaces in near-field. The top film will be mixed with nanoparticles of radius $r$ and volume fraction $f$.

lated using transfer matrix approach [21]. The hemispherical emissivity is given by the expression [6]

$$e(\omega) = \frac{c^2}{\omega^2} \int_0^{\omega/c} dk_\rho k_\rho \sum_{\mu=s,p} (1 - |\widetilde{R}_{h1}^{(\mu)}|^2 - |\widetilde{T}_{h1}^{(\mu)}|^2) \qquad (2.3)$$

where $\widetilde{R}_{h1}^{(\mu)}$ and $\widetilde{T}_{h1}^{(\mu)}$ are the polarized effective reflection and transmission coefficients, as shown in Fig. 2.1(a).

Far-field radiative heat transfer is described by Planck's law of thermal radiation [22]. This description, however, does not account for the presence of evanescent (surface) waves which dominate only near the boundaries. The expression of radiative transfer between closely spaced objects can be derived using dyadic Green's function formalism [23], and is given by

$$q_{1\to2}(T_1,T_2,L) = \int_0^\infty \frac{d\omega}{2\pi} [\Theta(\omega, T_1) - \Theta(\omega, T_2)] T_{1\to2}(\omega) \qquad (2.4)$$

where $\Theta(\omega, T) = (\hbar\omega/2)\coth(\hbar\omega/2k_BT)$ is the energy of harmonic oscillator at frequency $\omega$ and temperature $T$, $\hbar$ is the reduced Planck constant, and $k_B$ is the

22

Boltzmann constant. The function $T_{1\rightarrow2}(\omega)$ corresponds to the spectral transmissivity in radiative transfer between media 1 and 2 separated of distance $L$ and is expressed as [23]

$$
\begin{aligned}
T_{1\rightarrow2}(\omega) = & \int_0^{\omega/c} \frac{k_\rho dk_\rho}{2\pi} \sum_{\mu=s,p} \frac{(1-|\widetilde{R}_{h1}^{(\mu)}|^2)(1-|\widetilde{R}_{h2}^{(\mu)}|^2)}{|1-\widetilde{R}_{h1}^{(\mu)}\widetilde{R}_{h2}^{(\mu)}e^{2jk_{hz}L}|^2} \\
& + \int_{\omega/c}^{\infty} \frac{k_\rho dk_\rho}{2\pi} \sum_{\mu=s,p} \frac{4\Im(\widetilde{R}_{h1}^{(\mu)})\Im(\widetilde{R}_{h2}^{(\mu)})e^{-2|k_{hz}|L}}{|1-\widetilde{R}_{h1}^{(\mu)}\widetilde{R}_{h2}^{(\mu)}e^{-2|k_{hz}|L}|^2}
\end{aligned}
\tag{2.5}
$$

where $\widetilde{R}_{h1}^{(\mu)}$ and $\widetilde{R}_{h2}^{(\mu)}$ are polarized effective reflection coefficients of the two half spaces (calculated in the absence of other half space), and $k_{hz}$ is the $z$-component of wavevector in vacuum. The first term in Eq. (5.2) corresponds to propagating waves, while the second term describes the thermal transport due to evanescent waves, and its contribution is significant only for small values of gap $L$.

Clausius-Mossotti equation for the effective dielectric function, $\varepsilon_{eff}$, of the composite medium containing nanoparticle inclusions in a host material is given by [24, 25]

$$
\varepsilon_{eff} = \varepsilon_m \left( \frac{r^3 + 2\alpha_r f}{r^3 - \alpha_r f} \right)
\tag{2.6}
$$

where $\varepsilon_m$ is the dielectric function of the matrix, $\alpha_r$ is the electric dipole polarizability, $r$ and $f$ are the radius and volume fraction of nanoparticles respectively. The size dependent extension of Maxwell Garnett formula can be obtained by deriving an expression for electric dipole polarizability using Mie theory [17]

$$
\alpha_r = \frac{3jc^3}{2\omega^3\varepsilon_m^{3/2}} a_{1,r}
\tag{2.7}
$$

where $a_{1,r}$ is the first electric Mie coefficient given by

$$
a_{1,r} = \frac{\sqrt{\varepsilon_{np}}\psi_1(x_{np})\psi_1'(x_m) - \sqrt{\varepsilon_m}\psi_1(x_m)\psi_1'(x_{np})}{\sqrt{\varepsilon_{np}}\psi_1(x_{np})\xi_1'(x_m) - \sqrt{\varepsilon_m}\xi_1(x_m)\psi_1'(x_{np})}
\tag{2.8}
$$

where $\psi_1$ and $\xi_1$ are Riccati-Bessel functions of the first order given by $\psi_1(x) = xj_1(x)$ and $\xi_1(x) = xh_1^{(1)}(x)$ where $j_1$ and $h_1^{(1)}$ are first order spherical Bessel

functions and spherical Hankel functions of the first kind, respectively. Here, $'''$ indicates the first derivative. $x_m = \omega r \sqrt{\varepsilon_m}/c$ and $x_{np} = \omega r \sqrt{\varepsilon_{np}}/c$ are the size parameters of the matrix and the nanoparticles, respectively; $\varepsilon_{np}$ being the dielectric function of nanoparticles.

Effective medium approximation method is applicable when average distance between inclusions is much smaller than the wavelength of interest. If the dielectric inclusions of radius r can be imagined to be arranged in simple cubic lattice of lattice constant a, the condition for validity of the effective medium approximation is $\lambda_h >> a > 2r$. Where $\lambda_h$ is the wavelength in the host material [26]. We emphasize that since we use the approximation for thin-films doped with nanoparticles, its use may not be correct when the particle size is comparable to the thickness of the films. Also, as discussed in by Liu et al. [27], it can be argued that the use of effective medium theory (EMT) is questionable at nanoscale distances. Although such might be the case for the near-field calculations presented here, its detailed analysis is beyond the scope of this work and is left for future work. Despite of the limitations of Maxwell-Garnett-Mie theory and its application in the near-field regime, the results obtained should provide general trends and give considerable insight into optical properties of artificial materials. Further investigations by direct numerical simulation may be necessary to confirm the validity of EMT [28]. Moreover, these results will be constructive when judging the validity of the EMT in near-field by direct numerical calculations. We would like to keep these points open for speculation.

## 2.3 Results

The dielectric function is related to real ($n$) and imaginary ($\kappa$) parts of refractive index as $\sqrt{\varepsilon} = n + j\kappa$. For SiC and BN, the dielectric function has the form as

Figure 2.2: Hemispherical emissivity spectra for SiC or polystyrene (PS) thin film of thickness 0.4 $\mu$m mixed with BN and Au nanoparticles of 25 nm radius and different volume fractions (a) SiC film mixed with BN nanoparticles of various volume fractions, (b) SiC film mixed with Au nanoparticles of various volume fractions, (c) Polystyrene film mixed with BN nanoparticles of various volume fraction, and (d) Polystyrene film mixed with Au nanoparticles of various volume fractions. All spectral ranges begin at 0.35 $\mu$m.

[29, 30]

$$\varepsilon(\omega) = \varepsilon_\infty \frac{(\omega^2 - \omega_{LO}^2 + j\omega\gamma)}{(\omega^2 - \omega_{TO}^2 + j\omega\gamma)} \tag{2.9}$$

where $\omega_{TO}$ and $\omega_{LO}$ are transverse and longitudinal optical phonon frequencies and $\gamma$ is the damping constant. For SiC, the constants $\varepsilon_\infty$, $\omega_{TO}$, $\omega_{LO}$ and $\gamma$ are equal to 6.7, $9.83 \times 10^{-2}$ eV, 0.12 eV and $5.90 \times 10^{-4}$ eV respectively. The values of $\varepsilon_\infty$, $\omega_{TO}$, $\omega_{LO}$ and $\gamma$ for BN are 4.46, 0.1309 eV, 0.1616 eV and $6.55 \times 10^{-4}$ eV respectively. Data for the bulk gold (Au) is taken from Johnson and Christy [31]. Figure 2.2(a) considers the case of SiC film doped with NPs of BN. SiC film of 0.4 $\mu$m is on the top of Au film of 1 $\mu$m deposited on a substrate. Effect of change in NPs volume fraction ($f$) is studied. Volume fraction of BN nanoparticles is changed from 0% to 30% while keeping the radius of 25 nm. Thin film of pure SiC exhibits emission peaks at $\lambda_n^{SiC} \approx 10.33$ $\mu$m and $\lambda_k^{SiC} \approx 13$ $\mu$m. $\lambda_n$ is the

wavelength at which the real part of the refractive index becomes zero (zero-index material) [6, 32]. $\lambda_\kappa$ is the wavelength at which the real part of refractive index $(n)$ is large while the imaginary part of refractive index $(\kappa)$ is small [6]. These peaks are attributed to the presence of SPhPs, and the characteristic wavelengths of the dielectric function of SiC. Appearance of new peaks upon 5% inclusion of BN nanoparticles has been observed at $\lambda \approx 8.5$ $\mu$m and $\lambda \approx 11.5$ $\mu$m. When the volume fraction of NPs is increased further, each of these peaks splits into two giving rise to a total of six peaks. Locations of these peaks do not correspond to the characteristic wavelengths of BN ($\lambda_n^{BN} \approx 7.6$ $\mu$m and $\lambda_\kappa^{BN} \approx 9.8$ $\mu$m). In addition, there exists a small shift in the emission peak at $\lambda_\kappa^{SiC}$. This suggests an interaction between SiC matrix and BN NPs. Consider the case with 30% inclusion of BN. Figure 2.3(a) shows that the mixture has two additional locations where the refractive index is zero ($\lambda_{n1}^{mixture} \approx 8.5$ $\mu$m and $\lambda_{n2}^{mixture} \approx 11.7$ $\mu$m). Moreover, at two more points $n$ is large while imaginary part of refractive index is small, namely $\lambda_{\kappa 1}^{mixture} \approx 9$ $\mu$m and $\lambda_{\kappa 2}^{mixture} \approx 11.1$ $\mu$m These wavelengths correspond to the additional peaks. While the additional peaks are at the location of the characteristics of the refractive index of the mixture, it is interesting to note that peaks at $\approx 10.33$ $\mu$m and $\approx 12.98$ $\mu$m have no or little shift even at large volume fraction of 30%, because they are characteristic wavelengths of the host. Inclusion of BN leads to new SPhP leading to new peaks. Figure 2.2(b) shows the effect of Au nanoparticles in SiC thin film. When particle size is small, especially when the size is comparable to the mean free path of the free electrons, confinement effects become significant [25, 33]. The optical properties of metallic nanoparticles have shown size dependence [34]. We utilize a size-dependent dielectric function for Au nanoparticles of radius $r$ that takes care of electron scattering, which is given by
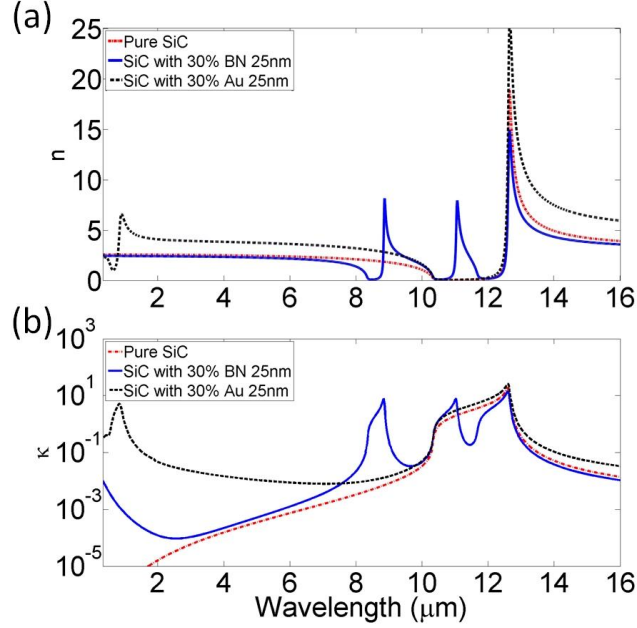
Figure 2.3: Refractive index characteristics of SiC doped with BN and Au nanoparticles: (a) Real part of refractive index $n$, and (b) imaginary part of refractive index $\kappa$, for SiC and SiC doped with 30% BN or Au nanoparticles.

[35]

$$\varepsilon(\omega, r) = \varepsilon_b(\omega) + \frac{\omega_p^2}{\omega^2 + j\omega\gamma_0} - \frac{\omega_p^2}{\omega^2 + j\omega(\gamma_0 + Av_f/r)} \tag{2.10}$$

where $\varepsilon_b$, $\omega_p$, $v_f$ and $\gamma_0$ are the bulk dielectric function, the plasma frequency, the Fermi velocity of free electrons and the electron damping, respectively. The values of $\varepsilon_b$ are taken from Johnson and Christy [31]. The parameters $\omega_p$, $v_f$ and $\gamma_0$ are taken to be 9.06 eV, 0.077 eV and $1.4 \times 10^6$ m/s, respectively. The proportionality constant $A$ that depends on the the electron scattering process at the surface of nanoparticles is assumed to be unity. Volume fraction is varied from 0 to 30% while NPs radius is kept constant (25 nm). Multiple oscillatory peaks are seen in the lower wavelength region upon addition of Au nanoparticles. A shift in the original peak of SiC at $\approx 13$ $\mu$m is seem when volume fraction is large (30%). While the presence of a peak at $\approx 10.33$ $\mu$m and a peak at $\approx 13$ $\mu$m can be related to $n$ and
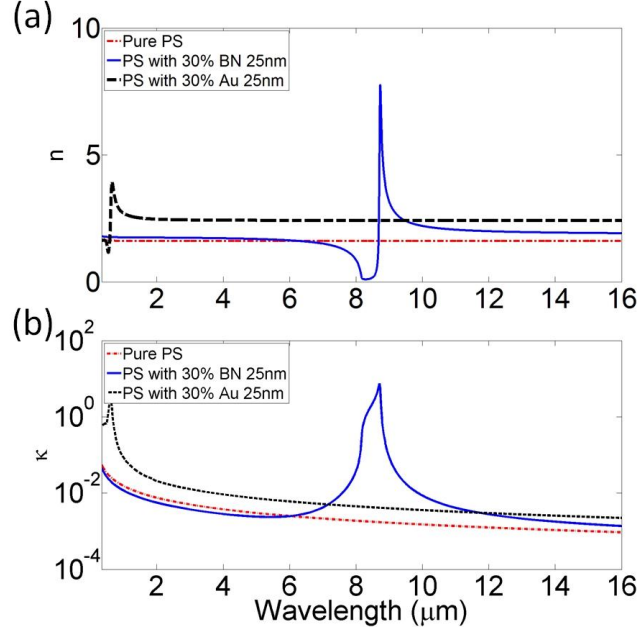
Figure 2.4: Refractive index characteristics of Polystyrene doped with BN and Au nanoparticles: (a) Real part of refractive index $n$, and (b) imaginary part of refractive index $\kappa$, for PS and PS doped with 30% BN or Au nanoparticles.

$\kappa$ plots shown in Figs. 2.3(a) and 2.3(b), multiple peaks between 0.35 $\mu$m to 8 $\mu$m cannot be explained using the refractive index characteristics. While change in refractive index is seen around 500 nm which corresponds to surface plasmon resonance of Au, one may expect a peak around 500 nm. Multiple peaks are observed instead. Figures 2.2(c) and 2.2(d) show emission spectra of polystyrene thin film doped with BN nanoparticles and Au nanoparticles respectively. The dielectric function of PS is in the form of [36]

$$\varepsilon(\omega) = 1 + \sum_{i=1}^{i=4} \frac{f_i}{(w_i^2 - \omega^2 - jg_i\omega)} \qquad (2.11)$$

where the parameters $f_i$, $w_i$, and $g_i$ are, in the units of eV, given by $f_i = [14.6, 96.9, 44.4, 136.9]$, $w_i = [6.35, 14.0, 11.0, 20.1]$ and $g_i = [0.65, 5.0, 3.5, 11.5]$, respectively. In case of BN, appearance of new peaks is quite similar to that in Fig. 2.2(a) and its relation with the refractive indices shown in Figs. 2.4(a) and 2.4(b) is obvious. Appearance of emission peaks at the locations of $\lambda_\kappa^{mixture}$ and

28

$\lambda_n^{mixture}$ is evident. However, when polystyrene film is doped with Au nanoparticles we once again see multiple peaks produced in the region 0.35 $\mu$m to 6 $\mu$m which are not related to the refractive index characteristics. Since polystyrene does not support either of SPhPs or SPPs, interaction between SPPs of Au and surface polariton of the host are not responsible for the multiple peaks. We hypothesize that the origin of multiple peaks is due to interaction of SPPs of Au and the boundaries of the thin film. In case of SiC film doped with Au nanoparticles the shift in the peak of $\approx$ 13 $\mu$m is due to interaction between SPPs of Au and SPhPs of SiC, in either cases (SiC and PS) the inclusion material does not produce new polaritons as seen in refractive index characteristics.

Figure 2.5 shows the effect of NPs size on the emission spectra. In Fig. 2.5(a), SiC film of 0.4 $\mu$m is doped with BN nanoparticles and volume fraction of BN NPs is kept constant at 10% and the radius is varied from 1 nm to 50 nm. The majority of emission spectrum shows no effect of BN particle size. However, effect of size is noticeable at wavelengths less than 1 $\mu$m. This is due to the fact that Mie scattering becomes important at shorter wavelengths giving rise to high peaks for larger particles. Figure 2.5(b) presents the calculation of emissivity for 0.4 $\mu$m thick polystyrene (PS) film doped with Au NPs. The volume fraction of NPs is fixed at 10% and particle size is changed from 1 nm to 50 nm. Unlike Fig. 2.5(a), Figure 2.5(b) shows a strong influence of particle size on the emissivity. While the spectrum in the visible region shows a negligible response to particle size, gold NPs greatly influence the near-infrared region between 1 $\mu$m to 4 $\mu$m. As the NP size is increased from 1 nm the emissivity peaks reduce in magnitude, showing smaller peaks for 10 nm and 25 nm. Emissivity for larger particles of 50 nm however is increased again and is comparable to that of NPs of 1 nm. This is due to the presence of two counteracting phenomena here. First is the change
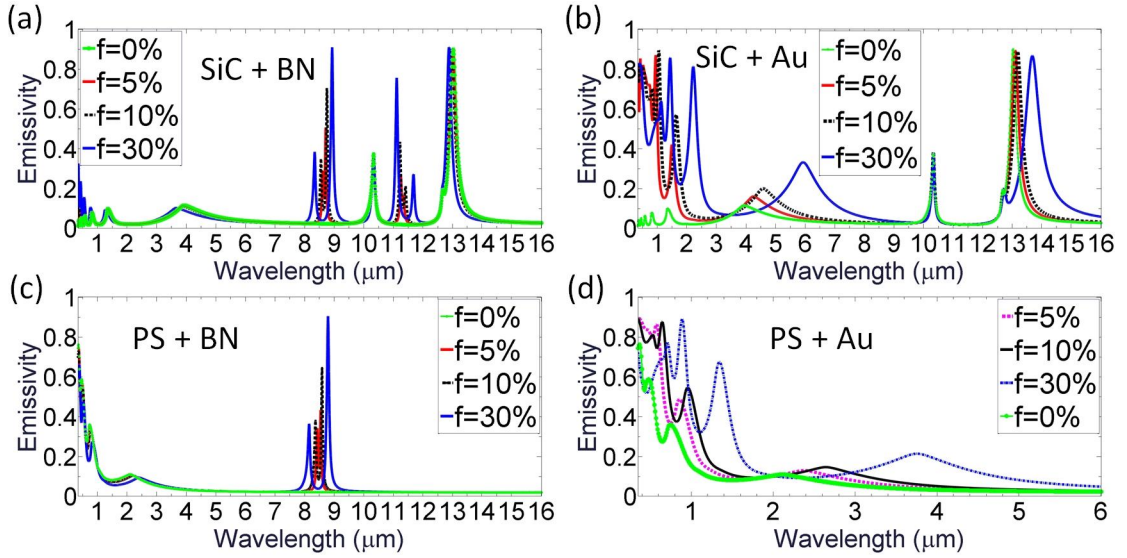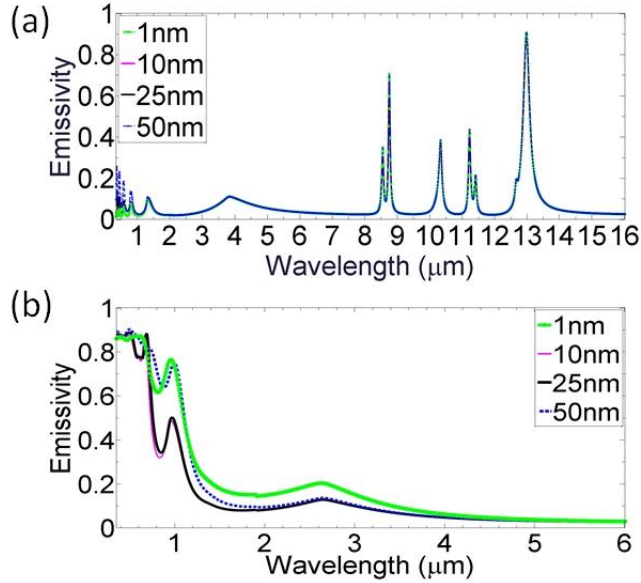
Figure 2.5: Hemispherical emissivity spectra for SiC or polystyrene (PS) thin film of thickness 0.4 $\mu$m mixed with BN and Au nanoparticles of volume fraction 10% and different radii (a) SiC film doped with BN nanoparticles and (b) Polystyrene thin film embedded with Au nanoparticles.

in dielectric function of Au NPs leading to decreased emissivity of larger particles and the second being Mie scattering of EM waves in the host causing an increase emissivity of larger particles.

Next, we present the effect of the doped nanoparticles on radiative heat transfer. We analyse radiative heat transfer between two identical multilayered structures at 300 K and 301 K as shown in Fig. 2.1(b). Each structure has a top layer of 0.4 $\mu$m deposited on 1 $\mu$m of Au. The top layer is doped with nanoparticles of 25 nm and different volume fractions. Figure 2.6 shows radiative heat flux vs distance between the structures and the normalized spectral density (defined as the ratio of $dq/d\omega$ to the maximum value over the range of wavelengths considered) at a distance of 100 nm is shown in the inset figures. Consider a structure with SiC layer doped with BN nanoparticles. Figure 2.6(a) shows very little change in overall heat transfer. While thin film of pure SiC shows nearly monochromatic heat transfer, selectivity is seen at additional bands of wavelength. These locations are wavelengths where
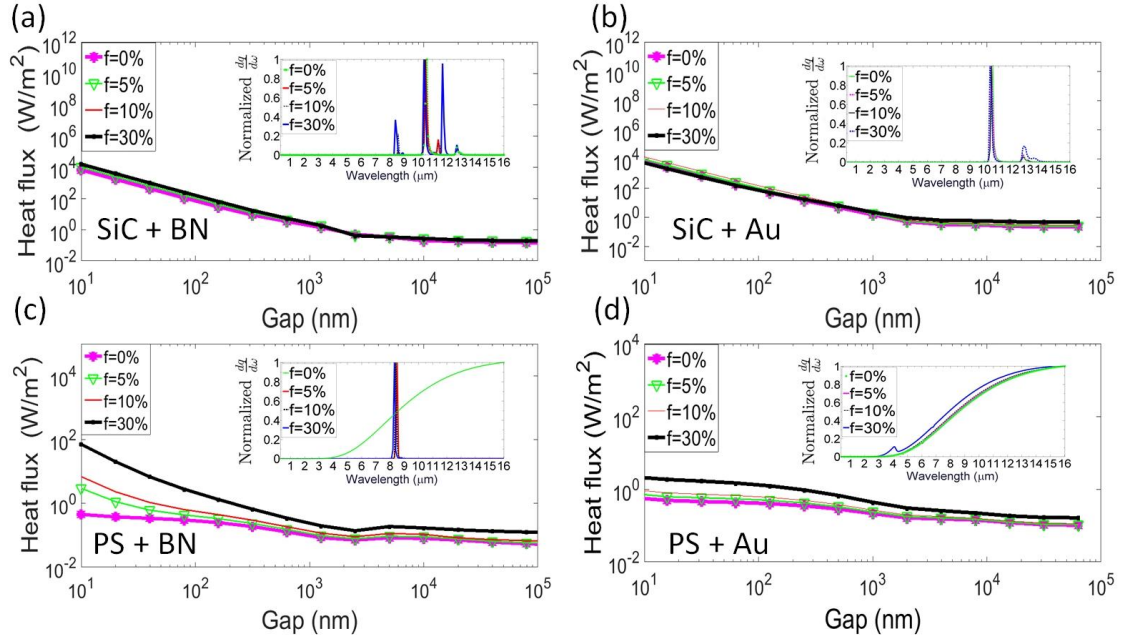
Figure 2.6: Near-field radiative heat flux between multilayered structures at 300 K and 301 K mixed with nanoparticles of radius 25 nm for different volume fractions, and the normalized spectral heat flux is displayed in the inset for the same configuration at a distance of 100 nm- each half space has nanoparticle-embedded thin layer of 0.4 $\mu$m on the top deposited on Au layer of 1 $\mu$m placed on substrate. Volume fraction of nanoparticles is varied. (a) SiC film doped with BN nanoparticles (b) SiC film doped with Au nanoparticles (c) polystyrene (PS) film mixed with BN nanoparticles and (d) PS film mixed with Au nanoparticles.

the effective refractive index of the mixture becomes zero (Figs. 2.3(a) and 2.3(b)). While the locations of the new peaks depends on the volume fraction, the peak corresponding to the host material is relatively unchanged. In Fig. 2.6(b), SiC film is doped with Au nanoparticles of radius 25 nm with different volume fractions. The change in total heat transfer characteristics is not significant with the addition of nanoparticles. Selectivity is observed near $\lambda = \lambda_1 \approx 10.33$ $\mu$m as in Mulet et al. [10], which is one of characteristic wavelengths of SiC. Moreover, the inclusion of Au nanoparticles has only a small impact on the selectivity in the near-field limit and this can be related to the refractive indices of the mixture (Figs. 2.3(a) and 2.3(b)). When the top layer is polystyrene doped with BN nanoparticles

(Fig. 2.6(c)), near-field heat flux is clearly dependent on volume fraction of the inclusion both in the near-field and far-field regime. Since polystyrene does not support SPPs/SPhPs, inclusion of BN clearly makes significant enhancement in heat transfer. The surface becomes selective at the wavelengths at which the real part of the effective refractive index becomes zero. When the PS film is doped with Au nanoparticles instead, the radiative heat transfer in Fig. 2.6(d), shows an increment with an increase in NPs volume fraction, both in the near-field as well as far-field limit. However, the normalized spectral density does not show any selectivity in the near-field. In summary, the wavelength selectivity of thin films in the near-field can be related to its effective refractive index in all four cases. This is logical as the selectivity is due to the presence of SPPs/SPhPs across the interfaces. It is interesting to note that, unlike in far-field regime, the selectivity is affected only when BN particles are used as inclusions. Addition of Au particles shows little or no impact on the selectivity in the near-field. This supports the idea that metallic nanoparticles do not induce new SPPs/SPhPs in the surfaces while dielectric nanoparticles such as BN produce new SPhP in the material.

## 2.4 Conclusion

We have demonstrated that nanoparticles influence the emission spectra of the multilayered structures. Wavelength selectivity can be altered and controlled by size and/or volume fraction of the NPs. Presence of NPs in a host material gives rise to an appearance of new emission peaks and a shift in the existing peaks in the emission spectra. When the metallic NPs are used, the effect of size is stronger as dielectric function of metallic NPs has a strong dependence of particle size due to electron scattering. We have also shown that volume fraction of the nanoparticles plays an important role in the near-field radiative heat transfer. If the NPs support SPhP, wavelength selectivity of thin films in the far field is at the

locations where the real part of effective refractive index of the mixture becomes zero or the imaginary part of refractive index is small while real part of the index is large. If the material of inclusion supports SPPs, as in metallic nanoparticles multiple emission peaks are seen which cannot related to $n$ and $\kappa$ values of the mixtures. (Our observation is limited to the case where the host material is thin-film.)

In the near-field, for NPs supporting SPhPs or SPPs the heat transfer is nearly monochromatic around the wavelength at which $n$ for the mixture becomes zero. It is observed that only SPhP supporting inclusions can influence the location of $\lambda_n$ of the mixture, hence wavelength selectivity of thin films in near-field has little or no effect due to the presence of metallic nanoparticles. This can be understood as the presence of NPs in the thin film does not induce new kind of SPPs/SPhPs resonance across the interfaces. This work broadens the range of designs and methods for wavelength selective emitters in both the far-field and near-field regime.

**List of References**

[1] S. Basu, Y. Chen, and Z. Zhang, "Microscale radiation in thermophotovoltaic devices-a review," *International Journal of Energy Research*, vol. 31, no. 6, pp. 689–716, 2007.

[2] C. McDonagh, C. S. Burke, and B. D. MacCraith, "Optical chemical sensors," *Chemical reviews*, vol. 108, no. 2, pp. 400–422, 2008.

[3] M. Pralle, N. Moelders, M. McNeal, I. Puscasu, A. Greenwald, J. Daly, E. Johnson, T. George, D. Choi, I. El-Kady, *et al.*, "Photonic crystal enhanced narrow-band infrared emitters," *Applied Physics Letters*, vol. 81, no. 25, pp. 4685–4687, 2002.

[4] B. Guha, C. Otey, C. B. Poitras, S. Fan, and M. Lipson, "Near-Field radiative cooling of nanostructures," *Nano letters*, vol. 12, no. 9, pp. 4546–4550, 2012.

[5] A. Narayanaswamy and G. Chen, "Thermal emission control with one-dimensional metallodielectric photonic crystals," *Physical Review B*, vol. 70, no. 12, p. 125101, 2004.

[6] A. Narayanaswamy, J. Mayo, and C. Canetta, "Infrared selective emitters with thin films of polar materials," *Applied Physics Letters*, vol. 104, no. 18, p. 183107, 2014.

[7] Y. Zheng and A. Narayanaswamy, "Patch contribution to near-field radiative energy transfer and van der Waals pressure between two half-spaces," *Physical Review A*, vol. 89, no. 2, p. 022512, 2014.

[8] H. Sai, H. Yugami, Y. Akiyama, Y. Kanamori, and K. Hane, "Spectral control of thermal emission by periodic microstructured surfaces in the near-infrared region," *JOSA A*, vol. 18, no. 7, pp. 1471–1476, 2001.

[9] P. Bermel, M. Ghebrebrhan, M. Harradon, Y. X. Yeng, I. Celanovic, J. D. Joannopoulos, and M. Soljacic, "Tailoring photonic metamaterial resonances for thermal radiation," *Nanoscale research letters*, vol. 6, no. 1, pp. 1–5, 2011.

[10] J.-P. Mulet, K. Joulain, R. Carminati, and J.-J. Greffet, "Enhanced radiative heat transfer at nanometric distances," *Microscale Thermophysical Engineering*, vol. 6, no. 3, pp. 209–222, 2002.

[11] Y. Zheng and A. Ghanekar, "Radiative energy and momentum transfer for various spherical shapes: A single sphere, a bubble, a spherical shell, and a coated sphere," *Journal of Applied Physics*, vol. 117, no. 6, p. 064314, 2015.

[12] M. Francoeur, S. Basu, and S. J. Petersen, "Electric and magnetic surface polariton mediated near-field radiative heat transfer between metamaterials made of silicon carbide particles," *Optics express*, vol. 19, no. 20, pp. 18 774–18 788, 2011.

[13] S. J. Petersen, S. Basu, B. Raeymaekers, and M. Francoeur, "Tuning near-field thermal radiative properties by quantifying sensitivity of mie resonance-based metamaterial design parameters," *Journal of Quantitative Spectroscopy and Radiative Transfer*, vol. 129, pp. 277–286, 2013.

[14] H. Gonome, M. Baneshi, J. Okajima, A. Komiya, N. Yamada, and S. Maruyama, "Control of thermal barrier performance by optimized nanoparticle size and experimental evaluation using a solar simulator," *Journal of Quantitative Spectroscopy and Radiative Transfer*, vol. 149, pp. 81–89, 2014.

[15] H. Gonome, M. Baneshi, J. Okajima, A. Komiya, and S. Maruyama, "Controlling the radiative properties of cool black-color coatings pigmented with cuo submicron particles," *Journal of Quantitative Spectroscopy and Radiative Transfer*, vol. 132, pp. 90–98, 2014.

[16] J. M. Garnett, "Colours in metal glasses, in metallic films, and in metallic solutions. ii," *Philosophical Transactions of the Royal Society of London. Series A, Containing Papers of a Mathematical or Physical Character*, pp. 237–288, 1906.

[17] W. T. Doyle, "Optical properties of a suspension of metal spheres," *Physical review B*, vol. 39, no. 14, p. 9852, 1989.

[18] C.-H. Wang, W.-Y. Shen, P.-S. Sheng, C.-Y. Lee, and H.-T. Chiu, "Deposition of mesoporous silicon carbide thin films from (me3si) 4sn: tin nanoparticles as in situ generated templates," *Chemistry of Materials*, vol. 19, no. 22, pp. 5250–5255, 2007.

[19] H. Wei and H. Eilers, "Electrical conductivity of thin-film composites containing silver nanoparticles embedded in a dielectric fluoropolymer matrix," *Thin Solid Films*, vol. 517, no. 2, pp. 575–581, 2008.

[20] W. C. Chew, *Waves and fields in inhomogeneous media.* IEEE press, 1995.

[21] M. Moharam, D. A. Pommet, E. B. Grann, and T. Gaylord, "Stable implementation of the rigorous coupled-wave analysis for surface-relief gratings: enhanced transmittance matrix approach," *JOSA A*, vol. 12, no. 5, pp. 1077–1086, 1995.

[22] M. Planck, *The theory of heat radiation.* Dover Publications, 2011.

[23] A. Narayanaswamy and Y. Zheng, "A Green's function formalism of energy and momentum transfer in fluctuational electrodynamics," *Journal of Quantitative Spectroscopy and Radiative Transfer*, vol. 132, pp. 12–21, 2014.

[24] V. Myroshnychenko, J. Rodríguez-Fernández, I. Pastoriza-Santos, A. M. Funston, C. Novo, P. Mulvaney, L. M. Liz-Marzán, and F. J. G. de Abajo, "Modelling the optical response of gold nanoparticles," *Chemical Society Reviews*, vol. 37, no. 9, pp. 1792–1805, 2008.

[25] U. Kreibig and M. Vollmer, *Optical properties of metal clusters.* Springer Berlin, 1995, vol. 25.

[26] M. S. Wheeler, "A scattering-based approach to the design, analysis, and experimental verification of magnetic metamaterials made from dielectrics," Ph.D. dissertation, 2010.

[27] X. Liu, T. Bright, and Z. Zhang, "Application conditions of effective medium theory in near-field radiative heat transfer between multilayered metamaterials," *Journal of Heat Transfer*, vol. 136, no. 9, p. 092703, 2014.

[28] B. Liu and S. Shen, "Broadband near-field radiative thermal emitter/absorber based on hyperbolic metamaterials: Direct numerical simulation by the wiener chaos expansion method," *Physical Review B*, vol. 87, no. 11, p. 115403, 2013.

[29] E. D. Palik, *Handbook of optical constants of solids*. Academic press, 1998, vol. 3.

[30] B. Neuner III, D. Korobkin, C. Fietz, D. Carole, G. Ferro, and G. Shvets, "Midinfrared Index Sensing of pL-Scale Analytes Based on Surface Phonon Polaritons in Silicon Carbide," *The Journal of Physical Chemistry C*, vol. 114, no. 16, pp. 7489–7491, 2010.

[31] P. B. Johnson and R.-W. Christy, "Optical constants of the noble metals," *Physical Review B*, vol. 6, no. 12, p. 4370, 1972.

[32] V. C. Nguyen, L. Chen, and K. Halterman, "Total transmission and total reflection by zero index metamaterials with defects," *Physical review letters*, vol. 105, no. 23, p. 233908, 2010.

[33] Y. He and T. Zeng, "First-principles study and model of dielectric functions of silver nanoparticles," *The Journal of Physical Chemistry C*, vol. 114, no. 42, pp. 18 023–18 030, 2010.

[34] K. L. Kelly, E. Coronado, L. L. Zhao, and G. C. Schatz, "The optical properties of metal nanoparticles: the influence of size, shape, and dielectric environment," *The Journal of Physical Chemistry B*, vol. 107, no. 3, pp. 668–677, 2003.

[35] H. Hövel, S. Fritz, A. Hilger, U. Kreibig, and M. Vollmer, "Width of cluster plasmon resonances: bulk dielectric functions and chemical interface damping," *Physical Review B*, vol. 48, no. 24, p. 18178, 1993.

[36] V. A. Parsegian, *Van der Waals forces: a handbook for biologists, chemists, engineers, and physicists*. Cambridge University Press, 2006.

# MANUSCRIPT 3

# A Novel and Efficient Mie-metamaterial Thermal Emitter for Thermophotovoltaic Systems

by

Alok Ghanekar,[1] Laura Lin,[1,2] and Yi Zheng[1]

[1]Department of Mechanical, Industrial and Systems Engineering, University of Rhode Island,

Kingston, RI 02881, USA

[2]Department of Mechanical Engineering, Technische Universität Braunschweig, 38106

Braunschweig, Germany

Corresponding Author: Yi Zheng

Department of Mechanical, Industrial and Systems Engineering

University of Rhode Island

Kingston, RI 02881, USA

Phone: +1 401-874-5184

Email Address: zheng@uri.edu

**Abstract**

We theoretically demonstrate a novel, efficient and cost effective thermal emitter using a Mie-resonance metamaterial for thermophotovoltaic (TPV) applications. We propose for the first time the design of a thermal emitter which is based on nanoparticle-embedded thin film. The emitter consists of a thin film of $SiO_2$ on the top of tungsten layer deposited on a substrate. The thin film is embedded with tungsten nanoparticles which alter the refractive index of the film. This gives rise to desired emissive properties in the wavelength range of 0.4 $\mu$m to 2 $\mu$m suitable for GaSb and InGaAs based photovoltaics. Effective dielectric properties are calculated using Maxwell-Garnett-Mie theory. Our calculations indicate this would significantly improve the efficiency of TPV cells. We introduce a new parameter to gauge the efficacy of thermal emitters and use it to compare different designs.

## 3.1    Introduction

Thermophotovoltaics (TPV) is a promising technology for heat recovery and an attractive alternative for existing electricity generation technologies [1, 2, 3]. A TPV system consists of a thermal emitter which operates at high temperatures (∼1500 K) [4, 5] and a photovoltaic cell and can directly convert thermal energy into electricity [6]. In principle, TPV systems can achieve an efficiency of Carnot engine for monochromatic radiation [7] and such TPV systems with efficiencies approaching the limit have been discussed in the literature [8, 9, 10]. In reality, efficiencies of TPV systems suffer from the mismatch between emission spectrum of emitter and absorption spectrum of PV cell [11]. External quantum efficiency (EQE) of a PV cell is defined as the fraction of incident photons converted into electron-hole pairs [12] and is indicative of the amount of current generated for a given incident photon wavelength. A PV cell has non-zero EQE above the band-gap, i.e. a PV cell can generate electric current only when incident photons
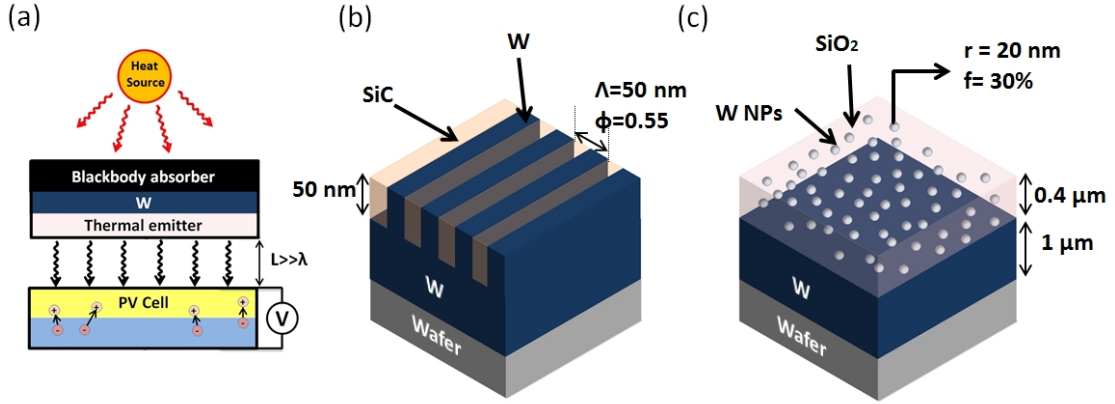
Figure 3.1: (a) Schematic of a typical TPV system with a thermal emitter/absorber and a PV cell. (b) An example of a thermal emitter based on 1-D grating structure of SiC and W on the top of W base. The grating thickness and period $\Lambda$=50 nm, filling ratio $\phi$=0.55. (c) A proposed design of thermal emitter consists of 0.4 $\mu$m thick $SiO_2$ layer on the top of 1 $\mu$m thick W layer deposited on the substrate. $SiO_2$ layer is doped with W nanoparticles of 20 nm radius with a volume fraction of 30%.

have higher energies than the bandgap of semiconductor material [13]. Moreover, absorption of incident photons having wavelength longer than bandgap wavelength is undesirable as it causes thermal leakage and reduces the efficiency [14]. So, in order to achieve high efficiency of a TPV system, goal is to develop a thermal emitter with high emissivity in the region of high external quantum efficiency (EQE) of PV cell and low emissivity in rest of the spectrum. Several studies have focused on using photonics crystals [15, 16], plasmonic metamaterials [17], single micro/nano sized spheres [18], doped materials [19, 20], surface gratings in order to obtain spectrally selective emission [21]. 1-D, 2-D and 3-D photonic crystals and surface gratings have also been developed [22, 23, 24]. Numerous works involve use of intermediate filters which reflect the low energy photons back to emitter [25, 26, 27, 28].

Metamaterials is another class of nanomaterials/nanostructures which has been the topic of many articles focused on selective thermal emitters. Liu et al [29] have

demonstrated a narrow-band mid infrared thermal emitter based on a metamaterial. Plasmonic metamaterials have also been explored for solar TPV applications as in [30, 31]. Woolf et al [32] have presented and also experimentally demonstrated a heterogeneous metasurface for selective emitters and predicted 22% conversion efficiency for InGaAs based TPV system at the operating temperature of 1300 K for the emitter. Use of refractory materials such as tungsten is common in the literature. These studies and several others [33, 34, 35, 36, 37, 38], although not specifically focused on TPV applications, involve complex surface patterns which are difficult to fabricate. In this paper, we propose for the first time the use of Mie-metamaterial thin films, i.e., nanoparticle-embedded thin films to design a novel, efficient and low cost thermal emitter suitable for GaSb and InGaAs based TPVs. Mie-metamaterials or Mie-resonance metamaterials are artificial materials which utilize Mie resonances of inclusions for the shaping of emission spectra. Several theoretical studies of nanoparticle inclusions into host materials have been performed [39, 40, 41]. However, literature pertaining to optical and emissive properties of nanoparticle embedded thin films is rare. Authors recently published a broad study on the role of polar and metallic nanoparticles on far-field and near-field thermal radiation from thin films by considering different cases of hypothetical Mie-metamaterial thin films [42]. In present study we exploit the idea by using thin films of $SiO_2$ embedded with tungsten (W) nanoparticles to design a novel thermal emitter specifically for GaSb and InGaAs based TPVs.

Schematic of a typical TPV system is shown in Fig. 6.1(a). Thermal radiation from the heat source is absorbed by the blackbody absorber. This heat is emitted by the selective thermal emitter only in the desired band of wavelengths in which the external quantum efficiency of the PV cell is high. Figure 6.1(b) depicts an example of 1-D grating structure that could be used to realize wavelength selective

radiative properties of thermal emitter. It comprises gratings of SiC and W of period $\Lambda = 50$ nm and filling ratio $\phi = 0.55$. Grating layer is 50 nm thick. It's emissive properties along with the emittance of 2-D grating structure considered in Zhao et al [13] will be compared to the Mie-metamaterial based thermal emitter of present study. The prime focus of this paper is the proposed design of thermal emitter shown in Fig. 6.1(c). It consists of a 0.4 $\mu$m thick film of $SiO_2$ on the top of 1 $\mu$m thick film of tungsten deposited on a substrate. Thickness of the layer of W makes sure that all the radiation from the substrate is reflected back and the radiative properties of the emitter are dictated by the top two layers alone. The $SiO_2$ film is doped with W nanoparticles of 20 nm radius. Inclusion of W nanoparticles changes the optical properties of the film and results in desired emission spectrum. Volume fraction of W nanoparticles was adjusted to 30% to achieve the best result. While the mixture of $SiO_2$ and W gives rise to spectrally selective emission for the PV, the choice of materials also makes sure that it will withstand high temperatures.

## 3.2 Theoretical Fundamentals

The hemispherical emissivity of the thermal emitter can be expressed as [42]

$$e(\omega) = \frac{c^2}{\omega^2} \int_0^{\omega/c} dk_\rho k_\rho \sum_{\mu=s,p} (1 - |\widetilde{R}_h^{(\mu)}|^2 - |\widetilde{T}_h^{(\mu)}|^2) \qquad (3.1)$$

where c is the speed of light in vacuum, $\omega$ is the angular frequency and $k_\rho$ is the magnitude of inplane wave vector. $\widetilde{R}_h^{(\mu)}$ and $\widetilde{T}_h^{(\mu)}$ are the polarization dependent effective reflection and transmission coefficients which can be calculated using the recursive relations of Fresnel coefficients of each interface [43]. The dielectric functions can be related to real ($n$) and imaginary ($\kappa$) parts of refractive index as $\sqrt{\varepsilon} = n + j\kappa$. Dielectric functions of the materials ($SiO_2$, W and SiC) considered in this paper are taken from literature [44, 45, 46]. Having very low temperature

coeffcients, room temperature values of dielectric function are used for $SiO_2$ and SiC [47, 48]. Dielectric properties of tungsten were also assumed to be unchaged as the operating temeprature is much less than the melting point. The top layer of the thermal emitter considered in our calculations is either 1-D grating structure or nanoparticle embedded thin-film. In both cases, it can be approximated as a homogeneous layer of an effective dielectric function.

If the period of grating ($\Lambda$) is much smaller than the wavelength of interest such as the case considered here, dielectric function of the grating layer can be approximated using effective medium theory [49]. We use second order effective medium approximation to calculate the effective dielectric function which is given by [49]

$$\varepsilon_{TE,2} = \varepsilon_{TE,0}\left[1 + \frac{\pi^2}{3}\left(\frac{\Lambda}{\lambda}\right)^2 \phi^2(1-\phi)^2 \frac{(\varepsilon_A - \varepsilon_B)^2}{\varepsilon_{TE,0}}\right] \tag{3.2a}$$

$$\varepsilon_{TM2} = \varepsilon_{TM0}\left[1 + \frac{\pi^2}{3}\left(\frac{\Lambda}{\lambda}\right)^2 \phi^2(1-\phi)^2(\varepsilon_A - \varepsilon_B)^2 \varepsilon_{TE,0}\left(\frac{\varepsilon_{TM0}}{\varepsilon_A \varepsilon_B}\right)^2\right] \tag{3.2b}$$

where $\varepsilon_A$ and $\varepsilon_B$ are the dielectric functions of the two materials in surface gratings, $\Lambda$ is the period and $\phi$ is the filling ratio. The expressions for zeroth order effective dielectric functions $\varepsilon_{TE,0}$ and $\varepsilon_{TM,0}$ are given by

$$\varepsilon_{TE,0} = \phi\varepsilon_A + (1-\phi)\varepsilon_B \tag{3.3a}$$

$$\varepsilon_{TM0} = \left(\frac{\phi}{\varepsilon_A} + \frac{1-\phi}{\varepsilon_B}\right)^{-1} \tag{3.3b}$$

For calculating the effective dielectric function the Mie-metamaterial, we use Clausius-Mossotti equation. [50, 51].

$$\varepsilon_{eff} = \varepsilon_m\left(\frac{r^3 + 2\alpha_r f}{r^3 - \alpha_r f}\right) \tag{3.4}$$

where $\varepsilon_m$ is the dielectric function of the matrix, $\alpha_r$ is the electric dipole polarizability, $r$ and $f$ are the radius and volume fraction of nanoparticles respectively. To consider the size effects of nanoparticle inclusions, we use the Maxwell Garnett

formula which employs the expression for electric dipole polarizability using Mie theory [52], $\alpha_r = 3jc^3 a_{1,r}/2\omega^3 \varepsilon_m^{3/2}$, where $a_{1,r}$ is the first electric Mie coefficient given by

$$a_{1,r} = \frac{\sqrt{\varepsilon_{np}}\psi_1(x_{np})\psi_1'(x_m) - \sqrt{\varepsilon_m}\psi_1(x_m)\psi_1'(x_{np})}{\sqrt{\varepsilon_{np}}\psi_1(x_{np})\xi_1'(x_m) - \sqrt{\varepsilon_m}\xi_1(x_m)\psi_1'(x_{np})} \qquad (3.5)$$

where $\psi_1$ and $\xi_1$ are Riccati-Bessel functions of the first order given by $\psi_1(x) = xj_1(x)$ and $\xi_1(x) = xh_1^{(1)}(x)$ where $j_1$ and $h_1^{(1)}$ are first order spherical Bessel functions and spherical Hankel functions of the first kind, respectively. Here, '' indicates the first derivative. $x_m = \omega r \sqrt{\varepsilon_m}/c$ and $x_{np} = \omega r \sqrt{\varepsilon_{np}}/c$ are the size parameters of the matrix and the nanoparticles, respectively; $\varepsilon_{np}$ being the dielectric function of nanoparticles.

It is worth mentioning that Maxwell-Garnett-Mie theory is applicable when average distance between inclusions is much smaller than the wavelength of interest [53]. This criteria is satisfied in the calculated presented. Also noteworthy is the fact that nanoparticle diameter (40 nm) is much smaller than the thickness of the thin film (0.4 $\mu$m) considered. Thus, effective medium theory holds true for the calculations presented in this study.

## 3.3    Results

Figure 6.2(a) illustrates the effect of W nanoparticle inclusions on the refractive indices of $SiO_2$ host. Pure $SiO_2$ has a near constant refractive index (n) $\sim 1.55$ and a negligible extinction coefficient ($\kappa$). Nano-sized W spheres ($2r = 40$ nm) much smaller than the operating wavelength are introduced into the $SiO_2$ matrix. This brings about an increased refractive index and extinction coefficient. Although real and imaginary parts of the refractive index have different implications, it is imperative that real and imaginary parts of the mixture depend on both the indices of its constituents. It is essential to point out that change in refractive indices of the mixture is a result of addition of new material as well as the Mie-scattering of
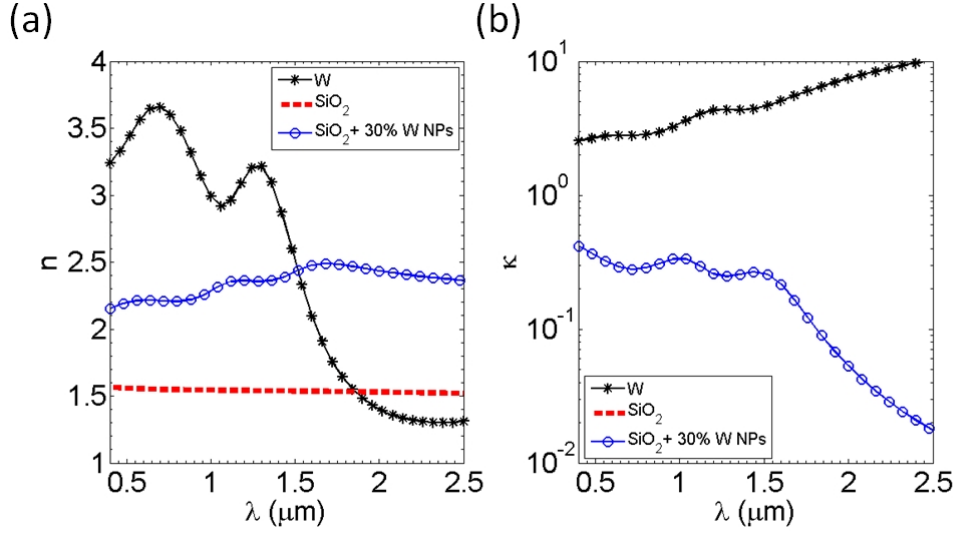
Figure 3.2: Refractive indices of W, $SiO_2$ and $SiO_2$ doped with W nanoparticles of volume fraction 30% and 20 nm radius. (a) Real part of refractive index. (b) Imaginary part of refractive index. Imaginary part of refractive index for $SiO_2$ is negligible for the range of wavelengths considered here [46].

electromagnetic waves by spherical nanoparticles. Consequently, refractive indices of the mixture depend on volume fraction and particle size. The resulting changes in the emission spectrum are displayed in Fig. 6.3(a). Owing to its metallic nature, W is moderately absorptive only at lower wavelengths and highly reflective beyond 2 $\mu$m. Although $SiO_2$ bulk has a high absorptivity/emissivity, 0.4 $\mu$m thick layer of $SiO_2$ is practically transparent for the entire spectrum. Therefore, both the bare tungsten and the combination of $SiO_2$ layer on tungsten base have low emissivity in the range of 0.4 to 2 $\mu$m and negligible emissivity for the majority of spectrum beyond 2 $\mu$m. Upon inclusion of W nanoparticles, emissivity is enhanced for spectral region of interest. The geometric parameters available for spectral shaping of the emissivity are thickness of $SiO_2$ film, volume fraction of W nanoparticles and particle radius. If size distribution of nanoparticles is available, it can be incorporated into the extended Maxwell-Garnett formula as in [55]. For the present study, the particle radius is fixed to 20 nm. Figure 6.3(a) also highlights the effect
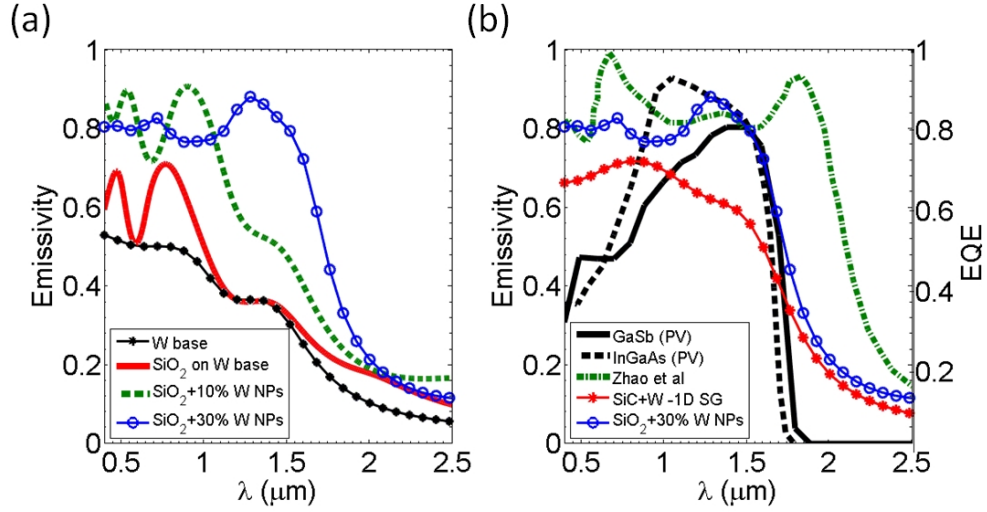
Figure 3.3: Emission spectra of different configurations. (a) Hemispherical emissivity of W, SiO$_2$ film of 0.4 $\mu$m deposited on W base and SiO$_2$ doped with W nanoparticles of 20 nm radius and different volume fractions. (b) Emission spectrum (left y-axis) of the final design is compared to the result presented by Zhao et al [13] and 1-D surface grating discussed in this study. The EQE plots (right y-axis) of PV cells are shown for comparison [54].

of volume fraction of W nanoparticles on emission spectra. An increase in volume fraction from 10% to 30% results in higher emissivity and the broadening of the emission spectrum. The final proposed configuration has the SiO$_2$ film thickness of 0.4 $\mu$m and 30% volume fraction of W nanoparticles. Note that calculated emissivity of W (black curve in Fig. 6.3(a)) matches well with high-temperature (1600 K) emissivivty reported in [56]. Also refractive index of SiO$_2$ has a low temeprature coefficient [57]. Therefore these materials are well suited for high temeprature applications.

The thermal emitter presented here is suitable for a typical TPV system consisting GaSb or InGaAs based photovoltaics. The EQE of the two PV cells is shown in Fig. 6.3(b). Both the GaSb and InGaAs based PV cells efficiently generate electricity if the wavelength of incident photons falls in the range of 0.4 $\mu$m to 2 $\mu$m. Configuration of the proposed design i.e. thickness of the SiO$_2$ layer,

radius and volume fraction of W nanoparticles was chosen to achieve best match between the emission spectrum and the EQE curve of the PV cells. Our design exhibits high emissivity ($>$ 0.8) in the wavelength range 0.4 $\mu$m to 1.7 $\mu$m and very low emissivity ($<$ 0.2) beyond 2 $\mu$m. The close match between the emission spectrum of the emitter and EQE curve PV cell ensures high conversion efficiency and minimizes the thermal leakage of long wavelength photons. For comparison, the emission spectrum of 1-D structure (Fig. 6.1(b)) and that of a 2-D grating structure discussed in Zhao et al [13] is also shown. It is apparent that the emission spectrum of the design presented here is comparable to that of 1-D structure and the 2-D structure presented in [13] for wavelengths below 1.7 $\mu$m. Although a substantial part of blackbody radiation at high temepraturs (1000 to 1500 K) exists between 2 to 6 $\mu$m, very little energy is emitted by proposed emitter in this region as emissivty is very low. Moreover, the proposed design has lower emissivity beyond 1.7 $\mu$m when compared to the 2-D design. This indicates much lower losses due to thermal leakage. It is worth mentioning that, while choice of materials in the present study is same as that used in [13], fabrication of thermal emitter based on tungsten embedded $SiO_2$ thin film is relatively simple. This guarantees low cost of large scale fabrication of such emitters. As refractory materials such as platinum and aluminum oxide ($Al_2O_3$) have been tested before for thermal emitter [32], they can also be explored for this new class of emitters.

## 3.4 Discussion

While the match between emission spectrum of the emitter and the EQE curve of the PV cell can be a good indicator of TPV system's performance, the emitter temperature has an equally important role as it decides the dominant wavelength and can dictate the overall efficiency. Therefore, discussion of conversion efficiency cannot be left out in this work. Ideal emitter has an $e(\omega) = 1$ above bandgap and

$e(\omega) = 0$ below the bandgap. The conversion efficiency of the TPV system could be defined as the ratio of the power output of the PV cell to the power incident on the PV cell given by

$$\eta = \frac{P_{out}}{P_{rad}} \tag{3.6}$$

where $P_{rad}$ is the power radiated by the emitter [58]

$$P_{rad} = \int_0^\infty \frac{\omega^2}{4\pi^2 c^2} \frac{\hbar\omega}{\left(e^{\hbar\omega/k_B T} - 1\right)} e(\omega) d\omega \tag{3.7}$$

The power output, $P_{out}$ is proportional to the number density of the photons above bandgap and the EQE of PV cell defined as [32]

$$P_{out} = qV_{OC}FF \int_0^\infty \overline{n}(\omega, T) e(\omega) \eta_{EQE}(\omega) d\omega \tag{3.8}$$

where $q$, $V_{OC}$, $FF$ and $\eta_{EQE}$ are electronic charge, open circuit voltage, fill factor and EQE of PV cell, respectively. $\overline{n}(\omega, T)$ is the number density of incident photons

$$\overline{n}(\omega, T) = \frac{\omega^2}{4\pi^2 c^2} \frac{1}{\left(e^{\hbar\omega/k_B T} - 1\right)} \tag{3.9}$$

Now consider a hypothetical TPV system with a thermal emitter which has no radiation below the bandgap but covers only a fraction of spectrum above bandgap with $e(\omega) = 1$. Such a system would have lower power output than the one with ideal thermal emitter despite having maximum efficiency with no losses. It is apparent that conversion efficiency of the TPV system alone cannot be regarded as a criterion to gauge the efficacy of a thermal emitter. Therefore we propose a new parameter to calculate the effectiveness of the thermal emitter for a given PV cell and emitter temperature. The parameter termed as effectiveness index is defined as the ratio of the efficiency of the TPV system to the efficiency of the TPV system with ideal thermal emitter at the same temperature and for the given PV cell, $\beta_{emitter} = \eta_{Real}/\eta_{Ideal}$, where subscripts *Real* and *Ideal* refer to TPV systems

47

with thermal emitter of consideration and an idealized thermal emitter at the same temperature. So,

$$\beta_{emitter} = \left(\frac{P_{out}}{P_{rad}}\right)_{Real} \times \left(\frac{P_{rad}}{P_{out}}\right)_{Ideal} \qquad (3.10)$$

While this norm, $\beta_{emitter}$ doesn't elaborate anything about the efficiency of the TPV system as a whole, it is a good measure to compare the effectiveness of different thermal emitters for a given PV cell and emitter temperature. Note that if $\beta_{emitter} > 1$, it implies that the TPV system is efficient but only a part of the spectrum of the EQE is being utilized and the output power is less than what an ideal emitter would produce. Therefore, the goal is to get $\beta_{emitter}$ close to 1 but not exceed 1. It is assumed that the emitter has a much higher temperature than the PV cell, which has a negligible reflection coefficient. While calculating effectiveness indices for different thermal emitters and a given PV cell, it is assumed that PV cell temeprature and its EQE do not vary.

We calculate the effectiveness of the thermal emitter for GaSb PV cell and at emitter temperature 1500 K for the designs presented in Fig. 6.3(b). Our proposed design has an effectiveness index $\beta_{emitter} = 0.72$ while its value for the 1-D design and the one considered in [13] is 0.78 and 0.65 respectively. It is important to note that despite having lower emissivity, the 1-D design has higher effectiveness index because it has lower emissivity beyond 2 $\mu$m, thermal wavelength at 1500 K being 1.93 $\mu$m. Structure discussed in [13] shows lower effectiveness index as it has higher emissivity below the bandgap. Effectiveness index of the aforementioned designs at 1300 K is $\beta_{emitter} = 0.6, 0.68$ and 0.58 respectively. As the thermal wavelength shifts to 2.3 $\mu$m, losses increase which clearly demonstrates the role of temperature and the dominant thermal wavelength governing the efficiency.

Thus, we have presented for the first time a thermal emitter which consists of Mie-metamaterial based thin film. Dielectric properties of SiO$_2$ thin films are

influenced by the inclusions of W nanoparticles. This manifests into the spectral shaping of thermal radiation from the surface of the emitter. The best possible emission spectrum is realized by adjusting the thickness of the film, radius and volume fraction of nanoparticles. The emission spectrum of the design matches well with the EQE of GaSb and InGaAs based PV cells that indicates high conversion efficiency. Emission spectrum of the present design is on par with previously proposed design based on 2-D grating structures. Very low emission for $\lambda > 2$ $\mu$m minimizes the leakage of long wavelength photons below the TPV band-gap. Materials chosen for the design ($SiO_2$ and W) are suitable from fabrication perspective and can withstand high operating temperatures of the TPV system. Moreover, fabrication of the proposed nanostructure is relatively simple as compared to surface gratings making it cost effective. Nanoparticle radius, volume fraction and film thickness offer a good tunability for tailoring of emission spectrum. We also explored a new parameter named as effectiveness index that can be used as a good indicator to compare efficacy of thermal emitter for a given PV cell and operating temperature. This study gives valuable insights into design opportunities for selective thermal emitters that can be applied for TPV systems.

## Acknowledgments

## List of References

[1] S. Basu, Y. Chen, and Z. Zhang, "Microscale radiation in thermophotovoltaic devices-a review," *International Journal of Energy Research*, vol. 31, no. 6,

pp. 689–716, 2007.

[2] M. Bosi, C. Ferrari, F. Melino, M. Pinelli, P. Spina, and M. Venturini, "Thermophotovoltaic generation: a state of the art review," *Proceedings ECOS*, 2012.

[3] T. Coutts, "A review of progress in thermophotovoltaic generation of electricity," *Renewable and Sustainable Energy Reviews*, vol. 3, no. 2, pp. 77–184, 1999.

[4] G. Colangelo, A. De Risi, and D. Laforgia, "Experimental study of a burner with high temperature heat recovery system for tpv applications," *Energy conversion and management*, vol. 47, no. 9, pp. 1192–1206, 2006.

[5] B. Wernsman, R. R. Siergiej, S. D. Link, R. G. Mahorter, M. N. Palmisiano, R. J. Wehrer, R. W. Schultz, G. P. Schmuck, R. L. Messham, S. Murray, *et al.*, "Greater than 20% radiant heat conversion efficiency of a thermophotovoltaic radiator/module system using reflective spectral control," *Electron Devices, IEEE Transactions on*, vol. 51, no. 3, pp. 512–515, 2004.

[6] D. C. White, B. D. Wedlock, and J. Blair, "Recent advances in thermal energy conversion," in *15th Annual Proceedings, Power Sources Conference*, 1961, pp. 125–132.

[7] J. K. Tong, W.-C. Hsu, Y. Huang, S. V. Boriskina, and G. Chen, "Thin-film'thermal well'emitters and absorbers for high-efficiency thermophotovoltaics," *arXiv preprint arXiv:1502.02061*, 2015.

[8] N.-P. Harder and P. Würfel, "Theoretical limits of thermophotovoltaic solar energy conversion," *Semiconductor Science and Technology*, vol. 18, no. 5, p. S151, 2003.

[9] E. Rephaeli and S. Fan, "Absorber and emitter for solar thermo-photovoltaic systems to achieve efficiency exceeding the shockley-queisser limit," *Optics express*, vol. 17, no. 17, pp. 15 145–15 159, 2009.

[10] P. Wurfel and W. Ruppel, "Upper limit of thermophotovoltaic solar-energy conversion," *Electron Devices, IEEE Transactions on*, vol. 27, no. 4, pp. 745–750, 1980.

[11] P. Bermel, M. Ghebrebrhan, W. Chan, Y. X. Yeng, M. Araghchini, R. Hamam, C. H. Marton, K. F. Jensen, M. Soljačić, J. D. Joannopoulos, *et al.*, "Design and global optimization of high-efficiency thermophotovoltaic systems," *Optics express*, vol. 18, no. 103, pp. A314–A334, 2010.

[12] W. R. Chan, P. Bermel, R. C. Pilawa-Podgurski, C. H. Marton, K. F. Jensen, J. J. Senkevich, J. D. Joannopoulos, M. Soljačić, and I. Celanovic,

"Toward high-energy-density, high-efficiency, and moderate-temperature chip-scale thermophotovoltaics," *Proceedings of the National Academy of Sciences*, vol. 110, no. 14, pp. 5309–5314, 2013.

[13] B. Zhao, L. Wang, Y. Shuai, and Z. M. Zhang, "Thermophotovoltaic emitters based on a two-dimensional grating/thin-film nanostructure," *International Journal of Heat and Mass Transfer*, vol. 67, pp. 637–645, 2013.

[14] L. Wang and Z. Zhang, "Wavelength-selective and diffuse emitter enhanced by magnetic polaritons for thermophotovoltaics," *Applied Physics Letters*, vol. 100, no. 6, p. 063902, 2012.

[15] P. Nagpal, S. E. Han, A. Stein, and D. J. Norris, "Efficient low-temperature thermophotovoltaic emitters from metallic photonic crystals," *Nano letters*, vol. 8, no. 10, pp. 3238–3243, 2008.

[16] K. A. Arpin, M. D. Losego, A. N. Cloud, H. Ning, J. Mallek, N. P. Sergeant, L. Zhu, Z. Yu, B. Kalanyan, G. N. Parsons, *et al.*, "Three-dimensional self-assembled photonic crystals with high temperature stability for thermal emission modification," *Nature communications*, vol. 4, 2013.

[17] M.-W. Tsai, T.-H. Chuang, C.-Y. Meng, Y.-T. Chang, and S.-C. Lee, "High performance midinfrared narrow-band plasmonic thermal emitter," *Applied physics letters*, vol. 89, no. 17, p. 173116, 2006.

[18] Y. Zheng and A. Ghanekar, "Radiative energy and momentum transfer for various spherical shapes: A single sphere, a bubble, a spherical shell, and a coated sphere," *Journal of Applied Physics*, vol. 117, no. 6, p. 064314, 2015.

[19] L. Ferguson and F. Dogan, "Spectral analysis of transition metal-doped mgo matched emitters for thermophotovoltaic energy conversion," *Journal of materials science*, vol. 37, no. 7, pp. 1301–1308, 2002.

[20] A. Licciulli, D. Diso, G. Torsello, S. Tundo, A. Maffezzoli, M. Lomascolo, and M. Mazzer, "The challenge of high-performance selective emitters for thermophotovoltaic applications," *Semiconductor Science and Technology*, vol. 18, no. 5, p. S174, 2003.

[21] Y. Nam, Y. X. Yeng, A. Lenert, P. Bermel, I. Celanovic, M. Soljačić, and E. N. Wang, "Solar thermophotovoltaic energy conversion systems with two-dimensional tantalum photonic crystal absorbers and emitters," *Solar Energy Materials and Solar Cells*, vol. 122, pp. 287–296, 2014.

[22] A. Heinzel, V. Boerner, A. Gombert, B. Bläsi, V. Wittwer, and J. Luther, "Radiation filters and emitters for the nir based on periodically structured metal surfaces," *Journal of Modern Optics*, vol. 47, no. 13, pp. 2399–2419, 2000.

[23] J. Fleming, S. Lin, I. El-Kady, R. Biswas, and K. Ho, "All-metallic three-dimensional photonic crystals with a large infrared bandgap," *Nature*, vol. 417, no. 6884, pp. 52–55, 2002.

[24] H. Sai, Y. Kanamori, and H. Yugami, "Tuning of the thermal radiation spectrum in the near-infrared region by metallic surface microstructures," *Journal of Micromechanics and Microengineering*, vol. 15, no. 9, p. S243, 2005.

[25] I. Celanovic, F. O'Sullivan, N. Jovanovic, M. Qi, and J. G. Kassakian, "1d and 2d photonic crystals for thermophotovoltaic applications," in *Photonics Europe*. International Society for Optics and Photonics, 2004, pp. 416–422.

[26] G. Kiziltas, J. L. Volakis, and N. Kikuchi, "Design of a frequency selective structure with inhomogeneous substrates as a thermophotovoltaic filter," *Antennas and Propagation, IEEE Transactions on*, vol. 53, no. 7, pp. 2282–2289, 2005.

[27] H. Höfler, H. Paul, W. Ruppel, and P. Würfel, "Interference filters for thermophotovoltaic solar energy conversion," *Solar Cells*, vol. 10, no. 3, pp. 273–286, 1983.

[28] G. Liu, Y. Xuan, Y. Han, and Q. Li, "Investigation of one-dimensional si/sio2 hotonic crystals for thermophotovoltaic filter," *Science in China Series E: Technological Sciences*, vol. 51, no. 11, pp. 2031–2039, 2008.

[29] X. Liu, T. Tyler, T. Starr, A. F. Starr, N. M. Jokerst, and W. J. Padilla, "Taming the blackbody with infrared metamaterials as selective thermal emitters," *Physical review letters*, vol. 107, no. 4, p. 045901, 2011.

[30] C. Wu, B. Neuner III, J. John, A. Milder, B. Zollars, S. Savoy, and G. Shvets, "Metamaterial-based integrated plasmonic absorber/emitter for solar thermophotovoltaic systems," *Journal of Optics*, vol. 14, no. 2, p. 024005, 2012.

[31] S. Molesky, C. J. Dewalt, and Z. Jacob, "High temperature epsilon-near-zero and epsilon-near-pole metamaterial emitters for thermophotovoltaics," *Optics express*, vol. 21, no. 101, pp. A96–A110, 2013.

[32] D. Woolf, J. Hensley, J. Cederberg, D. Bethke, A. Grine, and E. Shaner, "Heterogeneous metasurface for high temperature selective emission," *Applied Physics Letters*, vol. 105, no. 8, p. 081110, 2014.

[33] H. Wang and L. Wang, "Perfect selective metamaterial solar absorbers," *Optics express*, vol. 21, no. 106, pp. A1078–A1093, 2013.

[34] C. Argyropoulos, K. Q. Le, N. Mattiucci, G. DAguanno, and A. Alu, "Broadband absorbers and selective emitters based on plasmonic brewster metasurfaces," *Physical Review B*, vol. 87, no. 20, p. 205112, 2013.

[35] C.-W. Cheng, M. N. Abbas, C.-W. Chiu, K.-T. Lai, M.-H. Shih, and Y.-C. Chang, "Wide-angle polarization independent infrared broadband absorbers based on metallic multi-sized disk arrays," *Optics express*, vol. 20, no. 9, pp. 10 376–10 381, 2012.

[36] C. Wu, N. Arju, G. Kelp, J. A. Fan, J. Dominguez, E. Gonzales, E. Tutuc, I. Brener, and G. Shvets, "Spectrally selective chiral silicon metasurfaces based on infrared fano resonances," *Nature communications*, vol. 5, 2014.

[37] P.-E. Chang, Y.-W. Jiang, H.-H. Chen, Y.-T. Chang, Y.-T. Wu, L. D.-C. Tzuang, Y.-H. Ye, and S.-C. Lee, "Wavelength selective plasmonic thermal emitter by polarization utilizing fabry-pérot type resonances," *Applied Physics Letters*, vol. 98, no. 7, p. 073111, 2011.

[38] B. Zhu, Z. Wang, C. Huang, Y. Feng, J. Zhao, and T. Jiang, "Polarization insensitive metamaterial absorber with wide incident angle," *Progress In Electromagnetics Research*, vol. 101, pp. 231–239, 2010.

[39] M. Francoeur, S. Basu, and S. J. Petersen, "Electric and magnetic surface polariton mediated near-field radiative heat transfer between metamaterials made of silicon carbide particles," *Optics express*, vol. 19, no. 20, pp. 18 774–18 788, 2011.

[40] Q. Zhao, J. Zhou, F. Zhang, and D. Lippens, "Mie resonance-based dielectric metamaterials," *Materials Today*, vol. 12, no. 12, pp. 60–69, 2009.

[41] M. S. Wheeler, J. S. Aitchison, and M. Mojahedi, "Three-dimensional array of dielectric spheres with an isotropic negative permeability at infrared frequencies," *Physical Review B*, vol. 72, no. 19, p. 193103, 2005.

[42] A. Ghanekar, L. Lin, J. Su, H. Sun, and Y. Zheng, "Role of nanoparticles in wavelength selectivity of multilayered structures in the far-field and near-field regimes," *Optics Express*, vol. 23, no. 19, pp. A1129–A1139, 2015.

[43] W. C. Chew, *Waves and fields in inhomogeneous media*. IEEE press, 1995.

[44] L. Gao, F. Lemarchand, and M. Lequime, "Refractive index determination of sio2 layer in the uv/vis/nir range: spectrophotometric reverse engineering on single and bi-layer designs," *Journal of the European Optical Society-Rapid publications*, vol. 8, 2013.

[45] A. D. Rakić, A. B. Djurišić, J. M. Elazar, and M. L. Majewski, "Optical properties of metallic films for vertical-cavity optoelectronic devices," *Applied optics*, vol. 37, no. 22, pp. 5271–5283, 1998.

[46] E. D. Palik, *Handbook of optical constants of solids*. Academic press, 1998, vol. 3.

[47] P. Timans, *Advances in Rapid Thermal and Integrated Processing, ed. F. Roozeboom.* Dordrecht, The Netherlands: Kluwer Academic Publishers, The Netherlands, 1996.

[48] C. Xu, S. Wang, G. Wang, J. Liang, S. Wang, L. Bai, J. Yang, and X. Chen, "Temperature dependence of refractive indices for 4h-and 6h-sic," *Journal of Applied Physics*, vol. 115, no. 11, p. 113501, 2014.

[49] Y.-B. Chen, Z. Zhang, and P. Timans, "Radiative properties of patterned wafers with nanoscale linewidth," *Journal of Heat Transfer*, vol. 129, no. 1, pp. 79–90, 2007.

[50] V. Myroshnychenko, J. Rodríguez-Fernández, I. Pastoriza-Santos, A. M. Funston, C. Novo, P. Mulvaney, L. M. Liz-Marzán, and F. J. G. de Abajo, "Modelling the optical response of gold nanoparticles," *Chemical Society Reviews*, vol. 37, no. 9, pp. 1792–1805, 2008.

[51] U. Kreibig and M. Vollmer, *Optical properties of metal clusters.* Springer Berlin, 1995, vol. 25.

[52] W. T. Doyle, "Optical properties of a suspension of metal spheres," *Physical review B*, vol. 39, no. 14, p. 9852, 1989.

[53] M. S. Wheeler, "A scattering-based approach to the design, analysis, and experimental verification of magnetic metamaterials made from dielectrics," Ph.D. dissertation, 2010.

[54] M. G. M. Y. B. B. O. V. Sulima, A. W. Bett and P. S.Dutta, "Proc. 5th TPV Conf., Rome, Italy, September 2002 (AIP, New York, 1999)," p. p 402.

[55] Y. Battie, A. Resano-Garcia, N. Chaoui, Y. Zhang, and A. E. Naciri, "Extended maxwell-garnett-mie formulation applied to size dispersion of metallic nanoparticles embedded in host liquid matrix," *The Journal of Chemical Physics*, vol. 140, no. 4, p. 044705, 2014.

[56] S. Roberts, "Optical properties of nickel and tungsten and their interpretation according to drude's formula," *Physical Review*, vol. 114, no. 1, p. 104, 1959.

[57] P. Timans, "The thermal radiative properties of semiconductors," in *Advances in rapid thermal and integrated processing.* Springer, 1996, pp. 35–101.

[58] M. Planck, *The theory of heat radiation.* Dover Publications, 2011.

# MANUSCRIPT 4

## Mie-Metamaterials Based Thermal Emitter For Near-Field Thermophotovoltaic Systems

by

Alok Ghanekar[1], Yanpei Tian[1], Sinong Zhang[2], Yali Cui[2,3] and Yi Zheng[1]

[1] Department of Mechanical, Industrial and Systems Engineering, University of Rhode Island,

Kingston, RI 02881, USA

[2] College of Life Sciences, Northwest University, Xian, Shaanxi 710069, China

[3] National Engineering Research Center for Miniaturized Detection Systems, Northwest

University, Xian, Shaanxi 710069, China

(Has been published in Materials.)

Corresponding Author: Yi Zheng

Department of Mechanical, Industrial and Systems Engineering

University of Rhode Island

Kingston, RI 02881, USA

Phone: +1 401-874-5184

Email Address: zheng@uri.edu

**Abstract**

In this work, we theoretically analyze the performance characteristics of a near-field thermophotovoltaic system consisting a Mie-metamaterial emitter and GaSb based photovoltaic cell at separations less than the thermal wavelength. The emitter consists of tungsten nanoparticle-embedded thin film of $SiO_2$ deposited on bulk tungsten. Numerical results presented here are obtained using formulae derived from dyadic Green's function formalism and Maxwell-Garnett-Mie theory. We show that, by inclusion of tungsten nanoparticles, the thin layer of $SiO_2$ acts like an effective medium that enhances selective radiative heat transfer for the photons above the band gap of GaSb. We analyze TPV performance for various volume fractions of tungsten nanoparticles and thickness of $SiO_2$.

## 4.1 Introduction

Thermophotovoltaics (TPV) have been the focus of several works as an alternative to power generation technologies and a technology for waste heat recovery systems [1, 2, 3]. A typical TPV system consists of a high temperature ($\sim$1500 K) thermal emitter and a photovoltaic (PV) cell that converts the energy of incident photons into electricity. While ideal TPV systems convert radiative energy into electricity at an efficiency of the Carnot engine, practical TPV systems suffer from mismatch between the emission spectra of the emitter and absorption spectra of PV cell [4, 5, 6, 7, 8]. Several studies investigate the use of metamaterials [9, 10, 11], surface gratings and photonics crystals [12, 13, 14, 15, 16, 17] and complex surface patterns [18] to improve efficiency of TPV system. In the recent few years, it was demonstrated that near-field thermal radiation has a great potential in improving TPV systems [19, 20, 21, 22, 23, 24]. Several theoretical studies were focused on exploiting near-field coupling of surface waves between emitter and PV cell at nanometer separation to improve the efficiency. It is challenging to develop materi-

56

als that can withstand high temperatures as well as allow an enhanced coupling of surface waves for the energies above the band gap of PV cell. One-dimensional gratings, hyperbolic metamaterials and photonic crystals have shown a great potential in TPV applications. Dielectric mixtures and nanoparticle embedded thin films can also be utilized to tune near-field thermal radiation [25]. It has been demonstrated earlier that Mie-metamaterials or Mie-resonance metamaterials that utilize Mie resonances of inclusions into host materials can be used for spectral tuning of near-field thermal radiation. Authors earlier demonstrated the possible use of tungsten nanoparticle-embedded thin film of $SiO_2$ to achieve a selective thermal emitter for far-field TPV system [26]. Effect of nanoparticle inclusions into host material on near-field radiative heat transfer has been investigated in several theoretical studies [27, 28, 29]. Stemming from earlier work, we demonstrate the use of a Mie-metamaterial thermal emitter that consists of tungsten nanoparticles embedded into a thin film of $SiO_2$ deposited on thick layer of tungsten for near-field TPV system. We also explore possible alternative of W nanoparticles by refractive materials such as titanium nitride (TiN), tantalum (Ta) and molybdenum (Mo). We investigate the performance of such a TPV system for various configurations. While many recent works have dealt with gratings, photonic crystals and other metamaterials, this is the first time nanoparticle-embedded thin films have been investigated for near-field TPV system. The configuration of near-field TPV system considered in the present study is shown in Fig. 6.1. The emitter side is a Mie-metamaterial consisting tungsten nanoparticle-embedded in $SiO_2$ thin film on the top of a tungsten layer. Radius of nanoparticles is fixed to 20 nm. Their volume fraction and thickness of $SiO_2$ layer can be varied to investigate behaviour of the system. The layer of tungsten blocks radiation from the substrate making the emitter essentially opaque. PV cell considered here is GaSb (which has a bandgap
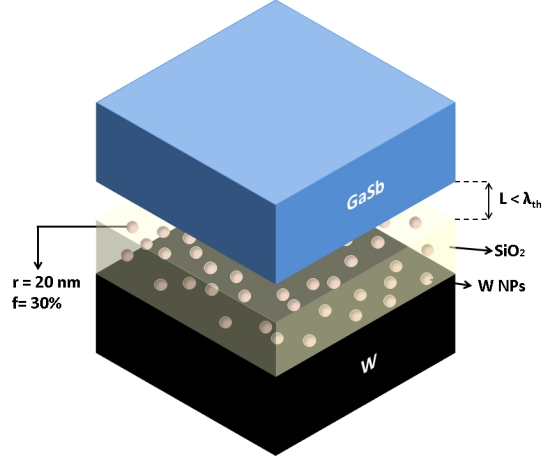
Figure 4.1: Schematic of near-field thermophotovoltaic system consisting the proposed thermal emitter and GaSb based PV cell at separation less than the thermal wavelength.

of 0.726 eV) whose properties can be found in Ref. [30]. Calculations reports in this work are for emitter temperature of 1500 K while PV cell is assumed to be at 300 K. The separation between the emitter and PV cell is comparable or less than the thermal wavelength at 1500 K ($\lambda_{th}$= 1.93 $\mu$m).

While we concern ourselves with mostly the theoretical side of proposed thermal emitter, there are various ways to fabricate nanoparticle embedded thin films. For example, it has been demonstrated that a stack of metallic nanoparticle arrays and $SiO_2$ arrays can be fabricated [?]. Alternatively, as suggested by [?], core-shell nanoparticle arrays can be fabricated using tungsten core and $SiO_2$ shell. This is followed by sputtering or chemical vapor deposition of $SiO_2$. Nanoparticles-$SiO_2$ composites also can be fabricated using sputtering deposition process. A mixture of W and $SiO_2$ powders can be prepared using PVDF (Polyvinylidene fluoride) and sintering/pressing onto a sputtering cooling plate. W-$SiO_2$ composites can be fabricated by RF sputtering of W followed by sputtering of W-$SiO_2$ powder. During the sputtering process, tungsten nanoparticles would form.
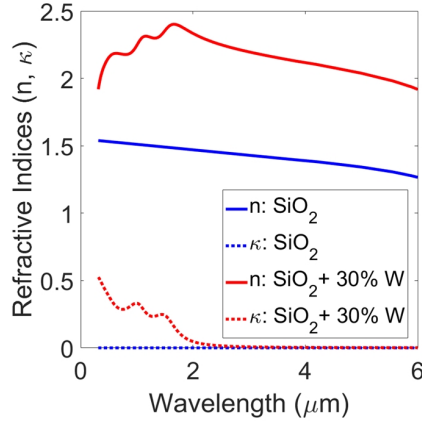
Figure 4.2: Real (n) and imaginary ($\kappa$) parts of refractive indices of pure $SiO_2$ and $SiO_2$ with 30% tungsten nanoparticles.

## 4.2 Results and Discussion

Refractive indices of plain $SiO_2$ and that of $SiO_2$ mixed with 30% nanoparticles of tungsten are shown in Fig. 6.2. Effect of nanoparticle inclusions can be observed. $SiO_2$ has a near constant value of refractive index $(n)$ and a negligible extinction coefficient $(\kappa)$ in the spectral range of our interest. Dielectric mixture of $SiO_2$ and tungsten displays an overall increased effective refractive index and a higher absorption coefficient for wavelengths shorter than 2.5 $\mu$m.

It is crucial to reduce the spectral energy below the band-gap of PV cell in order to improve the overall thermal efficiency of the TPV system. Coupling of surface waves dictates whether radiative transfer would be enhanced or suppressed. The goal is to enhance radiative transfer above the bandgap without significantly enhancing radiation below the bandgap of PV cell. In order to assess the impact of nanoparticle inclusions, we investigate spectral heat flux of the proposed TPV system for various configurations. Spectral heat flux across the proposed thermal emitter at a separation of $L = 100$ nm for various compositions is plotted in Fig. 6.3. Emitter with a 0.3 $\mu$m layer of $SiO_2$ on tungsten has lower heat flux across the spectrum when compared to plain tungsten as seen in Fig. 6.3 (a). Upon inclu-
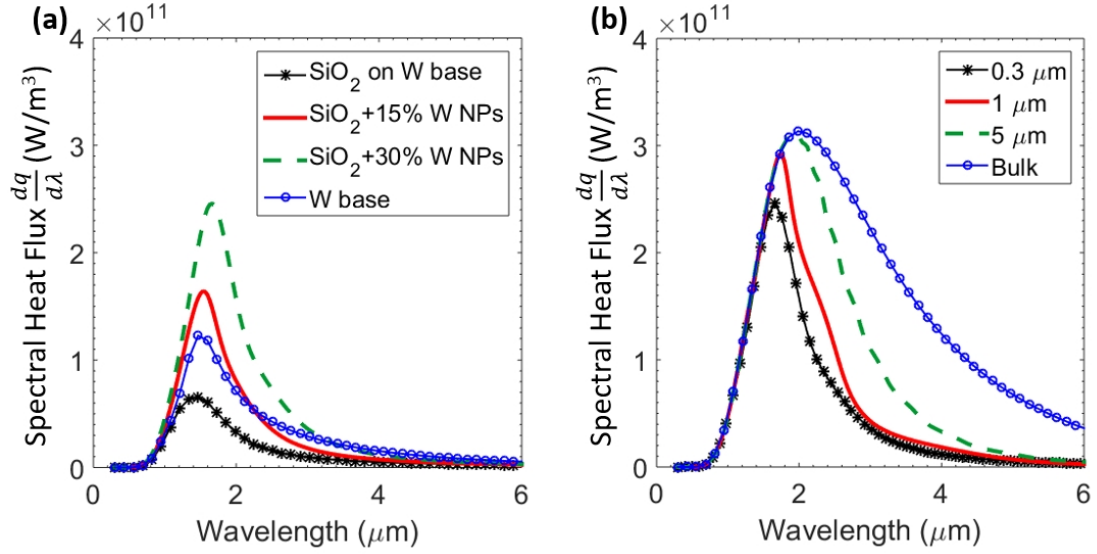
Figure 4.3: Spectral heat flux across the proposed emitter and the GaSb PV cell at a separation of L = 100 nm for (a) various volume fraction of W nanoparticles - 0%, 15% and 30 % compared to bulk W emitter; (b) various thicknesses of $SiO_2$ layer - 0.3 $\mu$m, 1 $\mu$m, 5 $\mu$m and bulk respectively.

sion of tungsten nanoparticles however, spectral heat flux is increased and is more selective towards shorter wavelengths ($\lambda < 2$ $\mu$m). While spectral heat flux shows increase over the entire range, it is more prominent for energies above the band-gap leading to less fraction of energy lost. An increased absorption coefficient in the shorter wavelengths can be accounted for enhanced coupling of surface modes in that range. To demonstrate the effect of reducing bulk layer to thin layer, Fig. 6.3 (b) illustrates spectral responses for various thicknesses of $SiO_2$ layer and fixed volume fraction of 30%. While a bulk layer of $SiO_2$ mixed with tungsten nanoparticle show broadband heat transfer, it can be clearly seen that, thinner layers of $SiO_2$ yield more selective spectral response while maximum spectral heat flux remains relatively same. It can be observed that radiation at longer wavelengths is more sensitive to layer thickness. It is imperative that such a configuration is more desirable for minimizing losses due to long wavelength photons. In principle, it is possible to tune the near-field thermal radiation by changing volume fraction of
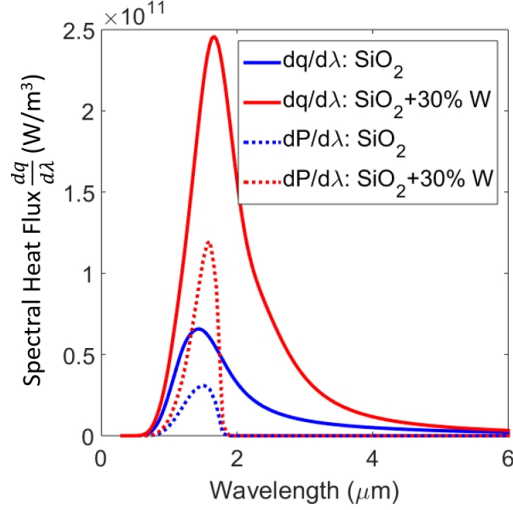
Figure 4.4: Predicted spectral density of output power (dashed lines) from GaSb PV cell for emitter with pure $SiO_2$ thin film and $SiO_2$ with 30% of W nanoparticles for separation of 100 nm compared with corresponding spectral heat fluxes (solid lines).

nanoparticles and thickness of the $SiO_2$ layer to achieve optimal configuration for a given operating temperature and separation.

We now investigate the power output of the GaSb PV cell as a result of near-field radiative heat transfer at a separation of 100 nm. To assess the overall performance of the TPV system, we model the PV cell as discussed in section 4.3. We calculate spectral density of output power along with the total output power. Figure 6.4 shows calculated spectral density of output power from PV cell for the emitter with pure $SiO_2$ layer of 0.3 $\mu$m thickness on tungsten and $SiO_2$ layer with 30% tungsten nanoparticles. The emitter with tungsten nanoparticle embedded thin film of $SiO_2$ displays an enhanced output power contribution above the bandgap of GaSb PV cell when compared the emitter to pure $SiO_2$ layer. For comparison spectral heat flux across the interface of the same configurations are also shown. The total heat flux and total power output of the PV cell of these configurations are plotted against separation up to 10 nm in Fig. 4.5. For gaps larger than 1 $\mu$m (far-field), heat flux and consequently power power and system efficiencies
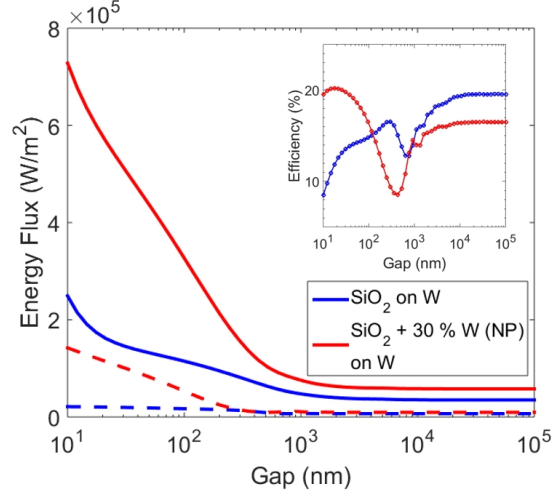
Figure 4.5: Total heat flux (solid lines) and output power (dashed lines) of PV cell as a function of separation between the emitter and PV cell for an emitter pure SiO$_2$ film of 0.5 $\mu$m and SiO$_2$ films with W nanoparticles. Inset shows overall efficiency of the corresponding TPV systems plotted as a function of separation.

are independent of the distance. For separations less than 1 $\mu$m (near-field), the overall heat flux increases due to presence of evanescent waves. Consequently, the output power also rises monotonically as separation between the emitter and PV cell is reduced. The inset in Fig. 4.5 shows TPV system efficiency against distance for the same setups. While the trend in efficiencies is not as monotonous, for the separations smaller than 100 nm, the emitter with tungsten nanoparticles shows higher thermal efficiency than the one with pure SiO$_2$. This is supported by earlier results that show the increased selectivity at shorter wavelengths leading to lower losses. Interestingly, the emitter with pure SiO$_2$ has higher efficiency in the far-field. Nevertheless, such a configuration has lower output power. Oscillatory behaviour of efficiency has been observed before and can be attributed to vacuum gap behaving like a waveguide [4]. We would like to emphasize that, to further improve the performance of the TPV system the materials chosen are not necessarily optimal. For example, PV cells with lower band gap such as InGaAs and InGaSb or the quaternary alloys like InGaAsSb can be used. This can allow use of lower

62
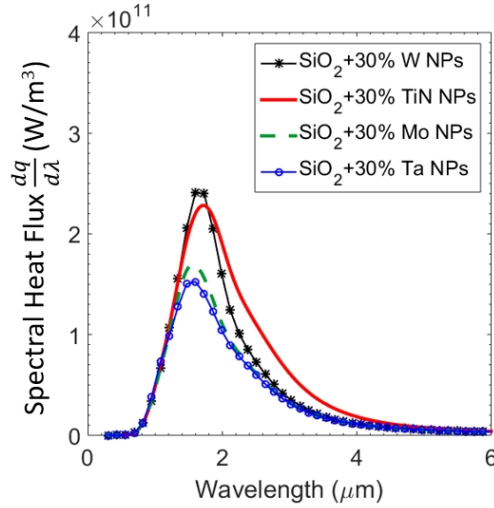
Figure 4.6: Spectral heat flux across the emitter consisting nanoparticles of alternative materials and the GaSb PV cell at a separation of L = 100 nm for volume fraction of 30%.

emitter temperature or higher efficiencies and output power at the same operating temperatures. Alternatively, other materials such as $Al_2O_3$ (in place of $SiO_2$) and Platinum, Molybdenum, Tantalum and Titanium Nitride (in place of W) can be investigated for thermal emitter structure. We show a possible replacement of W by refractory materials such as Titanium Nitride (TiN), Molybdenum (Mo) and Tantalum (Ta) using our calculations in Fig. 4.6. Spectral heat flux between the PV cell and emitter with $SiO_2$ layer of 0.3 $\mu$m thickness and 30% nanoparticles at a separation of 100 nm is shown. For comparison, heat flux with tungsten nanoparticles is shown. Corresponding values of total heat flux for W, TiN, Mo, and Ta nanoparticles is $3.72{\times}10^5$, $3.81{\times}10^5$, $2.68{\times}10^5$ and $2.57{\times}10^5$ W/m$^2$, respectively. From Fig. 4.6 it appears that emitter with TiN and W nanoparticles display higher heat flux for this particular configuration. Emitter with tungsten nanoparticles shows better selectivity than TiN. Various combinations of material type and dimensions can be investigated to tune the emission spectra.

Overall, we have numerically investigated for the first time, near-field thermophoto-

voltaic system that uses Mie-metamaterial based thermal emitter and a PV cell at a separation less than the thermal wavelength. We have theoretically demonstrated an enhanced wavelength selective thermal emitter for near-field thermophotovoltaic system using a Mie-resonance metamaterial. Thermal emitter consists of tungsten nanoparticle-embedded thin film of $SiO_2$ deposited on thick tungsten substrate. We analyze performance of such a TPV device for various cases. We study the effect of volume fraction, layer thickness of $SiO_2$ and separation between emitter and PV cell. The embedded tungsten nanoparticles in the thin film can alter the refractive index of the film and allow spectral control of near-field radiative transfer across the emitter and the PV cell. We evaluate energy conversion efficiency of the proposed near-field thermophotovoltaic system. The results show that the structure of Mie-metamaterial thermal emitter can significantly improve the efficiency of thermophotovoltaic system. Improvement in spectral selectivity as well as overall heat transfer can be accounted for increased power output and efficiency. We show that, by changing volume fraction of nanoparticles and thickness of $SiO_2$ it is possible to tune the near-field thermal radiation to obtain enhanced output power and high thermal efficiency. Materials considered can withstand high temperatures and suitable for thermal emitter.

## 4.3 Materials and Methods

The expression of radiative transfer between closely spaced bodies can be derived using dyadic Green's function approach [31], and is given by

$$q_{1\to2}(T_1,T_2,L) = \int_0^\infty \frac{d\omega}{2\pi} [\Theta(\omega, T_1) - \Theta(\omega, T_2)] T_{1\to2}(\omega) \qquad (4.1)$$

where $\Theta(\omega, T) = (\hbar\omega/2)\coth(\hbar\omega/2k_BT)$ is the energy of harmonic oscillator at frequency $\omega$ and temperature $T$, $\hbar$ is the reduced Planck constant, and $k_B$ is the Boltzmann constant. The function $T_{1\to2}(\omega)$ corresponds to the spectral transmissivity in radiative transfer between media 1 and 2 separated of distance $L$ and is

expressed as [31]

$$T_{1 \to 2}(\omega) = \int_0^{\omega/c} \frac{k_\rho dk_\rho}{2\pi} \sum_{\mu=s,p} \frac{(1 - |\widetilde{R}_{h1}^{(\mu)}|^2)(1 - |\widetilde{R}_{h2}^{(\mu)}|^2)}{|1 - \widetilde{R}_{h1}^{(\mu)} \widetilde{R}_{h2}^{(\mu)} e^{2jk_{hz}L}|^2}$$
$$+ \int_{\omega/c}^{\infty} \frac{k_\rho dk_\rho}{2\pi} \sum_{\mu=s,p} \frac{4\Im(\widetilde{R}_{h1}^{(\mu)})\Im(\widetilde{R}_{h2}^{(\mu)})e^{-2|k_{hz}|L}}{|1 - \widetilde{R}_{h1}^{(\mu)} \widetilde{R}_{h2}^{(\mu)} e^{-2|k_{hz}|L}|^2}$$

(4.2)

where $\widetilde{R}_{h1}^{(\mu)}$ and $\widetilde{R}_{h2}^{(\mu)}$ are polarized effective reflection coefficients of the two half spaces (calculated in the absence of other half space), and $k_{hz}$ is the $z$-component of wavevector in vacuum. The first term in Eq. (5.2) corresponds to propagating waves, while the second term describes the thermal transport due to evanescent waves, and its contribution is significant only for small values of gap $L$. For a structure having $N$-layer media having $(N-1)$ interfaces, the expression for the generalized reflection coefficient at the interface between region $i$ and region $i+1$ is given by [32],

$$\widetilde{R}_{i,i+1}^{(\mu)} = \frac{R_{i,i+1}^{(\mu)} + \widetilde{R}_{i+1,i+2}^{(\mu)} e^{2jk_{i+1,z}(d_{i+1}-d_i)}}{1 + R_{i,i+1}^{(\mu)} \widetilde{R}_{i+1,i+2}^{(\mu)} e^{2jk_{i+1,z}(d_{i+1}-d_i)}}$$

(4.3)

where $R_{i,i+1}^{(\mu)}$ is the Fresnel reflection coefficient at the interface between the layer $i$ and $i+1$, and $\widetilde{R}_{i+1,i+2}^{(\mu)}$ is the generalized reflection coefficient at the interface between the layer $i+1$ and $i+2$, $\mu = s$ (or $p$) refers to transverse electric (or magnetic) polarization, $z = -d_i$ is the location of the $i$th interface. $k_{i,z} = \sqrt{\varepsilon_i(\omega)\omega^2/c^2 - k_\rho^2}$ is the normal $z$-component of the wave vector in medium $i$ wherein $\varepsilon_i(\omega)$ is the relative permittivity of the medium $i$ as a function of angular frequency $\omega$, $c$ is the speed of light in vacuum and $k_\rho$ is the magnitude of the in-plane wave vector. With $\widetilde{R}_{N,N+1}^{(\mu)} = 0$, the above equation provides a recursive relation to calculate the reflection coefficients $\widetilde{R}_{i,i+1}^{(\mu)}$ in all regions. For calculating the effective dielectric function the Mie-metamaterial, we use Clausius-Mossotti equation. [33, 34].

$$\varepsilon_{eff} = \varepsilon_m \left( \frac{r^3 + 2\alpha_r f}{r^3 - \alpha_r f} \right)$$

(4.4)

where $\varepsilon_m$ is the dielectric function of the matrix, $\alpha_r$ is the electric dipole polarizability, $r$ and $f$ are the radius and volume fraction of nanoparticles respectively. To consider the size effects of nanoparticle inclusions, we use the Maxwell Garnett formula which employs the expression for electric dipole polarizability using Mie theory [35], $\alpha_r = 3jc^3 a_{1,r}/2\omega^3 \varepsilon_m^{3/2}$, where $a_{1,r}$ is the first electric Mie coefficient given by

$$a_{1,r} = \frac{\sqrt{\varepsilon_{np}}\psi_1(x_{np})\psi_1'(x_m) - \sqrt{\varepsilon_m}\psi_1(x_m)\psi_1'(x_{np})}{\sqrt{\varepsilon_{np}}\psi_1(x_{np})\xi_1'(x_m) - \sqrt{\varepsilon_m}\xi_1(x_m)\psi_1'(x_{np})} \qquad (4.5)$$

where $\psi_1$ and $\xi_1$ are Riccati-Bessel functions of the first order given by $\psi_1(x) = xj_1(x)$ and $\xi_1(x) = xh_1^{(1)}(x)$ where $j_1$ and $h_1^{(1)}$ are first order spherical Bessel functions and spherical Hankel functions of the first kind, respectively. Here, "'" indicates the first derivative. $x_m = \omega r \sqrt{\varepsilon_m}/c$ and $x_{np} = \omega r \sqrt{\varepsilon_{np}}/c$ are the size parameters of the matrix and the nanoparticles, respectively; $\varepsilon_{np}$ being the dielectric function of nanoparticles. It is worth mentioning that Maxwell-Garnett-Mie theory is applicable when average distance between inclusions is much smaller than the wavelength of interest [36]. This criteria is satisfied in the calculated presented. Since nanoparticle diameter (40 nm) is much smaller than the thickness of the thin film (0.3 $\mu$m) considered, effective medium theory holds true for the calculations presented in this study. Dielectric functions of the materials ($SiO_2$ and W) considered in this paper are taken from literature [37, 38]. Having very low temperature coefficients, room temperature values of dielectric function are used for $SiO_2$ [39]. Dielectric properties of tungsten were also assumed to be unchanged as the operating temperature is much less than the melting point.

Near-field thermal radiation and charge transport in PV cell can be theoretically modelled by accounting for charge density distribution due to number of photons absorbed at different cell depth [22]. Due to limitations of the present study, we employ a simplistic model to calculate output power of PV cell. We assume that

quantum efficiency of PV cell in the near-field would be the same as that in the far-field. Therefore, short circuit current can be calculated as [22]

$$I_{SC} = \int_{E_g/\hbar}^{\infty} \frac{e}{\hbar\omega} \cdot EQE_{GaSb}(\omega) \cdot \frac{dq}{d\omega} d\omega \qquad (4.6)$$

where $E_g$ is the bandgap of GaSb cell, $EQE_{GaSb}$ is external quantum efficiency, $dq/d\omega$ is spectral heat flux and $e$ is the electronic charge. Dark current can be calculated by,

$$I_0 = \frac{eD_n n_i^2}{L_n N_n} + \frac{eD_p n_i^2}{L_p N_p}; \qquad (4.7)$$

where $D_n$ and $D_p$ are diffusivities of electrons and holes, respectively, $n_i$ is the intrinsic carrier concentration, $N_n$ and $N_p$ are concentrations of electrons and holes, respectively, while diffusion lengths $L_n$ and $L_p$ can be calculated in terms of diffusivity and recombination lifetime $\tau$ using,

$$L_x = \sqrt{D \cdot \tau} \qquad (4.8)$$

Total recombination lifetime is calculated by,

$$1/t_{tot} = 1/\tau_R + 1/\tau_{SHR} + 1/\tau_{Au} \qquad (4.9)$$

where $\tau_R$, $\tau_{SHR}$ and $\tau_{Au}$ are radiative recombination, Shockley-Hall recombination and Augar recombination, respectively [40]. Open circuit voltage is calculated using,

$$V_{OC} = (k_B T_{PV}/e)ln(I_{SC}/I_0 + 1) \qquad (4.10)$$

Output power of the PV cell is given by,

$$P_{out} = I_{SC}V_{OC}(1 - 1/z)[1 - ln(z)/z] \qquad (4.11)$$

where $z = ln(I_{SC}/I_0)$ and efficiency of the TPV system is given by,

$$\eta = P_{out}/Q_{rad} \qquad (4.12)$$

For our calculations, intrinsic carrier concentration was assumed to be $4.3 \times 10^{12}$ cm$^{-3}$. Carrier concentration of electrons and holes were assumed to be equal to $N_n = N_p = 10^{17}$ cm$^{-3}$. The recombination lifetimes are taken to be $\tau_R = 40$ ns, $\tau_{SHR} = 10$ ns and $\tau_{Au} = 20$ $\mu$s. Carrier diffusivities are $D_n = 129$ cm$^2$/s and $D_p = 39$ cm$^2$/s for electrons and holes, respectively.

**Acknowledgments**

**List of References**

[1] S. Basu, Y. Chen, and Z. Zhang, "Microscale radiation in thermophotovoltaic devices-a review," *International Journal of Energy Research*, vol. 31, no. 6, pp. 689–716, 2007.

[2] M. Bosi, C. Ferrari, F. Melino, M. Pinelli, P. Spina, and M. Venturini, "Thermophotovoltaic generation: a state of the art review," *Proceedings ECOS*, 2012.

[3] T. Coutts, "A review of progress in thermophotovoltaic generation of electricity," *Renewable and Sustainable Energy Reviews*, vol. 3, no. 2, pp. 77–184, 1999.

[4] J. K. Tong, W.-C. Hsu, Y. Huang, S. V. Boriskina, and G. Chen, "Thin-film'thermal well'emitters and absorbers for high-efficiency thermophotovoltaics," *arXiv preprint arXiv:1502.02061*, 2015.

[5] N.-P. Harder and P. Würfel, "Theoretical limits of thermophotovoltaic solar energy conversion," *Semiconductor Science and Technology*, vol. 18, no. 5, p. S151, 2003.

[6] E. Rephaeli and S. Fan, "Absorber and emitter for solar thermo-photovoltaic systems to achieve efficiency exceeding the shockley-queisser limit," *Optics express*, vol. 17, no. 17, pp. 15 145–15 159, 2009.

[7] P. Wurfel and W. Ruppel, "Upper limit of thermophotovoltaic solar-energy conversion," *Electron Devices, IEEE Transactions on*, vol. 27, no. 4, pp. 745–750, 1980.

[8] P. Bermel, M. Ghebrebrhan, W. Chan, Y. X. Yeng, M. Araghchini, R. Hamam, C. H. Marton, K. F. Jensen, M. Soljačić, J. D. Joannopoulos, *et al.*, "Design and global optimization of high-efficiency thermophotovoltaic systems," *Optics express*, vol. 18, no. 103, pp. A314–A334, 2010.

[9] X. Liu, T. Tyler, T. Starr, A. F. Starr, N. M. Jokerst, and W. J. Padilla, "Taming the blackbody with infrared metamaterials as selective thermal emitters," *Physical review letters*, vol. 107, no. 4, p. 045901, 2011.

[10] C. Wu, B. Neuner III, J. John, A. Milder, B. Zollars, S. Savoy, and G. Shvets, "Metamaterial-based integrated plasmonic absorber/emitter for solar thermo-photovoltaic systems," *Journal of Optics*, vol. 14, no. 2, p. 024005, 2012.

[11] S. Molesky, C. J. Dewalt, and Z. Jacob, "High temperature epsilon-near-zero and epsilon-near-pole metamaterial emitters for thermophotovoltaics," *Optics express*, vol. 21, no. 101, pp. A96–A110, 2013.

[12] P. Nagpal, S. E. Han, A. Stein, and D. J. Norris, "Efficient low-temperature thermophotovoltaic emitters from metallic photonic crystals," *Nano letters*, vol. 8, no. 10, pp. 3238–3243, 2008.

[13] K. A. Arpin, M. D. Losego, A. N. Cloud, H. Ning, J. Mallek, N. P. Sergeant, L. Zhu, Z. Yu, B. Kalanyan, G. N. Parsons, *et al.*, "Three-dimensional self-assembled photonic crystals with high temperature stability for thermal emission modification," *Nature communications*, vol. 4, 2013.

[14] A. Heinzel, V. Boerner, A. Gombert, B. Bläsi, V. Wittwer, and J. Luther, "Radiation filters and emitters for the nir based on periodically structured metal surfaces," *Journal of Modern Optics*, vol. 47, no. 13, pp. 2399–2419, 2000.

[15] J. Fleming, S. Lin, I. El-Kady, R. Biswas, and K. Ho, "All-metallic three-dimensional photonic crystals with a large infrared bandgap," *Nature*, vol. 417, no. 6884, pp. 52–55, 2002.

[16] H. Sai, Y. Kanamori, and H. Yugami, "Tuning of the thermal radiation spectrum in the near-infrared region by metallic surface microstructures," *Journal of Micromechanics and Microengineering*, vol. 15, no. 9, p. S243, 2005.

[17] A. Ghanekar, M. Sun, Z. Zhang, and Y. Zheng, "Optimal design of wavelength selective thermal emitter for thermophotovoltaic applications," *Journal of Thermal Science and Engineering Applications*.

[18] D. Woolf, J. Hensley, J. Cederberg, D. Bethke, A. Grine, and E. Shaner, "Heterogeneous metasurface for high temperature selective emission," *Applied Physics Letters*, vol. 105, no. 8, p. 081110, 2014.

[19] A. Narayanaswamy and G. Chen, "Surface modes for near field thermophotovoltaics," *Applied Physics Letters*, vol. 82, no. 20, pp. 3544–3546, 2003.

[20] R. DiMatteo, P. Greiff, D. Seltzer, D. Meulenberg, E. Brown, E. Carlen, K. Kaiser, S. Finberg, H. Nguyen, J. Azarkevich, *et al.*, "M icron-gap t hermo p hoto v oltaics (mtpv)," in *AIP Conference Proceedings*, vol. 738, no. 1. AIP, 2004, pp. 42–51.

[21] M. Laroche, R. Carminati, and J.-J. Greffet, "Near-field thermophotovoltaic energy conversion," *Journal of Applied Physics*, vol. 100, no. 6, p. 063704, 2006.

[22] K. Park, S. Basu, W. P. King, and Z. Zhang, "Performance analysis of near-field thermophotovoltaic devices considering absorption distribution," *Journal of Quantitative Spectroscopy and Radiative Transfer*, vol. 109, no. 2, pp. 305–316, 2008.

[23] M. Francoeur, R. Vaillon, and M. P. Mengüç, "Thermal impacts on the performance of nanoscale-gap thermophotovoltaic power generators," *IEEE Transactions on Energy Conversion*, vol. 26, no. 2, pp. 686–698, 2011.

[24] T. Bright, L. Wang, and Z. Zhang, "Performance of near-field thermophotovoltaic cells enhanced with a backside reflector," *Journal of Heat Transfer*, vol. 136, no. 6, p. 062701, 2014.

[25] A. Ghanekar, L. Lin, J. Su, H. Sun, and Y. Zheng, "Role of nanoparticles in wavelength selectivity of multilayered structures in the far-field and near-field regimes," *Optics Express*, vol. 23, no. 19, pp. A1129–A1139, 2015.

[26] A. Ghanekar, L. Lin, and Y. Zheng, "Novel and efficient mie-metamaterial thermal emitter for thermophotovoltaic systems," *Optics express*, vol. 24, no. 10, pp. A868–A877, 2016.

[27] M. Francoeur, S. Basu, and S. J. Petersen, "Electric and magnetic surface polariton mediated near-field radiative heat transfer between metamaterials made of silicon carbide particles," *Optics express*, vol. 19, no. 20, pp. 18 774–18 788, 2011.

[28] Q. Zhao, J. Zhou, F. Zhang, and D. Lippens, "Mie resonance-based dielectric metamaterials," *Materials Today*, vol. 12, no. 12, pp. 60–69, 2009.

[29] M. S. Wheeler, J. S. Aitchison, and M. Mojahedi, "Three-dimensional array of dielectric spheres with an isotropic negative permeability at infrared frequencies," *Physical Review B*, vol. 72, no. 19, p. 193103, 2005.

[30] S. Adachi, "Optical dispersion relations for gap, gaas, gasb, inp, inas, insb, al x ga1- x as, and in1- x ga x as y p1- y," *Journal of Applied Physics*, vol. 66, no. 12, pp. 6030–6040, 1989.

[31] A. Narayanaswamy and Y. Zheng, "A Green's function formalism of energy and momentum transfer in fluctuational electrodynamics," *Journal of Quantitative Spectroscopy and Radiative Transfer*, vol. 132, pp. 12–21, 2014.

[32] W. C. Chew, *Waves and fields in inhomogeneous media*. IEEE press, 1995.

[33] V. Myroshnychenko, J. Rodríguez-Fernández, I. Pastoriza-Santos, A. M. Funston, C. Novo, P. Mulvaney, L. M. Liz-Marzán, and F. J. G. de Abajo, "Modelling the optical response of gold nanoparticles," *Chemical Society Reviews*, vol. 37, no. 9, pp. 1792–1805, 2008.

[34] U. Kreibig and M. Vollmer, *Optical properties of metal clusters*. Springer Berlin, 1995, vol. 25.

[35] W. T. Doyle, "Optical properties of a suspension of metal spheres," *Physical review B*, vol. 39, no. 14, p. 9852, 1989.

[36] M. S. Wheeler, "A scattering-based approach to the design, analysis, and experimental verification of magnetic metamaterials made from dielectrics," Ph.D. dissertation, 2010.

[37] L. Gao, F. Lemarchand, and M. Lequime, "Refractive index determination of sio2 layer in the uv/vis/nir range: spectrophotometric reverse engineering on single and bi-layer designs," *Journal of the European Optical Society-Rapid publications*, vol. 8, 2013.

[38] A. D. Rakić, A. B. Djurišić, J. M. Elazar, and M. L. Majewski, "Optical properties of metallic films for vertical-cavity optoelectronic devices," *Applied optics*, vol. 37, no. 22, pp. 5271–5283, 1998.

[39] P. Timans, *Advances in Rapid Thermal and Integrated Processing, ed. F. Roozeboom*. Dordrecht, The Netherlands: Kluwer Academic Publishers, The Netherlands, 1996.

[40] J. P. McKelvey, "Solid state and semiconductor physics," 1966.

# High Contrast Far-Field Radiative Thermal Diode

by

Alok Ghanekar[1], Gang Xiao[2], and Yi Zheng[1]

[1] Department of Mechanical, Industrial and Systems Engineering, University of Rhode Island,

Kingston, RI 02881, USA

[2] Department of Physics, Brown University, Providence, RI 02912, USA

Corresponding Author: Yi Zheng

Department of Mechanical, Industrial and Systems Engineering

University of Rhode Island

Kingston, RI 02881, USA

Phone: +1 401-874-5184

Email Address: zheng@uri.edu

**Abstract**

We propose a theoretical concept of a far-field radiative thermal rectification device that uses a phase change material to achieve a high degree of asymmetry in radiative heat transfer. The proposed device has a multilayer structure on one side and a blackbody on other side. The multilayer structure consists of transparent thin film of KBr sandwiched between a thin film of $VO_2$ and a reflecting layer of gold. When $VO_2$ is in its insulating phase, the structure is highly reflective due to the two transparent layers on highly reflective gold. When $VO_2$ is in the metallic phase, Fabry-Perot type of resonance occurs and the tri-layer structure acts like a wide-angle antireflection coating achieved by destructive interference of partially reflected waves making it highly absorptive for majority of spectral range of thermal radiation. The proposed structure forms the active part of configuration that acts like a far-field radiative thermal diode. Thermal rectification greater than 11 is obtained for a temperature bias of 20 K, which is the highest rectification ever predicted for far-field radiative diode configurations.

## 5.1   Introduction

Thermal diode [1], thermal transistors [2], thermal memory element [3] and similar thermal analogues of electronic devices have been topic of theoretical as well as experimental works. While earlier research has been on conduction (phonon) based devices [4, 5, 6, 7, 8], more recent studies have been focusing on radiation (photon) based thermal rectifiers [9, 10, 11, 12]. Thermal rectification has numerous applications in thermal management, thermal logic gates [13, 14, 15] and information processing [16].

Analogous to electrical diode, thermal diode is a rectification device wherein magnitude of heat flux strongly depends on the sign of applied temperature bias. To quantify rectification, we employ the widely used definition of rectification ra-

tio, i.e., $R = (Q_f - Q_r)/Q_r$ where $Q_f$ and $Q_r$ refer to forward and reverse heat flux, respectively [17]. Alternatively, rectification coefficient can be defined as $\eta = (Q_f - Q_r)/max(Q_r, Q_f)$. There are numerous studies pertaining to near-field and far-field thermal radiation based rectification devices that exploit temperature dependent properties of a phase change materials such as vanadium dioxide ($VO_2$) and $La_{0.7}Ca_{0.15}Sr_{0.15}MnO_3$ (LCSMO) [18, 11, 19]. A number of studies deal with far-field thermal radiation [20, 21] while several others focus on modulation of radiative heat transfer in the near-field regime [22, 23, 24, 25, 18, 26, 19]. Ben-Abdallah and Biehs introduced a $VO_2$ based simple far-field radiative thermal diode, while Prodhomme, et al., [27] proposed a far-field thermal transistor that uses a $VO_2$ base between a blackbody collector and a blackbody emitter. Zhu, et al., [28] showed that temperature dependent optical properties of SiC can be used to attain negative differential conductance. Van Zwol, et al., [22] proposed that one can take advantage of the phase transition from crystalline to amorphous state in AIST (an alloy of Ag, In, Sb, and Te) driven by a current pulse to obtain a large contrast in heat flux. In far-field limit, rectification is due to the change in emissive properties of a phase change material. In near-field limit, the difference in the coupling strength of polaritons or tunneling of surface waves between structures leads to thermal rectification. In general, it is observed that a higher rectification can be achieved in the near-field regime than in the far-field. However, it is challenging to develop such devices operating on the principle of near-field radiative transfer. Spectral control has been studied to affect radiative heat transfer in both the far-field as well as near-field. Customization of absorption/emission spectra is often achieved by the use of multilayer thin film structures [29], nanoparticles [30, 31], dielectric mixtures [32, 33], photonic crystals [34, 35], 1-D/2-D gratings [36] and metamaterials [37, 38]. Absorbers that utilize Fabry-Perot cavities [39, 40],
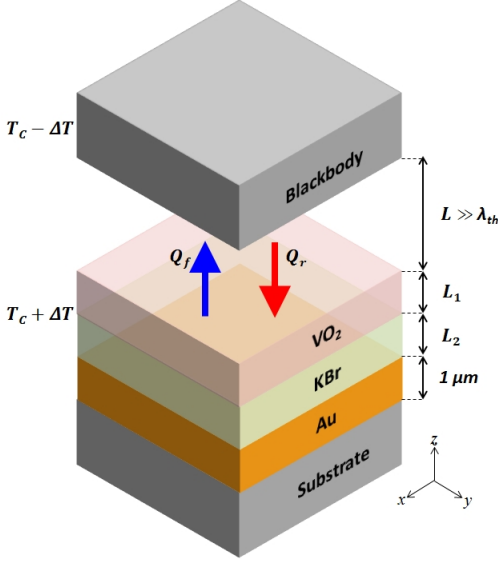
Figure 5.1: Schematic of a far-field thermal diode with a high rectification ratio. The active component has a tri-layer structure consisting of $VO_2$, KBr and gold thin films on a substrate with thicknesses $L_1$, $L_2$ and 1 $\mu$m, respectively. The passive component is a blackbody. $T_c = 341$ K is the phase transition temperature of $VO_2$.

Salibury screens [41] and Jaumann absorbers [42] and ultra-thin lossy thin films bounded by transparent substrate and superstate [43, 44, 45] have been investigated for decades. Quite notably, Nefzaoui, et al., [46] proposed using multilayer structures consisting of thin films (e.g., Si, HDSi and gold) to obtain thermal rectification. Kats, el al., [47] have theoretically and experimentally demonstrated that a thin-film of $VO_2$ on sapphire shows strong modulation of absorbance upon phase transition, particularly, at wavelength of 11.6 $\mu$m. Taylor, et al., [48] recently proposed an emitter consisting a dielectric spacer between $VO_2$ film and a reflecting substrate to achieve dynamic radiative cooling upon phase transition of $VO_2$. Fabry-Perot resonance was achieved at 10 $\mu$m wavelength. As discussed later, we show that, by tuning the resonance at right wavelength, maximum rectification can be achieved in the proposed design.

$VO_2$ has often been used in thermal rectification devices, because its phase-change

from an insulator to a metal can be switched reversibly within a short time ($\sim$100 fs) [49]. The common devices use either a bulk $VO_2$ solid or its thin-film form. In this work, we present a $VO_2$ based far-field thermal rectification device with a simple multilayer structure. We predict a record rectification factor of greater than 11 ($\eta$ >0.91).

A typical far-field thermal diode has two planar components separated by a distance much larger than thermal wavelength. The active component is made of a phase-change solid, whereas the passive component stays inert. Figure 6.1 illustrates the vertical structure of our proposed thermal diode. The active component contains a tri-layer structure consisting of $VO_2$, potassium bromide (KBr) and gold thin films on a substrate. Thicknesses of $VO_2$ and KBr layers can be tuned to maximize rectification. The thickness of gold layer is fixed at 1 $\mu$m to block radiation from the substrate. For a given temperature bias, maximum (far-field) radiative heat transfer would be possible when both sides are blackbodies, while minimum heat transfer would take place when at least one side is a highly reflective mirror. Ideally, the active component should exhibit a transition from blackbody to reflective surface upon the reversal of a temperature bias which induces the phase change. This is exactly our design attempts to achieve. Therefore, the passive component is chosen to be a blackbody. Any material other than a blackbody would not yield maximum rectification. Structure 1 and 2 are at temperature $T_1$ = $T_C + \Delta T$ and $T_2 = T_C - \Delta T$, respectively. The mean temperature is chosen to be the phase transition temperature of $VO_2$ ($T_C$ = 341 K). When $T_1 > T_2$ (referred to as forward bias), $VO_2$ layer is in its metallic phase; and when $T_1 < T_2$ (reverse bias), $VO_2$ layer becomes insulating with its optical axis aligned along the vertical direction, i.e., z-axis.

Phase transition of $VO_2$ is not abrupt [49, 50] and a complete insulator-metal tran-
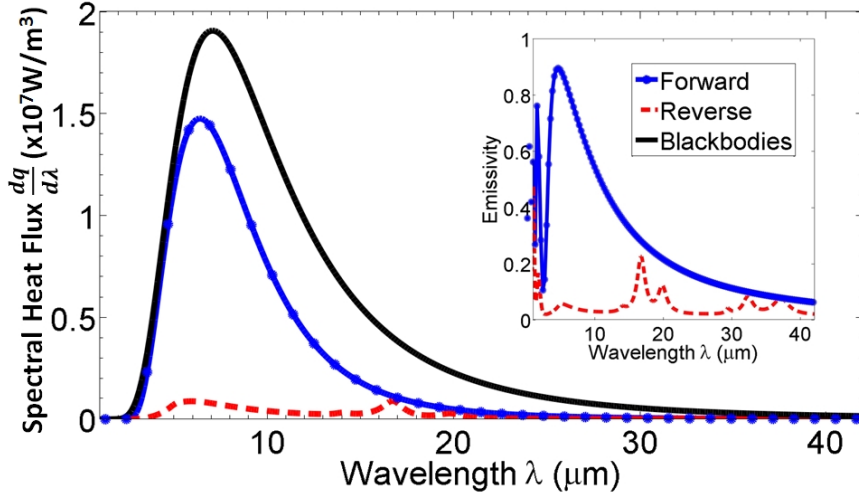
Figure 5.2: Spectral heat flux across the optimized thermal diode in forward and reverse bias scenarios. Spectral heat flux between blackbodies at temperatures 331 K and 351 K is shown for reference. Inset shows hemispherical emissivity of the active component of the diode for the forward and reverse bias.

sition does not occur until 350 K [26]. Rectification ratio depends on temperature bias as the temperature dependence of radiative heat transfer is essentially nonlinear. We calculate rectification values at a minimal temperature bias of 20 K i.e., $\Delta T = \pm 10$ K. Although transition of $VO_2$ exhibits a thermal hysteresis of about 8 K as presented in Ref. [49] and Ref. [51], the phase transition is reversible. As we report heat flux values at 10 K above and below the critical temperature of $VO_2$, hysteresis behavior is beyond the scope of this study.

## 5.2 Results and Discussion

A multilayer structure can be designed to attain high absorbance or reflectance based on its dimensions and material properties. Multilayers with constituent thicknesses much smaller than the incident wavelength of light have been studied before [52]. We show that in a $VO_2$ based multilayer structure, the dramatic change in the optical property of $VO_2$ upon phase-change facilitates an extensive variation in the surface reflectivity.

Concept shown in Fig. 6.1 has variable dimensions of $VO_2$ ($L_1$) and KBr ($L_2$) layer. These dimensions were optimized by running Genetic Algorithm to maximize rectification ratio. MATLAB's optimization toolbox was used to run Genetic Algorithm to perform optimization. Default values of population size (50), fitness scaling (rank), crossover fraction (0.8), stopping criteria (100 generations) were selected in the optimization toolbox. No tuning of optimization parameters was required as number of variables was only two. Lower and upper bounds on both $L_1$ and $L_2$ were kept at 25 nm and 2 $\mu$m, respectively. Optimal dimensions were found to be $L_1 = 25$ nm and $L_2 = 880$ nm, both are practical values. Further discussion will be focused on the design with these dimensions.

Figure 6.2 shows spectral heat flux ($dq/d\lambda$) of the proposed thermal diode in forward and reverse direction with temperature bias 20 K ($\Delta T = 10$ K). Forward heat flux is significantly higher than reverse flux as is clear from Fig. 6.2. A comparison is shown for heat flux across blackbodies at temperatures 331 K and 351 K, respectively. Inset in Fig. 6.2 displays angle-averaged emissivity of the active component in both scenarios. When $VO_2$ is metallic, the structure on the active component has high emissivity near the thermal wavelength ($\lambda_{th} = 1.27\hbar c/k_B T = 8.5$ $\mu$m for 341 K). As a significant portion of blackbody radiation falls within this range, this gives rise to a high heat flux in forward bias. However, when $VO_2$ is insulating, the structure has very low emissivity in the broad spectrum. The tri-layer structure behaves like a highly reflecting mirror resulting in very low heat flux. Consequently, high contrast in heat flow is achieved leading to a high rectification ratio of 11.3 ($\eta = 0.918$). In order to highlight the diode-like characteristics, heat flux across the device has been plotted against themeprature difference in Fig. 6.3. For comparison, simple case of bulk $VO_2$ is also shown, it has a rectification coeffcient of $\eta = 0.49$. Note that, effect of thermal hystersis is not considered here

for simplicity. Angle dependent spectral reflectivity of the active component of the thermal diode is plotted in Fig. 6.4 for the forward and reverse bias cases. When $VO_2$ is metallic, the tri-layer structure acts like a wide-angle antireflection coating for wavelengths between 4 $\mu$m to 10 $\mu$m. The dark spot in Fig. 6.4 corresponds to Fabry-Perot type of resonance that occurs around $\lambda = 4n_{KBr}(\lambda)L_2 = 5.3$ $\mu$m [47]. High absorption/emission in this wavelength region favors radiative heat transfer as thermal wavelength falls within this range. In reverse bias, the structure is highly reflective in a broad range of wavelengths giving rise to a very low absorption. Note that for thermal wavelength of 8.5 $\mu$m, Fabry-Perot resonance occurs (for metallic $VO_2$) when thickness of KBr layer is $L_2 = \lambda_{th}/4n_{KBr}(\lambda_{th}) = 1.4$ $\mu$m. This configuration however, would not necessarily achieve maximum rectification as the structure may not be purely reflecting when $VO_2$ is its insulating phase. Contrasting reflective properties of the structure are due to constructive and de-
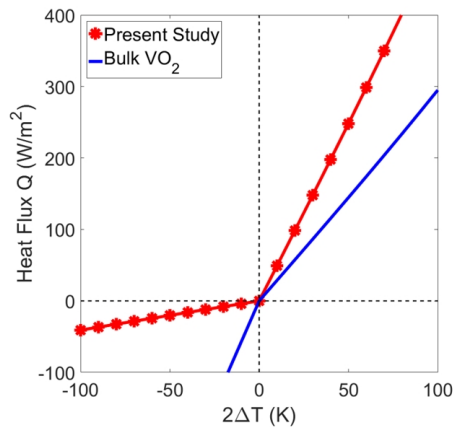


Figure 5.3: Heat flux plotted against temperature difference for thermal diode with bulk $VO_2$ and present structure.
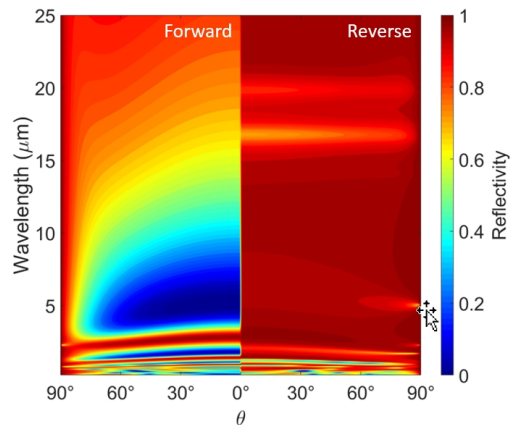
Figure 5.4: Angle dependent reflectivity of the active component of thermal diode plotted against wavelength and angle of incidence under forward and reverse bias.

structive interferences of electromagnetic waves generated by partial reflections at interfaces. As an electromagnetic wave travels through the media, it is partially

reflected at each interface leading to multiple reflections from each layer. This causes interference of electromagnetic waves due to each partial reflection. Effective reflection coefficient of the structure is the phasor sum of these reflection coefficients due to (an infinite number of) individual reflections. When $VO_2$ is metallic, phasor sum of partial reflections results in destructive interference in the wavelength range of 4 $\mu$m to 10 $\mu$m. As a result, the structure is highly absorptive in the range. When $VO_2$ is insulating, individual reflections add up to a large value making the structure highly reflective for a broad range of the spectrum.

Figure 5.5 shows phasor diagram of partial reflections at air-$VO_2$ interface and $VO_2$-KBr interface for TE polarized incident ray of wavelength $\lambda_{th} = 8.5$ $\mu$m and angle of incidence $10°$. $\widetilde{R}_{1,2}$ is the effective reflection coefficient at air-$VO_2$ interface and $\widetilde{R}_{2,3}$ is the effective reflection coefficient at $VO_2$-KBr interface due to multiple reflections within KBr layer. They can be expressed as geometric series whose terms are relative amplitudes of partial waves due to first, second and third reflection and so on. For both metallic as well as insulating $VO_2$, the magnitude of $\widetilde{R}_{2,3}$, $|\widetilde{R}_{2,3}|$, is large. However, when $VO_2$ is in metallic phase, each partial reflection results in a phase-shift such that partial waves add up destructively leading to a small value of $|\widetilde{R}_{1,2}|$ and low reflectivity, especially in the wavelength range centered around thermal wavelength. On the other hand, in reverse bias (insulating $VO_2$) phasors add constructively, giving rise to highly reflective surface properties for a broad range of wavelengths. A similar phenomenon can be observed for TM polarization as well. As KBr is transparent and has a negligible extinction coefficient for most of infrared region, much of the absorption takes place within the $VO_2$ layer. Transparent layer of KBr mainly influences the reflective properties by altering the phase of the light propagating through the media. Potentially, any other material transparent to infrared light such as magnesium fluoride or intrinsic
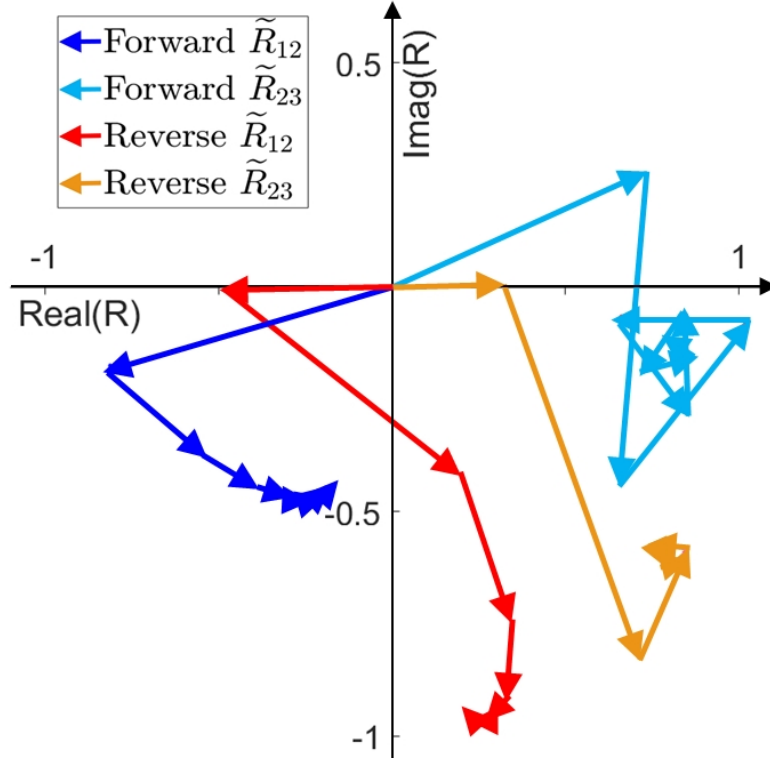
Figure 5.5: Effective reflection coefficient at air-VO$_2$ interface ($\widetilde{R}_{1,2}$) and VO$_2$-KBr interface ($\widetilde{R}_{2,3}$) as phasor sum of reflection coefficients due to each reflection for TE polarized incident plane wave of wavelength $\lambda_{th} = 8.5$ $\mu$m and angle of incidence $10°$

silicon can be used in this concept. However, optimal dimensions of such a device might be different.

In summary, we present a VO$_2$ based far-field radiative thermal diode structure with a high rectification ratio of 11.3. The active component of the proposed device has a tri-layer structure consisting thin films of VO$_2$, KBr and gold. As VO$_2$ undergoes phase change around 341 K, reflecting properties of the surface are dramatically changed in the spectral region that contributes to significant amount of thermal radiation. Facilitated by Fabry-Perot type of resonance around 5.3 $\mu$m, metallic VO$_2$ makes the structure behave like a wide-angle antireflection coating while insulating VO$_2$ makes it highly reflecting. As a result, high degree of asymmetry in radiative heat transfer is predicted across the tri-layer structure

and a blackbody. Contrasting reflecting properties of the structure can be explained using constructive and destructive interference of partial reflections across the interfaces. We optimized layer thicknesses to maximize rectification. Thermal rectification greater than 11 is predicted for temperature difference of 20 K and it is highest among far-field radiative diodes that have been studied. Possibility of attaining higher rectification could be investigated in future by using alternate transparent materials, thinner films of $VO_2$ and/or using more number of alternating $VO_2$/dielectric layers. Such devices can find numerous applications such as thermal logic devices and thermal management systems.

## 5.3   Methods

To calculate heat flux in forward and reverse bias across our far-field thermal diode, we use the well known expression of radiative transfer obtained through dyadic Green's function formalism [53]. Radiative transfer between two planar objects is given by

$$Q_{1\to2}(T_1,T_2,L) = \int_0^\infty \frac{d\omega}{2\pi} [\Theta(\omega,T_1) - \Theta(\omega,T_2)] T_{1\to2}(\omega,L) \qquad (5.1)$$

where $\Theta(\omega,T) = (\hbar\omega/2)\coth(\hbar\omega/2k_BT)$ is the energy of a harmonic oscillator at frequency $\omega$ and temperature $T$, $\hbar$ is the reduced Planck constant, and $k_B$ is the Boltzmann constant. The function $T_{1\to2}(\omega,L)$ corresponds to the spectral transmissivity in radiative transfer between media 1 and 2 with a separation of $L$ and is expressed as [53]

$$T_{1\to2}(\omega,L) = \int_0^{\omega/c} \frac{k_\rho dk_\rho}{2\pi} \sum_{\substack{\mu=TE, \\ TM}} \frac{(1-|\widetilde{R}_{h1}^{(\mu)}|^2)(1-|\widetilde{R}_{h2}^{(\mu)}|^2)}{|1-\widetilde{R}_{h1}^{(\mu)}\widetilde{R}_{h2}^{(\mu)}e^{2jk_{hz}L}|^2} \qquad (5.2)$$

where $\widetilde{R}_{h1}^{(\mu)}$ and $\widetilde{R}_{h2}^{(\mu)}$ are polarized effective reflection coefficients of the two half spaces (calculated in the absence of other half space), $\mu = TE$ (or $TM$) refers to transverse electric (or magnetic) polarization and $k_{hz}$ is the $z$-component of

wavevector in vacuum. Here, $j$ is the imaginary unit. For a structure having $N$-layer media having $(N-1)$ interfaces, by solving the boundary conditions at the interfaces, one can obtain the expression for the generalized reflection coefficient at the interface between regions $i$ and $i+1$ [54],

$$\widetilde{R}_{i,i+1}^{(\mu)} = \frac{R_{i,i+1}^{(\mu)} + \widetilde{R}_{i+1,i+2}^{(\mu)} e^{2jk_{i+1,z}(d_{i+1}-d_i)}}{1 + R_{i,i+1}^{(\mu)} \widetilde{R}_{i+1,i+2}^{(\mu)} e^{2jk_{i+1,z}(d_{i+1}-d_i)}} \qquad (5.3)$$

where $R_{i,i+1}^{(\mu)}$ is the Fresnel reflection coefficient at the interface between the layers $i$ and $i+1$, and $\widetilde{R}_{i+1,i+2}^{(\mu)}$ is the generalized reflection coefficient at the interface between the layers $i+1$ and $i+2$, $z = -d_i$ is the location of the $i$th interface. $k_{i,z} = \sqrt{\varepsilon_i(\omega)\omega^2/c^2 - k_\rho^2}$ is the normal $z$-component of the wave vector in medium $i$, wherein $\varepsilon_i(\omega)$ is the relative permittivity of the medium $i$ as a function of angular frequency $\omega$, $c$ is the speed of light in vacuum and $k_\rho$ is the magnitude of the in-plane wave vector. With $\widetilde{R}_{N,N+1}^{(\mu)} = 0$, the above equation provides a recursive relation to calculate the reflection coefficients $\widetilde{R}_{i,i+1}^{(\mu)}$ in all regions. Note that Eq. 5.2 has only one integral corresponding to propagating waves. The terms due to evanescent waves are ignored as separation between the two half spaces is much larger than the thermal wavelength $(L \gg \lambda_{th})$. The hemispherical emissivity of the active component can be expressed as [32]

$$e(\omega) = \frac{c^2}{\omega^2} \int_0^{\omega/c} dk_\rho k_\rho \sum_{\mu=s,p} (1 - |\widetilde{R}_h^{(\mu)}|^2) \qquad (5.4)$$

Note that the term for tranmissivity has been omitted as a layer of gold makes the structure opaque.

Insulating $VO_2$ (below 341 K) is anisotropic. In a plane $(x-y$ plane in Fig. 6.1) perpendicular to optical axis known as the ordinary mode, its dielectric function is $\varepsilon_O$ and it is $\varepsilon_E$ along the optical axis (extraordinary mode). Both $\varepsilon_O$ and $\varepsilon_E$ can be calculated using the classical oscillator formula $\varepsilon(\omega) = \varepsilon_\infty + \sum_{i=1}^{N} \frac{S_i \omega_i^2}{\omega_i^2 - j\gamma_i\omega - \omega^2}$.

Values of high-frequency constant $\varepsilon_\infty$, phonon frequency $\omega_i$, scattering rate $\gamma_i$ and oscillator strength $S_i$ are taken from Ref. [55]. There are eight phonon modes for ordinary and nine phonon modes for extraordinary dielectric function. In the metallic state, VO$_2$ is isotropic and Drude model [55] is used to describe the dielectric function i.e., $\varepsilon(\omega) = \dfrac{-\omega_p^2 \varepsilon_\infty}{\omega^2 - j\omega\Gamma}$. Refractive indices of KBr are taken from Ref. [56], while dielectric properties of gold can be found in Ref. [57]. Blackbody is assumed to have a constant dielectric function $\varepsilon = 1 + 0.001j$.

**List of References**

[1] B. Li, L. Wang, and G. Casati, "Thermal diode: Rectification of heat flux," *Physical review letters*, vol. 93, no. 18, p. 184301, 2004.

[2] B. Li, L. Wang, and G. Casati, "Negative differential thermal resistance and thermal transistor," *Applied Physics Letters*, vol. 88, no. 14, p. 143501, 2006.

[3] L. Wang and B. Li, "Thermal memory: a storage of phononic information," *Physical review letters*, vol. 101, no. 26, p. 267203, 2008.

[4] W. Kobayashi, Y. Teraoka, and I. Terasaki, "An oxide thermal rectifier," *Applied Physics Letters*, vol. 95, no. 17, p. 171905, 2009.

[5] D. Sawaki, W. Kobayashi, Y. Moritomo, and I. Terasaki, "Thermal rectification in bulk materials with asymmetric shape," *arXiv preprint arXiv:1102.4182*, 2011.

[6] W. Kobayashi, D. Sawaki, T. Omura, T. Katsufuji, Y. Moritomo, and I. Terasaki, "Thermal rectification in the vicinity of a structural phase transition," *Applied Physics Express*, vol. 5, no. 2, p. 027302, 2012.

[7] C. Chang, D. Okawa, A. Majumdar, and A. Zettl, "Solid-state thermal rectifier," *Science*, vol. 314, no. 5802, pp. 1121–1124, 2006.

[8] M. J. Martínez-Pérez, A. Fornieri, and F. Giazotto, "Rectification of electronic heat current by a hybrid thermal diode," *Nature nanotechnology*, vol. 10, no. 4, pp. 303–307, 2015.

[9] P. Ben-Abdallah and S.-A. Biehs, "Near-field thermal transistor," *Physical review letters*, vol. 112, no. 4, p. 044301, 2014.

[10] P. Ben-Abdallah and S.-A. Biehs, "Phase-change radiative thermal diode," *Applied Physics Letters*, vol. 103, no. 19, p. 191907, 2013.

[11] C. R. Otey, W. T. Lau, and S. Fan, "Thermal rectification through vacuum," *Physical Review Letters*, vol. 104, no. 15, p. 154301, 2010.

[12] Z. Chen, C. Wong, S. Lubner, S. Yee, J. Miller, W. Jang, C. Hardin, A. Fong, J. E. Garay, and C. Dames, "A photon thermal diode," *Nature communications*, vol. 5, 2014.

[13] L. Wang and B. Li, "Phononics gets hot," *Phys. World*, vol. 21, pp. 27–29, 2008.

[14] L. Wang and B. Li, "Thermal logic gates: computation with phonons," *Physical review letters*, vol. 99, no. 17, p. 177208, 2007.

[15] P. Ben-Abdallah and S.-A. Biehs, "Towards boolean operations with thermal photons," *Physical Review B*, vol. 94, no. 24, p. 241401, 2016.

[16] N. Li, J. Ren, L. Wang, G. Zhang, P. Hänggi, and B. Li, "Colloquium: Phononics: Manipulating heat flow with electronic analogs and beyond," *Reviews of Modern Physics*, vol. 84, no. 3, p. 1045, 2012.

[17] B. Song, A. Fiorino, E. Meyhofer, and P. Reddy, "Near-field radiative thermal transport: From theory to experiment," *AIP Advances*, vol. 5, no. 5, p. 053503, 2015.

[18] Y. Yang, S. Basu, and L. Wang, "Radiation-based near-field thermal rectification with phase transition materials," *Applied Physics Letters*, vol. 103, no. 16, p. 163101, 2013.

[19] J. Huang, Q. Li, Z. Zheng, and Y. Xuan, "Thermal rectification based on thermochromic materials," *International Journal of Heat and Mass Transfer*, vol. 67, pp. 575–580, 2013.

[20] E. Nefzaoui, K. Joulain, J. Drevillon, and Y. Ezzahri, "Radiative thermal rectification using superconducting materials," *Applied Physics Letters*, vol. 104, no. 10, p. 103905, 2014.

[21] K. Joulain, Y. Ezzahri, J. Drevillon, and P. Ben-Abdallah, "Modulation and amplification of radiative far field heat transfer: Towards a simple radiative thermal transistor," *Applied Physics Letters*, vol. 106, no. 13, p. 133505, 2015.

[22] P. Van Zwol, K. Joulain, P. Ben-Abdallah, J.-J. Greffet, and J. Chevrier, "Fast nanoscale heat-flux modulation with phase-change materials," *Physical Review B*, vol. 83, no. 20, p. 201404, 2011.

[23] P. Van Zwol, L. Ranno, and J. Chevrier, "Tuning near field radiative heat flux through surface excitations with a metal insulator transition," *Physical review letters*, vol. 108, no. 23, p. 234301, 2012.

[24] F. Menges, M. Dittberner, L. Novotny, D. Passarello, S. Parkin, M. Spieser, H. Riel, and B. Gotsmann, "Thermal radiative near field transport between vanadium dioxide and silicon oxide across the metal insulator transition," *Applied Physics Letters*, vol. 108, no. 17, p. 171904, 2016.

[25] A. Ghanekar, J. Ji, and Y. Zheng, "High-rectification near-field thermal diode using phase change periodic nanostructure," *Applied Physics Letters*, vol. 109, no. 12, p. 123106, 2016.

[26] Y. Yang, S. Basu, and L. Wang, "Vacuum thermal switch made of phase transition materials considering thin film and substrate effects," *Journal of Quantitative Spectroscopy and Radiative Transfer*, vol. 158, pp. 69–77, 2015.

[27] H. Prod'homme, J. Ordonez-Miranda, Y. Ezzahri, J. Drevillon, and K. Joulain, "Optimized thermal amplification in a radiative transistor," *Journal of Applied Physics*, vol. 119, no. 19, p. 194502, 2016.

[28] L. Zhu, C. R. Otey, and S. Fan, "Negative differential thermal conductance through vacuum," *Applied Physics Letters*, vol. 100, no. 4, p. 044104, 2012.

[29] K.-T. Lee, C. Ji, and L. J. Guo, "Wide-angle, polarization-independent ultra-thin broadband visible absorbers," *Applied Physics Letters*, vol. 108, no. 3, p. 031107, 2016.

[30] Y. Zheng and A. Ghanekar, "Radiative energy and momentum transfer for various spherical shapes: A single sphere, a bubble, a spherical shell, and a coated sphere," *Journal of Applied Physics*, vol. 117, no. 6, p. 064314, 2015.

[31] L. Zhu, C. R. Otey, and S. Fan, "Ultrahigh-contrast and large-bandwidth thermal rectification in near-field electromagnetic thermal transfer between nanoparticles," *Physical Review B*, vol. 88, no. 18, p. 184301, 2013.

[32] A. Ghanekar, L. Lin, J. Su, H. Sun, and Y. Zheng, "Role of nanoparticles in wavelength selectivity of multilayered structures in the far-field and near-field regimes," *Optics Express*, vol. 23, no. 19, pp. A1129–A1139, 2015.

[33] A. Ghanekar, L. Lin, and Y. Zheng, "Novel and efficient mie-metamaterial thermal emitter for thermophotovoltaic systems," *Optics express*, vol. 24, no. 10, pp. A868–A877, 2016.

[34] V. Rinnerbauer, A. Lenert, D. M. Bierman, Y. X. Yeng, W. R. Chan, R. D. Geil, J. J. Senkevich, J. D. Joannopoulos, E. N. Wang, M. Soljačić, *et al.*, "Metallic photonic crystal absorber-emitter for efficient spectral control in high-temperature solar thermophotovoltaics," *Advanced Energy Materials*, vol. 4, no. 12, 2014.

[35] J. B. Chou, Y. X. Yeng, A. Lenert, V. Rinnerbauer, I. Celanovic, M. Soljačić, E. N. Wang, and S.-G. Kim, "Design of wide-angle selective absorbers/emitters with dielectric filled metallic photonic crystals for energy applications," *Optics express*, vol. 22, no. 101, pp. A144–A154, 2014.

[36] S.-A. Biehs, F. S. Rosa, and P. Ben-Abdallah, "Modulation of near-field heat transfer between two gratings," *Applied Physics Letters*, vol. 98, no. 24, p. 243102, 2011.

[37] N. I. Zheludev and Y. S. Kivshar, "From metamaterials to metadevices," *Nature materials*, vol. 11, no. 11, pp. 917–924, 2012.

[38] N. Yu and F. Capasso, "Flat optics with designer metasurfaces," *Nature materials*, vol. 13, no. 2, pp. 139–150, 2014.

[39] M. S. Ünlü and S. Strite, "Resonant cavity enhanced photonic devices," *Journal of Applied Physics*, vol. 78, no. 2, pp. 607–639, 1995.

[40] K. Kishino, M. S. Unlu, J.-I. Chyi, J. Reed, L. Arsenault, and H. Morkoc, "Resonant cavity-enhanced (rce) photodetectors," *IEEE Journal of Quantum Electronics*, vol. 27, no. 8, pp. 2025–2034, 1991.

[41] R. L. Fante and M. T. Mccormack, "Reflection properties of the salisbury screen," *IEEE transactions on antennas and propagation*, vol. 36, no. 10, pp. 1443–1454, 1988.

[42] Y. RaDi, C. Simovski, and S. Tretyakov, "Thin perfect absorbers for electromagnetic waves: theory, design, and realizations," *Physical Review Applied*, vol. 3, no. 3, p. 037001, 2015.

[43] H. Bosman, Y. Lau, and R. Gilgenbach, "Microwave absorption on a thin film," *Applied Physics Letters*, vol. 82, no. 9, pp. 1353–1355, 2003.

[44] C. Hägglund, S. P. Apell, and B. Kasemo, "Maximized optical absorption in ultrathin films and its application to plasmon-based two-dimensional photovoltaics," *Nano letters*, vol. 10, no. 8, pp. 3135–3141, 2010.

[45] M. Pu, Q. Feng, M. Wang, C. Hu, C. Huang, X. Ma, Z. Zhao, C. Wang, and X. Luo, "Ultrathin broadband nearly perfect absorber with symmetrical coherent illumination," *Optics express*, vol. 20, no. 3, pp. 2246–2254, 2012.

[46] E. Nefzaoui, J. Drevillon, Y. Ezzahri, and K. Joulain, "Simple far-field radiative thermal rectifier using fabry–perot cavities based infrared selective emitters," *Applied optics*, vol. 53, no. 16, pp. 3479–3485, 2014.

[47] M. A. Kats, D. Sharma, J. Lin, P. Genevet, R. Blanchard, Z. Yang, M. M. Qazilbash, D. Basov, S. Ramanathan, and F. Capasso, "Ultra-thin perfect absorber employing a tunable phase change material," *Applied Physics Letters*, vol. 101, no. 22, p. 221101, 2012.

[48] S. Taylor, Y. Yang, and L. Wang, "Vanadium dioxide based fabry-perot emitter for dynamic radiative cooling applications," *Journal of Quantitative Spectroscopy and Radiative Transfer*, 2017.

[49] M. Qazilbash, M. Brehm, G. Andreev, A. Frenzel, P.-C. Ho, B.-G. Chae, B.-J. Kim, S. J. Yun, H.-T. Kim, A. Balatsky, and O. Shpyrko, "Infrared spectroscopy and nano-imaging of the insulator-to-metal transition in vanadium dioxide," *Physical Review B*, vol. 79, no. 7, p. 075107, 2009.

[50] A. Frenzel, M. M. Qazilbash, M. Brehm, B.-G. Chae, B.-J. Kim, H.-T. Kim, A. Balatsky, F. Keilmann, and D. Basov, "Inhomogeneous electronic state near the insulator-to-metal transition in the correlated oxide vo 2," *Physical Review B*, vol. 80, no. 11, p. 115115, 2009.

[51] J. Ordonez-Miranda, Y. Ezzahri, J. Drevillon, and K. Joulain, "Transistor-like device for heating and cooling based on the thermal hysteresis of vo 2," *Physical Review Applied*, vol. 6, no. 5, p. 054003, 2016.

[52] M. A. Kats and F. Capasso, "Optical absorbers based on strong interference in ultra-thin films (laser photonics rev. 10 (5)/2016)," *Laser & Photonics Reviews*, vol. 10, no. 5, pp. 699–699, 2016.

[53] A. Narayanaswamy and Y. Zheng, "A Green's function formalism of energy and momentum transfer in fluctuational electrodynamics," *Journal of Quantitative Spectroscopy and Radiative Transfer*, vol. 132, pp. 12–21, 2014.

[54] W. C. Chew, *Waves and fields in inhomogeneous media.* IEEE press, 1995.

[55] A. Barker Jr, H. Verleur, and H. Guggenheim, "Infrared optical properties of vanadium dioxide above and below the transition temperature," *Physical Review Letters*, vol. 17, no. 26, p. 1286, 1966.

[56] H. Li, "Refractive index of alkali halides and its wavelength and temperature derivatives," *Journal of physical and chemical reference data*, vol. 5, no. 2, pp. 329–528, 1976.

[57] P. B. Johnson and R.-W. Christy, "Optical constants of the noble metals," *Physical Review B*, vol. 6, no. 12, p. 4370, 1972.

**MANUSCRIPT 6**

**High-rectification Near-field Thermal Diode Using Phase Change Periodic Nanostructure**

by

Alok Ghanekar[1], Jun Ji[2], and Yi Zheng[1]

[1] Department of Mechanical, Industrial and Systems Engineering, University of Rhode Island,

Kingston, RI 02881, USA

[2] Department of Marine Engineering, Merchant Marine College, Shanghai Maritime University,

Shanghai, 201306, China

Corresponding Author: Yi Zheng

Department of Mechanical, Industrial and Systems Engineering

University of Rhode Island

Kingston, RI 02881, USA

Phone: +1 401-874-5184

Email Address: zheng@uri.edu

**Abstract**

We theoretically demonstrate workings of a near-field thermal rectification device that uses a phase change material to achieve asymmetry in radiative heat transfer. We exploit the temperature dependent dielectric properties of $VO_2$ due to metal-insulator transition near 341 K. Analogous to an electrical diode, heat transfer coefficient is high in one direction while it is considerably small when the polarity of temperature gradient is reversed. We show that thermal rectification can be greatly enhanced by using 1-D rectangular and triangular $VO_2$ surface gratings. With the introduction of periodic grating, rectification ratio is dramatically enhanced in the near-field due to reduced tunneling of surface waves across the interfaces for negative polarity. Our calculations predict that for minimal temperature difference of 20 K, rectification ratio as high as 16 can be obtained and it is maximum in existing literature for comparable operating temperatures and separation.

## 6.1   Introduction

The idea of thermal rectification devices such as thermal diode [1] and thermal equivalents of electronic devices such as thermal transistors [2] and memory element [3] has been around for more than a decade. These conduction (phonon) based thermal rectifiers have some limitations due to speed of acoustic phonons, presence of Kapitza resistances and nonlinear phonon-phonon interaction [4, 5]. Devices that utilize property of temperature dependent thermal conductivity [6, 7, 8] and solid state thermal rectifiers [9, 10] have also been demonstrated. Components based on thermal radiation (photons) have also been proposed [5, 11, 12, 13]. In this letter, we discuss radiative thermal rectification devices, which are contactless and do not suffer from above mentioned limitations [14]. They also have weaker nonlinearity [12]. Moreover, physics of thermal transport remains unchanged close and far from equilibrium in photonic devices [4]. Apart from thermal management and energy

storage, these thermal analogues of electronic devices could find applications in thermal circuits [15], thermal logic gates [16] and information processing [17]. Thermal diode is a device that is analogous to electrical diode and has a high degree of asymmetry in the magnitude of heat flow depending on the applied temperature bias. To gauge rectification, we use the widely used definition of rectification ratio, i.e. $R = (Q_f - Q_r)/Q_r$ where $Q_f$ and $Q_r$ refer to forward and reverse heat flux respectively [18]. The goal is to increase $R$ as much as possible so that $Q_f \gg Q_r$ and rectification is reasonably high to be utilized in a practical device. Studies pertaining to rectification devices other than thermal diodes also deal with achieving manipulation of heat flux. Most thermal rectification devices exploit temperature dependent properties of phase change materials by focusing on the use of bulk materials or thin-films to achieve thermal rectification. Non-contact rectification devices utilize change in dielectric properties of materials such as vanadium dioxide $(VO_2)$ and $La_{0.7}Ca_{0.15}Sr_{0.15}MnO_3$ (LCSMO) [19, 12, 20]. In far-field, rectification is due to change in emissive properties of a phase change structure. In near-field, difference in the degree of tunneling of surface waves between structures leads to thermal rectification. Consequently higher rectification can be achieved in the near-field regime. Zhu et al [21] utilized temperature dependent optical properties of SiC to put forward a method to attain negative differential conductance. Zwol et al [22] proposed rapid modulation of near-field radiative heat flux at a distance of 100 nm that utilizes fast transition in crystalline and amorphous states of AIST (an alloy of silver, indium, antimony and tellurium) that can be achieved using a current pulse. Zwol et al [23] and Menges et al [24] have experimentally demonstrated that phase change of $VO_2$ results in change of surface polariton states and significantly alters near-field radiative heat transfer. It has been theoretically calculated that bulk $VO_2$ and $SiO_2$ can achieve thermal rectification ratio of about
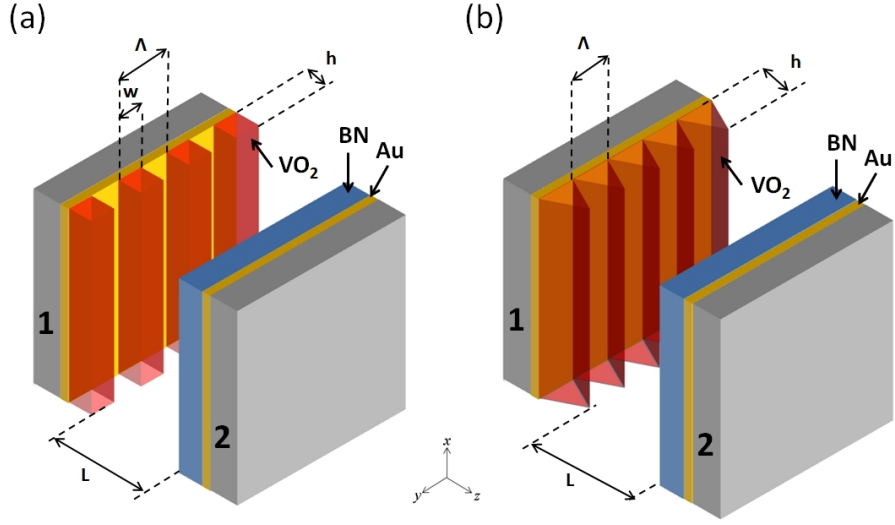
Figure 6.1: Schematics of near-field thermal diodes. (a) Active side has top layer of 1-D rectangular grating made of $VO_2$ of height $h$, width $w$, period $\Lambda$ and filling ratio $\phi$ on a gold layer deposited on a substrate. (b) Rectangular grating is replaced by a triangular one of height $h$ and period $\Lambda$. Passive counterpart of both designs consists of a BN layer on gold on the top of a substrate.

2 at a gap of 10 nm [19]. Yang et al [25] also proposed a $VO_2$ based near-field radiative thermal switch whose switching factor can reach up to 80% for gap of 10 nm. Using a combination of two phase change materials - $VO_2$ and LCSMO, Huang et al [20] achieved the rectification ratio of 7.7 at a gap of 10 nm, hot and cold temperatures being 80 K and 25 K, respectively.

Present study focuses on rectification in a near-field thermal diode and employs $VO_2$ as phase-transition material. $VO_2$ can be switched reversibly in a very short amount of time ($\sim$ 100 fs) from an insulating state to a metallic state [26]. To increase the rectification, one may try to use different materials. It has been observed that metamaterials such as mixtures of dielectric materials [27] and grating structures [28] can manipulate radiative transfer in near-field. Therefore they are candidates for enhancement of thermal rectification. Previous studies mainly dealt with bulk materials and thin films. Our calculations indicate that rectification ratio (key results shown in Fig. 6.2) can be raised significantly by using 1-D surface

gratings of $VO_2$.

A typical near-field thermal diode has two planar structures at a distance less than thermal wavelength [19]. One structure (hereafter referred to as active side) has a phase change material and its counterpart has fixed material properties (passive side). Figure 6.1 introduces the two concepts of thermal diode proposed in this letter that consists of two structures at a distance of $L = 100$ nm. In both concepts, structure 1 (active side) contains top layer of phase change material $VO_2$ at temperature $T_1 = 341$ K $+ \Delta T$. On the passive side, structure 2 has its temperature $T_2 = 341$ K $- \Delta T$. Mean temperature is chosen to be the phase transition temperature of $VO_2$ at 341 K. When $T_1 > T_2$ (referred to as forward bias), $VO_2$ layer is in metallic phase; when $T_1 < T_2$ (reverse bias), $VO_2$ layer is in insulator phase with its optical axis aligned along the distance between them. Proposed configurations will be discussed in more details along with results.

Phase transition of $VO_2$ is not homogeneous and it happens gradually along temeprature [26, 29]. Hence, transition from insulator to metallic phase should be considered complete only at 350 K [25]. We calculate rectification values at a minimal temperature difference of 20 K ($\Delta T = \pm 10$ K), as it reflects intrinsic properties of the proposed device around anchoring temperature. As the temperature dependence of radiative heat transfer is essentially non-linear, rectification ratio is a function of temperature difference (bias). It has been observed before that rectification ratio generally increases with bias near the anchoring temperature [11]. Higher rectification ratios have been predicted earlier, but mostly at larger biases and gaps smaller than 100 nm [19, 12, 20, 21, 22, 25]. The proposed concepts in this letter exhibit highest rectification ratio in the existing literature for comparable operating conditions and separations.

## 6.2 Theoretical Fundamentals

To calculate heat flux for forward and reverse bias across near-field thermal diode, we use the well known expression of near-field radiative transfer obtained through dyadic Green's function formalism [30]. Radiative transfer between closely spaced objects can be calculated by

$$Q_{1 \to 2}(T_1, T_2, L) = \int_0^\infty \frac{d\omega}{2\pi} [\Theta(\omega, T_1) - \Theta(\omega, T_2)] T_{1 \to 2}(\omega, L) \tag{6.1}$$

where $\Theta(\omega, T) = (\hbar\omega/2) \coth(\hbar\omega/2k_B T)$ is the energy of harmonic oscillator at frequency $\omega$ and temperature $T$, $\hbar$ is the reduced Planck constant, and $k_B$ is the Boltzmann constant. The function $T_{1 \to 2}(\omega, L)$ is known as the spectral transmissivity in radiative transfer between media 1 and 2 separated of distance $L$ [25, 27, 28, 30].

As our proposed designs involve 1-D grating structure of VO$_2$ in vacuum, we use second order approximation of effective medium theory to obtain the dielectric properties given by the expressions [31, 32, 33]

$$\varepsilon_{TE,2} = \varepsilon_{TE,0} \left[ 1 + \frac{\pi^2}{3} \left( \frac{\Lambda}{\lambda} \right)^2 \phi^2 (1 - \phi)^2 \frac{(\varepsilon_A - \varepsilon_B)^2}{\varepsilon_{TE,0}} \right] \tag{6.2a}$$

$$\varepsilon_{TM2} = \varepsilon_{TM0} \left[ 1 + \frac{\pi^2}{3} \left( \frac{\Lambda}{\lambda} \right)^2 \phi^2 (1 - \phi)^2 (\varepsilon_A - \varepsilon_B)^2 \varepsilon_{TE,0} \left( \frac{\varepsilon_{TM0}}{\varepsilon_A \varepsilon_B} \right)^2 \right] \tag{6.2b}$$

where $\varepsilon_A$ and $\varepsilon_B$ are dielectric functions of the two materials (VO$_2$ and vacuum) in surface gratings, $\lambda$ is the wavelength, $\Lambda$ is grating period and filling ratio $\phi = w/\Lambda$ where $w$ is width of VO$_2$ segment . The expressions for zeroth order effective dielectric functions $\varepsilon_{TE,0}$ and $\varepsilon_{TM,0}$ are given by [34, 31]

$$\varepsilon_{TE,0} = \phi\varepsilon_A + (1 - \phi)\varepsilon_B \tag{6.3a}$$

$$\varepsilon_{TM,0} = \left( \frac{\phi}{\varepsilon_A} + \frac{1 - \phi}{\varepsilon_B} \right)^{-1} \tag{6.3b}$$

For triangular gratings as shown in Fig. 6.1(b), gratings can be treated as a composition of multiple layers of rectangular gratings each having decreasing filling ratio and period equal to that of parent grating [34]. We confirm that slicing the triangular structure into 100 layers is sufficient to achieve converging values of near-field heat flux.

Effective medium approximation (EMA) holds true when grating period is much less than wavelength of interest [33]. As this study deals with temperatures around 341 K, grating period (50 nm) is much less than the thermal wavelength ($\sim 8.5$ $\mu$m). Thus the condition of EMA is satisfied. When dealing with near-field radiative transfer pertaining to periodic gratings, criterion for the validity of EMA is somewhat different and effective medium theory holds true as long as gap between the planar structures (100 nm in this case) is greater than the grating period [35] (see discussions about dashed lines in Fig. 6.2).

VO$_2$ in insulator state (below 341 K) is anisotropic. In a plane perpendicular to optical axis ($x - y$ plane in our case) known as ordinary mode, its dielectric function is $\varepsilon_O$ and it is $\varepsilon_E$ along the optical axis ($z$ axis, extraordinary mode). Both $\varepsilon_O$ and $\varepsilon_E$ can be calculated using classical oscillator formula $\varepsilon(\omega) = \varepsilon_\infty + \sum_{i=1}^{N} \dfrac{S_i \omega_i^2}{\omega_i^2 - j\gamma_i \omega - \omega^2}$. Experimental values of high-frequency constant $\varepsilon_\infty$, phonon frequency $\omega_i$, scattering rate $\gamma_i$ and oscillator strength $S_i$ can be found in Ref. [36]. Here, $j$ is the imaginary unit. There exist eight phonon modes for ordinary and nine phonon modes for extraordinary dielectric function. In metallic state, VO$_2$ is isotropic and Drude model [36] is used to describe the dielectric function that is given by $\varepsilon(\omega) = \dfrac{-\omega_p^2 \varepsilon_\infty}{\omega^2 - j\omega\Gamma}$. Dielectric function for BN [37] is of the form $\varepsilon(\omega) = \varepsilon_\infty \dfrac{(\omega^2 - \omega_{LO}^2 + j\omega\gamma)}{(\omega^2 - \omega_{TO}^2 + j\omega\gamma)}$. Here $\omega_{TO}$ and $\omega_{LO}$ are transverse and longitudinal optical phonon frequencies and $\gamma$ is the damping constant. The values of $\varepsilon_\infty$, $\omega_{TO}$, $\omega_{LO}$ and $\gamma$ for BN are 4.46, 0.1309 eV, 0.1616 eV and $6.55 \times 10^{-4}$ eV respectively.
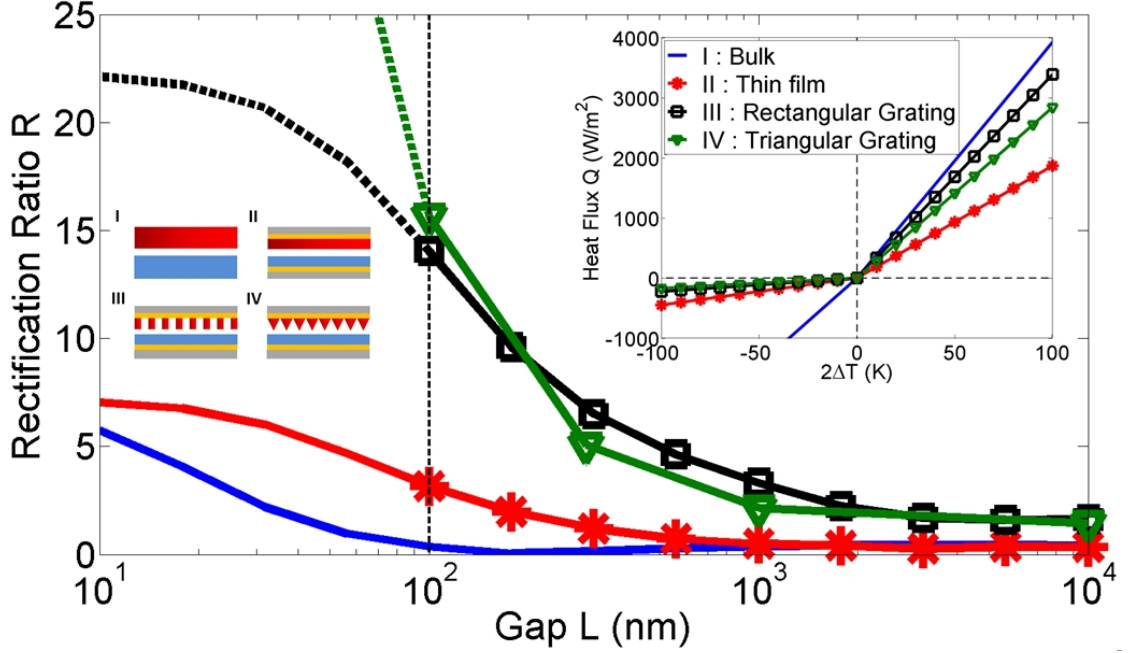
Figure 6.2: Gap-dependent rectification ratio for different thermal diode configurations. Passive structures are (I): Bulk BN, and (II), (III), (IV): 1 $\mu$m layer of BN over 1 $\mu$m layer of gold on a substrate. Active structures are (I): Bulk $VO_2$, (II): 1 $\mu$m layer of $VO_2$ on the top of 1 $\mu$m layer of gold on a substrate, (III): Rectangular 1-D grating of $VO_2$ with thickness $h$=0.5 $\mu$m, period $\Lambda$=50 nm and filling ratio $\phi$=0.3, (IV): Triangular grating of $VO_2$ with height $h$=0.5 $\mu$m and period $\Lambda$=50 nm. Inset figure shows heat flux as a function of temperature difference at 100 nm separation to highlight diode-like characteristics of different configurations.

Dielectric properties of gold can be found in Ref. [38].

## 6.3 Results

In order to explain the results of our calculations for the proposed designs shown in Fig. 6.1 we plot rectification ratio against gap for four different configurations in Fig. 6.2 for the temperature difference of 20 K ($\Delta T = \pm 10$ K). Before discussing the main design (Fig. 6.1(a)) we consider the simplistic case which consists of bulk $VO_2$ on active side and bulk BN on passive side (case I). As insulator $VO_2$ and metallic $VO_2$ have different optical properties, one expects to observe some degree of asymmetry in heat flow. Such a configuration exhibits weak rectification which gradually increases at smaller gaps when surface waves become dominant. Next

we consider using thin films. In case II, the active side has 1 $\mu$m layer of VO$_2$ over 1 $\mu$m thick gold and the passive side has 1 $\mu$m layer of BN on the top of 1 $\mu$m gold. 1 $\mu$m thick layer of gold is sufficient to block radiation from the substrate and to support the top layer as free standing thin layer is not practical [39]. This design shows an increased near-field rectification, far-field rectification being about the same. Rectification is stronger in near-field because of the asymmetry in heat flux due to different levels of tunneling of surface waves across the two interfaces. We now consider case III where thin film of VO$_2$ is replaced by a 1-D grating structure of height $h = 0.5$ $\mu$m, period $\Lambda = 50$ nm and filling ratio $\phi = 0.3$. The passive side remains the same as in case II. This configuration shows a significant enhancement in rectification and rectification value reaches around 14 at the gap of 100 nm. Figure 6.2 also shows dependence of rectification ratio on gap for an alternative design (case IV) depicted in Fig. 6.1(b). This design has a 1-D triangular structure of height $h = 0.5$ $\mu$m and period $\Lambda = 50$ nm on active side. While this structure shows a similar trend as case III, a sharp increase in rectification ratio can be seen at smaller gaps. Rectification ratio of 16 is reached at 100 nm gap. Although results for the distances smaller than 100 nm may not be accurate completely as gap becomes comparable to the grating period (displayed using dashed lines in Fig. 6.2). The trend is noteworthy for the triangular structure (case IV) as rectification ratio keeps increasing to higher values for shorter distances. Further investigations for triangular grating are beyond the scope of this study and left for future work. Numerical methods such as Wiener chaos expansion method [40] can be employed for calculation of near-field heat flux for distances shorter than the grating period. Figure 6.2 inset displays heat flux versus temperature difference for the four cases studied. Difference between slopes for forward and reverse bias is obvious. Diode-like characteristics are apparent especially for designs based on
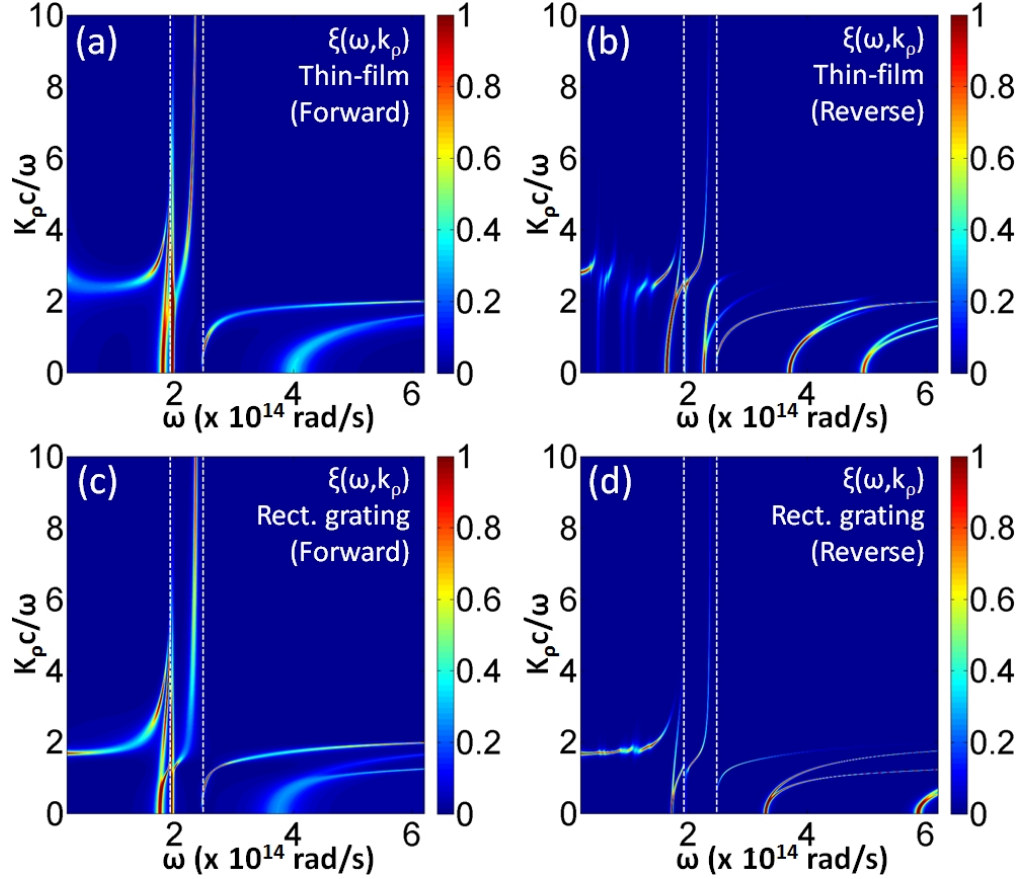
Figure 6.3: Coefficient of energy transmission $\xi(\omega, k_\rho)$ across the the two interfaces of thermal diode plotted against angular frequency $\omega$ and normalized parallel wavevector $k_\rho c/\omega$ for (a) case II: forward bias, (b) case II: reverse bias, (c) case III: forward bias, and (d) case III: reverse bias.

rectangular and triangular gratings. Different materials such as $SiO_2$, SiC, BN, gold and polystyrene and structures (thin film or bulk) can be used on passive side and strongly influence rectification. When 1 $\mu$m layer of BN is used over reflecting gold surface on passive side, it results in maximum rectification for case II. The choice of passive structure used here may not remain optimal when active structure is modified. In order to emphasize the effect of 1-D gratings on active side, we use the same structure on passive side for cases II, III and IV.

To illustrate why grating structure enhances the thermal rectification, we plot energy transmission coefficient $\xi(\omega, k_\rho)$ across the interfaces of thermal diode for case II (Figs. 6.3(a) and 6.3(b)) and Case III (Figs. 6.3(c) and 6.3(d)) at a gap of
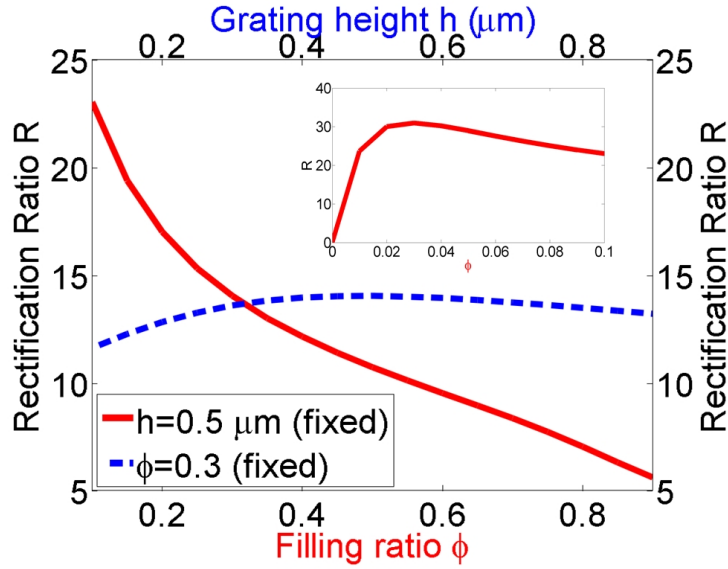
Figure 6.4: Effect of design parameters (filling ratio $\phi$ and grating height $h$) on the rectification ratio of thermal diode using rectangular gratings. Inset figure shows variation of rectification ratio near zero filling ratio. (Horizontal axis in main figure starts at 0.1.)

100 nm. Here $k_\rho c/\omega$ is normalized parallel wavevector. For both cases, transmission coefficient is close to unity for forward bias well beyond light line ($k_\rho c/\omega = 1$). Transmission is high for two prominent frequencies that are close to characteristic wavelengths of BN (7.6 $\mu$m and 9.8 $\mu$m), as shown by dashed lines. Since metallic VO$_2$ does not support surface phonon polariton in the infrared region [25], near-field radiative transfer is mainly attributed to the symmetric and antisymmetric surface phonons supported by the BN layer ($k_\rho c/\omega \gg 1$ in Fig. 6.3). In addition, there exists a secondary contribution due to Fabry-Perot modes and frustrated modes ($k_\rho c/\omega \approx 1$) in the near-field regime. High energy transmission in forward bias is due to tunneling of surface waves across interfaces. In reverse bias, although both BN and insulator VO$_2$ support surface phonon modes, they do not overlap and near-field radiative transfer is dominated by non-resonant surface waves. In addition, surface phonons of insulator VO$_2$ occur in frequency range where BN has low extinction coefficient ($\kappa \approx 0$), and vice versa. As a result, tunneling between

100

BN and insulator $VO_2$ is much weaker than that of BN and metallic $VO_2$, that leads to thermal rectification. We note that when thin film of $VO_2$ is replaced by a 1-D rectangular grating, transmission coefficient for reverse bias is reduced as seen in Figs. 6.3(b) and 6.3(d). Reduction in transmission coefficient comes from the presence of grating which suppresses the tunneling of surface waves supported by insulator $VO_2$ and BN. Tunneling between BN and metallic $VO_2$ however is relatively unchanged (Figs. 6.3(a) and 6.3(c)). Consequently, a higher rectification is achieved. Resulting difference in spectral heat fluxes can also be observed.

We analyze possible parameters that can influence the rectification for the design using 1-D rectangular grating (case III) for a gap of 100 nm in Fig. 6.4. Filling ratio is fixed to 0.3 and the grating height is varied from 0.1 to 0.9 $\mu$m (dashed line). We observe that peak rectification ratio is achieved when grating height is around 0.5 $\mu$m. Solid line in Fig. 6.4 shows variation in filling ratio for fixed grating height of 0.5 $\mu$m. Dependence of rectification on filling ratio is clearly stronger, as it directly affects the optical properties of grating structure therefore influencing the surface waves across the interfaces. For higher filling ratios, rectification values are lower, and understandably, are close to what is predicted for a thin film design (case II). Thermal rectification even higher than 20 can be predicted at smaller filling ratios. Rectification reaches maximum value when filling ratio is around 0.03, and it becomes zero when filling ratio is zero (Fig. 4 inset). However, filling ratio of 0.03 is impractical as grating period is 50 nm. Another parameter of interest would be grating period. Since we focus on gap of 100 nm we have to limit ourselves to periods less than 100 nm. As the period is much smaller than the dominant thermal wavelength, it has virtually no effect on rectification.

Thus we have demonstrated that an enhanced thermal rectification can be achieved using 1-D grating of phase change material $VO_2$. Our calculations indicate that

a reasonably high value of rectification ratio ($\sim 16$) can be obtained at a gap of 100 nm. Rectification ratio can be optimized by tuning parameters such as grating height and especially, filling ratio. Materials and structures on passive side also play a significant role in the rectification. Improved rectification is attributed to reduced tunneling of surface waves across the interfaces for reverse bias. Rectification ratio can be further increased to much higher values for distance shorter than 100 nm and it is a viable candidate for future investigations.

## Acknowledgments

## List of References

[1] B. Li, L. Wang, and G. Casati, "Thermal diode: Rectification of heat flux," *Physical review letters*, vol. 93, no. 18, p. 184301, 2004.

[2] B. Li, L. Wang, and G. Casati, "Negative differential thermal resistance and thermal transistor," *Applied Physics Letters*, vol. 88, no. 14, p. 143501, 2006.

[3] L. Wang and B. Li, "Thermal memory: a storage of phononic information," *Physical review letters*, vol. 101, no. 26, p. 267203, 2008.

[4] P. Ben-Abdallah and S.-A. Biehs, "Contactless heat flux control with photonic devices," *AIP Advances*, vol. 5, no. 5, p. 053502, 2015.

[5] P. Ben-Abdallah and S.-A. Biehs, "Near-field thermal transistor," *Physical review letters*, vol. 112, no. 4, p. 044301, 2014.

[6] W. Kobayashi, Y. Teraoka, and I. Terasaki, "An oxide thermal rectifier," *Applied Physics Letters*, vol. 95, no. 17, p. 171905, 2009.

[7] D. Sawaki, W. Kobayashi, Y. Moritomo, and I. Terasaki, "Thermal rectification in bulk materials with asymmetric shape," *arXiv preprint arXiv:1102.4182*, 2011.

[8] W. Kobayashi, D. Sawaki, T. Omura, T. Katsufuji, Y. Moritomo, and I. Terasaki, "Thermal rectification in the vicinity of a structural phase transition," *Applied Physics Express*, vol. 5, no. 2, p. 027302, 2012.

[9] C. Chang, D. Okawa, A. Majumdar, and A. Zettl, "Solid-state thermal rectifier," *Science*, vol. 314, no. 5802, pp. 1121–1124, 2006.

[10] M. J. Martínez-Pérez, A. Fornieri, and F. Giazotto, "Rectification of electronic heat current by a hybrid thermal diode," *Nature nanotechnology*, vol. 10, no. 4, pp. 303–307, 2015.

[11] P. Ben-Abdallah and S.-A. Biehs, "Phase-change radiative thermal diode," *Applied Physics Letters*, vol. 103, no. 19, p. 191907, 2013.

[12] C. R. Otey, W. T. Lau, and S. Fan, "Thermal rectification through vacuum," *Physical Review Letters*, vol. 104, no. 15, p. 154301, 2010.

[13] Z. Chen, C. Wong, S. Lubner, S. Yee, J. Miller, W. Jang, C. Hardin, A. Fong, J. E. Garay, and C. Dames, "A photon thermal diode," *Nature communications*, vol. 5, 2014.

[14] S. Dyakov, J. Dai, M. Yan, and M. Qiu, "Near field thermal memory device," *arXiv preprint arXiv:1408.5831*, 2014.

[15] L. Wang and B. Li, "Phononics gets hot," *Phys. World*, vol. 21, pp. 27–29, 2008.

[16] L. Wang and B. Li, "Thermal logic gates: computation with phonons," *Physical review letters*, vol. 99, no. 17, p. 177208, 2007.

[17] N. Li, J. Ren, L. Wang, G. Zhang, P. Hänggi, and B. Li, "Colloquium: Phononics: Manipulating heat flow with electronic analogs and beyond," *Reviews of Modern Physics*, vol. 84, no. 3, p. 1045, 2012.

[18] B. Song, A. Fiorino, E. Meyhofer, and P. Reddy, "Near-field radiative thermal transport: From theory to experiment," *AIP Advances*, vol. 5, no. 5, p. 053503, 2015.

[19] Y. Yang, S. Basu, and L. Wang, "Radiation-based near-field thermal rectification with phase transition materials," *Applied Physics Letters*, vol. 103, no. 16, p. 163101, 2013.

[20] J. Huang, Q. Li, Z. Zheng, and Y. Xuan, "Thermal rectification based on thermochromic materials," *International Journal of Heat and Mass Transfer*, vol. 67, pp. 575–580, 2013.

[21] L. Zhu, C. R. Otey, and S. Fan, "Negative differential thermal conductance through vacuum," *Applied Physics Letters*, vol. 100, no. 4, p. 044104, 2012.

[22] P. Van Zwol, K. Joulain, P. Ben-Abdallah, J.-J. Greffet, and J. Chevrier, "Fast nanoscale heat-flux modulation with phase-change materials," *Physical Review B*, vol. 83, no. 20, p. 201404, 2011.

[23] P. Van Zwol, L. Ranno, and J. Chevrier, "Tuning near field radiative heat flux through surface excitations with a metal insulator transition," *Physical review letters*, vol. 108, no. 23, p. 234301, 2012.

[24] F. Menges, M. Dittberner, L. Novotny, D. Passarello, S. Parkin, M. Spieser, H. Riel, and B. Gotsmann, "Thermal radiative near field transport between vanadium dioxide and silicon oxide across the metal insulator transition," *Applied Physics Letters*, vol. 108, no. 17, p. 171904, 2016.

[25] Y. Yang, S. Basu, and L. Wang, "Vacuum thermal switch made of phase transition materials considering thin film and substrate effects," *Journal of Quantitative Spectroscopy and Radiative Transfer*, vol. 158, pp. 69–77, 2015.

[26] M. Qazilbash, M. Brehm, G. Andreev, A. Frenzel, P.-C. Ho, B.-G. Chae, B.-J. Kim, S. J. Yun, H.-T. Kim, A. Balatsky, and O. Shpyrko, "Infrared spectroscopy and nano-imaging of the insulator-to-metal transition in vanadium dioxide," *Physical Review B*, vol. 79, no. 7, p. 075107, 2009.

[27] A. Ghanekar, L. Lin, J. Su, H. Sun, and Y. Zheng, "Role of nanoparticles in wavelength selectivity of multilayered structures in the far-field and near-field regimes," *Optics Express*, vol. 23, no. 19, pp. A1129–A1139, 2015.

[28] S.-A. Biehs, F. S. Rosa, and P. Ben-Abdallah, "Modulation of near-field heat transfer between two gratings," *Applied Physics Letters*, vol. 98, no. 24, p. 243102, 2011.

[29] A. Frenzel, M. M. Qazilbash, M. Brehm, B.-G. Chae, B.-J. Kim, H.-T. Kim, A. Balatsky, F. Keilmann, and D. Basov, "Inhomogeneous electronic state near the insulator-to-metal transition in the correlated oxide vo 2," *Physical Review B*, vol. 80, no. 11, p. 115115, 2009.

[30] A. Narayanaswamy and Y. Zheng, "A Green's function formalism of energy and momentum transfer in fluctuational electrodynamics," *Journal of Quantitative Spectroscopy and Radiative Transfer*, vol. 132, pp. 12–21, 2014.

[31] D. H. Raguin and G. M. Morris, "Antireflection structured surfaces for the infrared spectral region," *Applied Optics*, vol. 32, no. 7, pp. 1154–1167, 1993.

[32] P. Lalanne and D. Lemercier-Lalanne, "On the effective medium theory of subwavelength periodic structures," *Journal of Modern Optics*, vol. 43, no. 10, pp. 2063–2085, 1996.

[33] Y.-B. Chen, Z. Zhang, and P. Timans, "Radiative properties of patterned wafers with nanoscale linewidth," *Journal of Heat Transfer*, vol. 129, no. 1, pp. 79–90, 2007.

[34] E. Glytsis and T. K. Gaylord, "High-spatial-frequency binary and multilevel stairstep gratings: polarization-selective mirrors and broadband antireflection surfaces," *Applied optics*, vol. 31, no. 22, pp. 4459–4470, 1992.

[35] X. Liu, T. Bright, and Z. Zhang, "Application conditions of effective medium theory in near-field radiative heat transfer between multilayered metamaterials," *Journal of Heat Transfer*, vol. 136, no. 9, p. 092703, 2014.

[36] A. Barker Jr, H. Verleur, and H. Guggenheim, "Infrared optical properties of vanadium dioxide above and below the transition temperature," *Physical Review Letters*, vol. 17, no. 26, p. 1286, 1966.

[37] E. D. Palik, *Handbook of optical constants of solids*. Academic press, 1998, vol. 3.

[38] P. B. Johnson and R.-W. Christy, "Optical constants of the noble metals," *Physical Review B*, vol. 6, no. 12, p. 4370, 1972.

[39] A. Narayanaswamy, J. Mayo, and C. Canetta, "Infrared selective emitters with thin films of polar materials," *Applied Physics Letters*, vol. 104, no. 18, p. 183107, 2014.

[40] B. Liu and S. Shen, "Broadband near-field radiative thermal emitter/absorber based on hyperbolic metamaterials: Direct numerical simulation by the wiener chaos expansion method," *Physical Review B*, vol. 87, no. 11, p. 115403, 2013.

# BIBLIOGRAPHY

"http://www.microchem.com/prod-su8.htm."

Adachi, S., "Optical dispersion relations for gap, gaas, gasb, inp, inas, insb, al x ga1- x as, and in1- x ga x as y p1- y," *Journal of Applied Physics*, vol. 66, no. 12, pp. 6030–6040, 1989.

Argyropoulos, C., Le, K. Q., Mattiucci, N., DAguanno, G., and Alu, A., "Broadband absorbers and selective emitters based on plasmonic brewster metasurfaces," *Physical Review B*, vol. 87, no. 20, p. 205112, 2013.

Arpin, K. A., Losego, M. D., Cloud, A. N., Ning, H., Mallek, J., Sergeant, N. P., Zhu, L., Yu, Z., Kalanyan, B., Parsons, G. N., *et al.*, "Three-dimensional self-assembled photonic crystals with high temperature stability for thermal emission modification," *Nature communications*, vol. 4, 2013.

Barker Jr, A., Verleur, H., and Guggenheim, H., "Infrared optical properties of vanadium dioxide above and below the transition temperature," *Physical Review Letters*, vol. 17, no. 26, p. 1286, 1966.

Bartoli, B., Catalanotti, S., Coluzzi, B., Cuomo, V., Silvestrini, V., and Troise, G., "Nocturnal and diurnal performances of selective radiators," *Applied Energy*, vol. 3, no. 4, pp. 267–286, 1977.

Basu, S., Chen, Y., and Zhang, Z., "Microscale radiation in thermophotovoltaic devices-a review," *International Journal of Energy Research*, vol. 31, no. 6, pp. 689–716, 2007.

Battie, Y., Resano-Garcia, A., Chaoui, N., Zhang, Y., and Naciri, A. E., "Extended maxwell-garnett-mie formulation applied to size dispersion of metallic nanoparticles embedded in host liquid matrix," *The Journal of Chemical Physics*, vol. 140, no. 4, p. 044705, 2014.

Ben-Abdallah, P. and Biehs, S.-A., "Phase-change radiative thermal diode," *Applied Physics Letters*, vol. 103, no. 19, p. 191907, 2013.

Ben-Abdallah, P. and Biehs, S.-A., "Near-field thermal transistor," *Physical review letters*, vol. 112, no. 4, p. 044301, 2014.

Ben-Abdallah, P. and Biehs, S.-A., "Contactless heat flux control with photonic devices," *AIP Advances*, vol. 5, no. 5, p. 053502, 2015.

Ben-Abdallah, P. and Biehs, S.-A., "Towards boolean operations with thermal photons," *Physical Review B*, vol. 94, no. 24, p. 241401, 2016.

Bermel, P., Ghebrebrhan, M., Chan, W., Yeng, Y. X., Araghchini, M., Hamam, R., Marton, C. H., Jensen, K. F., Soljačić, M., Joannopoulos, J. D., *et al.*, "Design and global optimization of high-efficiency thermophotovoltaic systems," *Optics express*, vol. 18, no. 103, pp. A314–A334, 2010.

Bermel, P., Ghebrebrhan, M., Harradon, M., Yeng, Y. X., Celanovic, I., Joannopoulos, J. D., and Soljacic, M., "Tailoring photonic metamaterial resonances for thermal radiation," *Nanoscale research letters*, vol. 6, no. 1, pp. 1–5, 2011.

Biehs, S.-A., Rosa, F. S., and Ben-Abdallah, P., "Modulation of near-field heat transfer between two gratings," *Applied Physics Letters*, vol. 98, no. 24, p. 243102, 2011.

Bosi, M., Ferrari, C., Melino, F., Pinelli, M., Spina, P., and Venturini, M., "Thermophotovoltaic generation: a state of the art review," *Proceedings ECOS*, 2012.

Bosman, H., Lau, Y., and Gilgenbach, R., "Microwave absorption on a thin film," *Applied Physics Letters*, vol. 82, no. 9, pp. 1353–1355, 2003.

Bright, T., Wang, L., and Zhang, Z., "Performance of near-field thermophotovoltaic cells enhanced with a backside reflector," *Journal of Heat Transfer*, vol. 136, no. 6, p. 062701, 2014.

Celanovic, I., O'Sullivan, F., Jovanovic, N., Qi, M., and Kassakian, J. G., "1d and 2d photonic crystals for thermophotovoltaic applications," in *Photonics Europe*. International Society for Optics and Photonics, 2004, pp. 416–422.

Chan, W. R., Bermel, P., Pilawa-Podgurski, R. C., Marton, C. H., Jensen, K. F., Senkevich, J. J., Joannopoulos, J. D., Soljačić, M., and Celanovic, I., "Toward high-energy-density, high-efficiency, and moderate-temperature chip-scale thermophotovoltaics," *Proceedings of the National Academy of Sciences*, vol. 110, no. 14, pp. 5309–5314, 2013.

Chang, C., Okawa, D., Majumdar, A., and Zettl, A., "Solid-state thermal rectifier," *Science*, vol. 314, no. 5802, pp. 1121–1124, 2006.

Chang, P.-E., Jiang, Y.-W., Chen, H.-H., Chang, Y.-T., Wu, Y.-T., Tzuang, L. D.-C., Ye, Y.-H., and Lee, S.-C., "Wavelength selective plasmonic thermal emitter by polarization utilizing fabry-pérot type resonances," *Applied Physics Letters*, vol. 98, no. 7, p. 073111, 2011.

Chen, Y.-B., Zhang, Z., and Timans, P., "Radiative properties of patterned wafers with nanoscale linewidth," *Journal of Heat Transfer*, vol. 129, no. 1, pp. 79–90, 2007.

Chen, Z., Wong, C., Lubner, S., Yee, S., Miller, J., Jang, W., Hardin, C., Fong, A., Garay, J. E., and Dames, C., "A photon thermal diode," *Nature communications*, vol. 5, 2014.

Cheng, C.-W., Abbas, M. N., Chiu, C.-W., Lai, K.-T., Shih, M.-H., and Chang, Y.-C., "Wide-angle polarization independent infrared broadband absorbers based on metallic multi-sized disk arrays," *Optics express*, vol. 20, no. 9, pp. 10 376–10 381, 2012.

Chew, W. C., *Waves and fields in inhomogeneous media*. IEEE press, 1995.

Chou, J. B., Yeng, Y. X., Lenert, A., Rinnerbauer, V., Celanovic, I., Soljačić, M., Wang, E. N., and Kim, S.-G., "Design of wide-angle selective absorbers/emitters with dielectric filled metallic photonic crystals for energy applications," *Optics express*, vol. 22, no. 101, pp. A144–A154, 2014.

Colangelo, G., De Risi, A., and Laforgia, D., "Experimental study of a burner with high temperature heat recovery system for tpv applications," *Energy conversion and management*, vol. 47, no. 9, pp. 1192–1206, 2006.

Coutts, T., "A review of progress in thermophotovoltaic generation of electricity," *Renewable and Sustainable Energy Reviews*, vol. 3, no. 2, pp. 77–184, 1999.

del Campo, A. and Greiner, C., "Su-8: a photoresist for high-aspect-ratio and 3d submicron lithography," *Journal of Micromechanics and Microengineering*, vol. 17, no. 6, p. R81, 2007.

DiMatteo, R., Greiff, P., Seltzer, D., Meulenberg, D., Brown, E., Carlen, E., Kaiser, K., Finberg, S., Nguyen, H., Azarkevich, J., *et al.*, "M icron-gap t hermo p hoto v oltaics (mtpv)," in *AIP Conference Proceedings*, vol. 738, no. 1. AIP, 2004, pp. 42–51.

Doyle, W. T., "Optical properties of a suspension of metal spheres," *Physical review B*, vol. 39, no. 14, p. 9852, 1989.

Dyakov, S., Dai, J., Yan, M., and Qiu, M., "Near field thermal memory device," *arXiv preprint arXiv:1408.5831*, 2014.

Fante, R. L. and Mccormack, M. T., "Reflection properties of the salisbury screen," *IEEE transactions on antennas and propagation*, vol. 36, no. 10, pp. 1443–1454, 1988.

Felix, T., "Devices for lowering the temperature of a body by heat radiation therefrom," Mar. 21 1967, uS Patent 3,310,102.

Ferguson, L. and Dogan, F., "Spectral analysis of transition metal-doped mgo matched emitters for thermophotovoltaic energy conversion," *Journal of materials science*, vol. 37, no. 7, pp. 1301–1308, 2002.

Fleming, J., Lin, S., El-Kady, I., Biswas, R., and Ho, K., "All-metallic three-dimensional photonic crystals with a large infrared bandgap," *Nature*, vol. 417, no. 6884, pp. 52–55, 2002.

Francoeur, M., Basu, S., and Petersen, S. J., "Electric and magnetic surface polariton mediated near-field radiative heat transfer between metamaterials made of silicon carbide particles," *Optics express*, vol. 19, no. 20, pp. 18 774–18 788, 2011.

Francoeur, M., Vaillon, R., and Mengüç, M. P., "Thermal impacts on the performance of nanoscale-gap thermophotovoltaic power generators," *IEEE Transactions on Energy Conversion*, vol. 26, no. 2, pp. 686–698, 2011.

Frenzel, A., Qazilbash, M. M., Brehm, M., Chae, B.-G., Kim, B.-J., Kim, H.-T., Balatsky, A., Keilmann, F., and Basov, D., "Inhomogeneous electronic state near the insulator-to-metal transition in the correlated oxide vo 2," *Physical Review B*, vol. 80, no. 11, p. 115115, 2009.

Gao, L., Lemarchand, F., and Lequime, M., "Refractive index determination of sio2 layer in the uv/vis/nir range: spectrophotometric reverse engineering on single and bi-layer designs," *Journal of the European Optical Society-Rapid publications*, vol. 8, 2013.

Garnett, J. M., "Colours in metal glasses, in metallic films, and in metallic solutions. ii," *Philosophical Transactions of the Royal Society of London. Series A, Containing Papers of a Mathematical or Physical Character*, pp. 237–288, 1906.

Gentle, A. R. and Smith, G. B., "Radiative heat pumping from the earth using surface phonon resonant nanoparticles," *Nano letters*, vol. 10, no. 2, pp. 373–379, 2010.

Ghanekar, A., Ji, J., and Zheng, Y., "High-rectification near-field thermal diode using phase change periodic nanostructure," *Applied Physics Letters*, vol. 109, no. 12, p. 123106, 2016.

Ghanekar, A., Lin, L., Su, J., Sun, H., and Zheng, Y., "Role of nanoparticles in wavelength selectivity of multilayered structures in the far-field and near-field regimes," *Optics Express*, vol. 23, no. 19, pp. A1129–A1139, 2015.

Ghanekar, A., Lin, L., and Zheng, Y., "Novel and efficient mie-metamaterial thermal emitter for thermophotovoltaic systems," *Optics express*, vol. 24, no. 10, pp. A868–A877, 2016.

Ghanekar, A., Sun, M., Zhang, Z., and Zheng, Y., "Optimal design of wavelength selective thermal emitter for thermophotovoltaic applications," *Journal of Thermal Science and Engineering Applications*.

Glytsis, E. and Gaylord, T. K., "High-spatial-frequency binary and multilevel stairstep gratings: polarization-selective mirrors and broadband antireflection surfaces," *Applied optics*, vol. 31, no. 22, pp. 4459–4470, 1992.

Gonome, H., Baneshi, M., Okajima, J., Komiya, A., and Maruyama, S., "Controlling the radiative properties of cool black-color coatings pigmented with cuo submicron particles," *Journal of Quantitative Spectroscopy and Radiative Transfer*, vol. 132, pp. 90–98, 2014.

Gonome, H., Baneshi, M., Okajima, J., Komiya, A., Yamada, N., and Maruyama, S., "Control of thermal barrier performance by optimized nanoparticle size and experimental evaluation using a solar simulator," *Journal of Quantitative Spectroscopy and Radiative Transfer*, vol. 149, pp. 81–89, 2014.

Grenier, P., "Radiative cooling-inverse greenhouse effect," *Revue de Physique Appliquee*, vol. 14, pp. 87–90, 1979.

Guha, B., Otey, C., Poitras, C. B., Fan, S., and Lipson, M., "Near-Field radiative cooling of nanostructures," *Nano letters*, vol. 12, no. 9, pp. 4546–4550, 2012.

Hägglund, C., Apell, S. P., and Kasemo, B., "Maximized optical absorption in ultrathin films and its application to plasmon-based two-dimensional photovoltaics," *Nano letters*, vol. 10, no. 8, pp. 3135–3141, 2010.

Harder, N.-P. and Würfel, P., "Theoretical limits of thermophotovoltaic solar energy conversion," *Semiconductor Science and Technology*, vol. 18, no. 5, p. S151, 2003.

He, Y. and Zeng, T., "First-principles study and model of dielectric functions of silver nanoparticles," *The Journal of Physical Chemistry C*, vol. 114, no. 42, pp. 18 023–18 030, 2010.

Heilmann, A., *Polymer films with embedded metal nanoparticles.* Springer Science & Business Media, 2013, vol. 52.

Heinzel, A., Boerner, V., Gombert, A., Bläsi, B., Wittwer, V., and Luther, J., "Radiation filters and emitters for the nir based on periodically structured metal surfaces," *Journal of Modern Optics*, vol. 47, no. 13, pp. 2399–2419, 2000.

Höfler, H., Paul, H., Ruppel, W., and Würfel, P., "Interference filters for thermophotovoltaic solar energy conversion," *Solar Cells*, vol. 10, no. 3, pp. 273–286, 1983.

Hövel, H., Fritz, S., Hilger, A., Kreibig, U., and Vollmer, M., "Width of cluster plasmon resonances: bulk dielectric functions and chemical interface damping," *Physical Review B*, vol. 48, no. 24, p. 18178, 1993.

Huang, J., Li, Q., Zheng, Z., and Xuan, Y., "Thermal rectification based on thermochromic materials," *International Journal of Heat and Mass Transfer*, vol. 67, pp. 575–580, 2013.

Johnson, P. B. and Christy, R.-W., "Optical constants of the noble metals," *Physical Review B*, vol. 6, no. 12, p. 4370, 1972.

Joulain, K., Ezzahri, Y., Drevillon, J., and Ben-Abdallah, P., "Modulation and amplification of radiative far field heat transfer: Towards a simple radiative thermal transistor," *Applied Physics Letters*, vol. 106, no. 13, p. 133505, 2015.

Kats, M. A. and Capasso, F., "Optical absorbers based on strong interference in ultra-thin films (laser photonics rev. 10 (5)/2016)," *Laser & Photonics Reviews*, vol. 10, no. 5, pp. 699–699, 2016.

Kats, M. A., Sharma, D., Lin, J., Genevet, P., Blanchard, R., Yang, Z., Qazilbash, M. M., Basov, D., Ramanathan, S., and Capasso, F., "Ultra-thin perfect absorber employing a tunable phase change material," *Applied Physics Letters*, vol. 101, no. 22, p. 221101, 2012.

Kelly, K. L., Coronado, E., Zhao, L. L., and Schatz, G. C., "The optical properties of metal nanoparticles: the influence of size, shape, and dielectric environment," *The Journal of Physical Chemistry B*, vol. 107, no. 3, pp. 668–677, 2003.

Kishino, K., Unlu, M. S., Chyi, J.-I., Reed, J., Arsenault, L., and Morkoc, H., "Resonant cavity-enhanced (rce) photodetectors," *IEEE Journal of Quantum Electronics*, vol. 27, no. 8, pp. 2025–2034, 1991.

Kiziltas, G., Volakis, J. L., and Kikuchi, N., "Design of a frequency selective structure with inhomogeneous substrates as a thermophotovoltaic filter," *Antennas and Propagation, IEEE Transactions on*, vol. 53, no. 7, pp. 2282–2289, 2005.

Kobayashi, W., Sawaki, D., Omura, T., Katsufuji, T., Moritomo, Y., and Terasaki, I., "Thermal rectification in the vicinity of a structural phase transition," *Applied Physics Express*, vol. 5, no. 2, p. 027302, 2012.

Kobayashi, W., Teraoka, Y., and Terasaki, I., "An oxide thermal rectifier," *Applied Physics Letters*, vol. 95, no. 17, p. 171905, 2009.

Kreibig, U. and Vollmer, M., *Optical properties of metal clusters.* Springer Berlin, 1995, vol. 25.

LaBianca, N. C. and Gelorme, J. D., "High-aspect-ratio resist for thick-film applications," in *SPIE's 1995 Symposium on Microlithography*. International Society for Optics and Photonics, 1995, pp. 846–852.

Lalanne, P. and Lemercier-Lalanne, D., "On the effective medium theory of sub-wavelength periodic structures," *Journal of Modern Optics*, vol. 43, no. 10, pp. 2063–2085, 1996.

Laroche, M., Carminati, R., and Greffet, J.-J., "Near-field thermophotovoltaic energy conversion," *Journal of Applied Physics*, vol. 100, no. 6, p. 063704, 2006.

Lee, K.-T., Ji, C., and Guo, L. J., "Wide-angle, polarization-independent ultra-thin broadband visible absorbers," *Applied Physics Letters*, vol. 108, no. 3, p. 031107, 2016.

Li, B., Wang, L., and Casati, G., "Thermal diode: Rectification of heat flux," *Physical review letters*, vol. 93, no. 18, p. 184301, 2004.

Li, B., Wang, L., and Casati, G., "Negative differential thermal resistance and thermal transistor," *Applied Physics Letters*, vol. 88, no. 14, p. 143501, 2006.

Li, H., "Refractive index of alkali halides and its wavelength and temperature derivatives," *Journal of physical and chemical reference data*, vol. 5, no. 2, pp. 329–528, 1976.

Li, N., Ren, J., Wang, L., Zhang, G., Hänggi, P., and Li, B., "Colloquium: Phononics: Manipulating heat flow with electronic analogs and beyond," *Reviews of Modern Physics*, vol. 84, no. 3, p. 1045, 2012.

Licciulli, A., Diso, D., Torsello, G., Tundo, S., Maffezzoli, A., Lomascolo, M., and Mazzer, M., "The challenge of high-performance selective emitters for thermophotovoltaic applications," *Semiconductor Science and Technology*, vol. 18, no. 5, p. S174, 2003.

Liu, B. and Shen, S., "Broadband near-field radiative thermal emitter/absorber based on hyperbolic metamaterials: Direct numerical simulation by the wiener chaos expansion method," *Physical Review B*, vol. 87, no. 11, p. 115403, 2013.

Liu, G., Xuan, Y., Han, Y., and Li, Q., "Investigation of one-dimensional si/sio2 hotonic crystals for thermophotovoltaic filter," *Science in China Series E: Technological Sciences*, vol. 51, no. 11, pp. 2031–2039, 2008.

Liu, X., Tyler, T., Starr, T., Starr, A. F., Jokerst, N. M., and Padilla, W. J., "Taming the blackbody with infrared metamaterials as selective thermal emitters," *Physical review letters*, vol. 107, no. 4, p. 045901, 2011.

Liu, X., Bright, T., and Zhang, Z., "Application conditions of effective medium theory in near-field radiative heat transfer between multilayered metamaterials," *Journal of Heat Transfer*, vol. 136, no. 9, p. 092703, 2014.

Lorenz, H., Laudon, M., and Renaud, P., "Mechanical characterization of a new high-aspect-ratio near uv-photoresist," *Microelectronic Engineering*, vol. 41, pp. 371–374, 1998.

Martínez-Pérez, M. J., Fornieri, A., and Giazotto, F., "Rectification of electronic heat current by a hybrid thermal diode," *Nature nanotechnology*, vol. 10, no. 4, pp. 303–307, 2015.

McDonagh, C., Burke, C. S., and MacCraith, B. D., "Optical chemical sensors," *Chemical reviews*, vol. 108, no. 2, pp. 400–422, 2008.

McKelvey, J. P., "Solid state and semiconductor physics," 1966.

Menges, F., Dittberner, M., Novotny, L., Passarello, D., Parkin, S., Spieser, M., Riel, H., and Gotsmann, B., "Thermal radiative near field transport between vanadium dioxide and silicon oxide across the metal insulator transition," *Applied Physics Letters*, vol. 108, no. 17, p. 171904, 2016.

Moharam, M., Pommet, D. A., Grann, E. B., and Gaylord, T., "Stable implementation of the rigorous coupled-wave analysis for surface-relief gratings: enhanced transmittance matrix approach," *JOSA A*, vol. 12, no. 5, pp. 1077–1086, 1995.

Molesky, S., Dewalt, C. J., and Jacob, Z., "High temperature epsilon-near-zero and epsilon-near-pole metamaterial emitters for thermophotovoltaics," *Optics express*, vol. 21, no. 101, pp. A96–A110, 2013.

Motaharifar, E., Pierce, R., Islam, R., Henderson, R., Hsu, J., and Lee, M., "Broadband terahertz refraction index dispersion and loss of polymeric dielectric substrate and packaging materials," *Journal of Infrared, Millimeter, and Terahertz Waves*, vol. 39, no. 1, pp. 93–104, 2018.

Mulet, J.-P., Joulain, K., Carminati, R., and Greffet, J.-J., "Enhanced radiative heat transfer at nanometric distances," *Microscale Thermophysical Engineering*, vol. 6, no. 3, pp. 209–222, 2002.

Myroshnychenko, V., Rodríguez-Fernández, J., Pastoriza-Santos, I., Funston, A. M., Novo, C., Mulvaney, P., Liz-Marzán, L. M., and de Abajo, F. J. G., "Modelling the optical response of gold nanoparticles," *Chemical Society Reviews*, vol. 37, no. 9, pp. 1792–1805, 2008.

Nagpal, P., Han, S. E., Stein, A., and Norris, D. J., "Efficient low-temperature thermophotovoltaic emitters from metallic photonic crystals," *Nano letters*, vol. 8, no. 10, pp. 3238–3243, 2008.

Nam, Y., Yeng, Y. X., Lenert, A., Bermel, P., Celanovic, I., Soljačić, M., and Wang, E. N., "Solar thermophotovoltaic energy conversion systems with two-dimensional tantalum photonic crystal absorbers and emitters," *Solar Energy Materials and Solar Cells*, vol. 122, pp. 287–296, 2014.

Narayanaswamy, A. and Chen, G., "Surface modes for near field thermophotovoltaics," *Applied Physics Letters*, vol. 82, no. 20, pp. 3544–3546, 2003.

Narayanaswamy, A. and Chen, G., "Thermal emission control with one-dimensional metallodielectric photonic crystals," *Physical Review B*, vol. 70, no. 12, p. 125101, 2004.

Narayanaswamy, A., Mayo, J., and Canetta, C., "Infrared selective emitters with thin films of polar materials," *Applied Physics Letters*, vol. 104, no. 18, p. 183107, 2014.

Narayanaswamy, A. and Zheng, Y., "A Green's function formalism of energy and momentum transfer in fluctuational electrodynamics," *Journal of Quantitative Spectroscopy and Radiative Transfer*, vol. 132, pp. 12–21, 2014.

Nefzaoui, E., Drevillon, J., Ezzahri, Y., and Joulain, K., "Simple far-field radiative thermal rectifier using fabry–perot cavities based infrared selective emitters," *Applied optics*, vol. 53, no. 16, pp. 3479–3485, 2014.

Nefzaoui, E., Joulain, K., Drevillon, J., and Ezzahri, Y., "Radiative thermal rectification using superconducting materials," *Applied Physics Letters*, vol. 104, no. 10, p. 103905, 2014.

Nemani, K. V., Moodie, K. L., Brennick, J. B., Su, A., and Gimi, B., "In vitro and in vivo evaluation of su-8 biocompatibility," *Materials Science and Engineering: C*, vol. 33, no. 7, pp. 4453–4459, 2013.

Neuner III, B., Korobkin, D., Fietz, C., Carole, D., Ferro, G., and Shvets, G., "Midinfrared Index Sensing of pL-Scale Analytes Based on Surface Phonon Polaritons in Silicon Carbide," *The Journal of Physical Chemistry C*, vol. 114, no. 16, pp. 7489–7491, 2010.

Nguyen, V. C., Chen, L., and Halterman, K., "Total transmission and total reflection by zero index metamaterials with defects," *Physical review letters*, vol. 105, no. 23, p. 233908, 2010.

O. V. Sulima, A. W. Bett, M. G. M. Y. B. B. and S.Dutta, P., "Proc. 5th TPV Conf., Rome, Italy, September 2002 (AIP, New York, 1999)," p. p 402.

Ordonez-Miranda, J., Ezzahri, Y., Drevillon, J., and Joulain, K., "Transistorlike device for heating and cooling based on the thermal hysteresis of vo 2," *Physical Review Applied*, vol. 6, no. 5, p. 054003, 2016.

Otey, C. R., Lau, W. T., and Fan, S., "Thermal rectification through vacuum," *Physical Review Letters*, vol. 104, no. 15, p. 154301, 2010.

Palik, E. D., *Handbook of optical constants of solids.* Academic press, 1998, vol. 3.

Parida, O. P. and Bhat, N., "Characterization of optical properties of su-8 and fabrication of optical components," in *Int. Conf. on Opt. and Photon.(CSIO)*, 2009, pp. 4–7.

Park, K., Basu, S., King, W. P., and Zhang, Z., "Performance analysis of near-field thermophotovoltaic devices considering absorption distribution," *Journal of Quantitative Spectroscopy and Radiative Transfer*, vol. 109, no. 2, pp. 305–316, 2008.

Parsegian, V. A., *Van der Waals forces: a handbook for biologists, chemists, engineers, and physicists.* Cambridge University Press, 2006.

Petersen, S. J., Basu, S., Raeymaekers, B., and Francoeur, M., "Tuning near-field thermal radiative properties by quantifying sensitivity of mie resonance-based metamaterial design parameters," *Journal of Quantitative Spectroscopy and Radiative Transfer*, vol. 129, pp. 277–286, 2013.

Planck, M., *The theory of heat radiation.* Dover Publications, 2011.

Pralle, M., Moelders, N., McNeal, M., Puscasu, I., Greenwald, A., Daly, J., Johnson, E., George, T., Choi, D., El-Kady, I., *et al.*, "Photonic crystal enhanced narrow-band infrared emitters," *Applied Physics Letters*, vol. 81, no. 25, pp. 4685–4687, 2002.

Prod'homme, H., Ordonez-Miranda, J., Ezzahri, Y., Drevillon, J., and Joulain, K., "Optimized thermal amplification in a radiative transistor," *Journal of Applied Physics*, vol. 119, no. 19, p. 194502, 2016.

Pu, M., Feng, Q., Wang, M., Hu, C., Huang, C., Ma, X., Zhao, Z., Wang, C., and Luo, X., "Ultrathin broadband nearly perfect absorber with symmetrical coherent illumination," *Optics express*, vol. 20, no. 3, pp. 2246–2254, 2012.

Qazilbash, M., Brehm, M., Andreev, G., Frenzel, A., Ho, P.-C., Chae, B.-G., Kim, B.-J., Yun, S. J., Kim, H.-T., Balatsky, A., and Shpyrko, O., "Infrared spectroscopy and nano-imaging of the insulator-to-metal transition in vanadium dioxide," *Physical Review B*, vol. 79, no. 7, p. 075107, 2009.

RaDi, Y., Simovski, C., and Tretyakov, S., "Thin perfect absorbers for electromagnetic waves: theory, design, and realizations," *Physical Review Applied*, vol. 3, no. 3, p. 037001, 2015.

Raguin, D. H. and Morris, G. M., "Antireflection structured surfaces for the infrared spectral region," *Applied Optics*, vol. 32, no. 7, pp. 1154–1167, 1993.

Rakić, A. D., Djurišić, A. B., Elazar, J. M., and Majewski, M. L., "Optical properties of metallic films for vertical-cavity optoelectronic devices," *Applied optics*, vol. 37, no. 22, pp. 5271–5283, 1998.

Rephaeli, E. and Fan, S., "Absorber and emitter for solar thermo-photovoltaic systems to achieve efficiency exceeding the shockley-queisser limit," *Optics express*, vol. 17, no. 17, pp. 15 145–15 159, 2009.

Rinnerbauer, V., Lenert, A., Bierman, D. M., Yeng, Y. X., Chan, W. R., Geil, R. D., Senkevich, J. J., Joannopoulos, J. D., Wang, E. N., Soljačić, M., *et al.*, "Metallic photonic crystal absorber-emitter for efficient spectral control in high-temperature solar thermophotovoltaics," *Advanced Energy Materials*, vol. 4, no. 12, 2014.

Roberts, S., "Optical properties of nickel and tungsten and their interpretation according to drude's formula," *Physical Review*, vol. 114, no. 1, p. 104, 1959.

Sai, H., Kanamori, Y., and Yugami, H., "Tuning of the thermal radiation spectrum in the near-infrared region by metallic surface microstructures," *Journal of Micromechanics and Microengineering*, vol. 15, no. 9, p. S243, 2005.

Sai, H., Yugami, H., Akiyama, Y., Kanamori, Y., and Hane, K., "Spectral control of thermal emission by periodic microstructured surfaces in the near-infrared region," *JOSA A*, vol. 18, no. 7, pp. 1471–1476, 2001.

Sawaki, D., Kobayashi, W., Moritomo, Y., and Terasaki, I., "Thermal rectification in bulk materials with asymmetric shape," *arXiv preprint arXiv:1102.4182*, 2011.

Smith, B. C., *Infrared spectral interpretation: a systematic approach.* CRC press, 1998.

Smith, G., Deller, C., Swift, P., Gentle, A., Garrett, P., and Fisher, W., "Nanoparticle-doped polymer foils for use in solar control glazing," *Journal of Nanoparticle Research*, vol. 4, no. 1, pp. 157–165, 2002.

Song, B., Fiorino, A., Meyhofer, E., and Reddy, P., "Near-field radiative thermal transport: From theory to experiment," *AIP Advances*, vol. 5, no. 5, p. 053503, 2015.

Srinivasan, A., Czapla, B., Mayo, J., and Narayanaswamy, A., "Infrared dielectric function of polydimethylsiloxane and selective emission behavior," *Applied Physics Letters*, vol. 109, no. 6, p. 061905, 2016.

Sua, J., Gaob, F., Gub, Z., Daic, W., Cernigliaroc, G., and Sun, H., "Fabrication of su-8 based nanopatterns and their use as a nanoimprint mold," in *Proc. of SPIE Vol*, vol. 8974, 2014, pp. 897 409–1.

Tan, T., Wong, D., Lee, P., Rawat, R., and Patran, A., "Study of a chemically amplified resist for x-ray lithography by fourier transform infrared spectroscopy," *Applied spectroscopy*, vol. 58, no. 11, pp. 1288–1294, 2004.

Taylor, S., Yang, Y., and Wang, L., "Vanadium dioxide based fabry-perot emitter for dynamic radiative cooling applications," *Journal of Quantitative Spectroscopy and Radiative Transfer*, 2017.

Teh, W., Dürig, U., Drechsler, U., Smith, C., and Güntherodt, H.-J., "Effect of low numerical-aperture femtosecond two-photon absorption on (su-8) resist for ultrahigh-aspect-ratio microstereolithography," *Journal of applied physics*, vol. 97, no. 5, p. 054907, 2005.

Timans, P., *Advances in Rapid Thermal and Integrated Processing, ed. F. Roozeboom.* Dordrecht, The Netherlands: Kluwer Academic Publishers, The Netherlands, 1996.

Timans, P., "The thermal radiative properties of semiconductors," in *Advances in rapid thermal and integrated processing.* Springer, 1996, pp. 35–101.

Tong, J. K., Hsu, W.-C., Huang, Y., Boriskina, S. V., and Chen, G., "Thin-film'thermal well'emitters and absorbers for high-efficiency thermophotovoltaics," *arXiv preprint arXiv:1502.02061*, 2015.

Tsai, M.-W., Chuang, T.-H., Meng, C.-Y., Chang, Y.-T., and Lee, S.-C., "High performance midinfrared narrow-band plasmonic thermal emitter," *Applied physics letters*, vol. 89, no. 17, p. 173116, 2006.

Ünlü, M. S. and Strite, S., "Resonant cavity enhanced photonic devices," *Journal of Applied Physics*, vol. 78, no. 2, pp. 607–639, 1995.

Van Zwol, P., Joulain, K., Ben-Abdallah, P., Greffet, J.-J., and Chevrier, J., "Fast nanoscale heat-flux modulation with phase-change materials," *Physical Review B*, vol. 83, no. 20, p. 201404, 2011.

Van Zwol, P., Ranno, L., and Chevrier, J., "Tuning near field radiative heat flux through surface excitations with a metal insulator transition," *Physical review letters*, vol. 108, no. 23, p. 234301, 2012.

Verleur, H. W., "Determination of optical constants from reflectance or transmittance measurements on bulk crystals or thin films," *JOSA*, vol. 58, no. 10, pp. 1356–1364, 1968.

Wang, C.-H., Shen, W.-Y., Sheng, P.-S., Lee, C.-Y., and Chiu, H.-T., "Deposition of mesoporous silicon carbide thin films from (me3si) 4sn: tin nanoparticles as in situ generated templates," *Chemistry of Materials*, vol. 19, no. 22, pp. 5250–5255, 2007.

Wang, H. and Wang, L., "Perfect selective metamaterial solar absorbers," *Optics express*, vol. 21, no. 106, pp. A1078–A1093, 2013.

Wang, L. and Li, B., "Thermal logic gates: computation with phonons," *Physical review letters*, vol. 99, no. 17, p. 177208, 2007.

Wang, L. and Li, B., "Phononics gets hot," *Phys. World*, vol. 21, pp. 27–29, 2008.

Wang, L. and Li, B., "Thermal memory: a storage of phononic information," *Physical review letters*, vol. 101, no. 26, p. 267203, 2008.

Wang, L. and Zhang, Z., "Wavelength-selective and diffuse emitter enhanced by magnetic polaritons for thermophotovoltaics," *Applied Physics Letters*, vol. 100, no. 6, p. 063902, 2012.

Wang, X.-B., Sun, J., Chen, C.-M., Sun, X.-Q., Wang, F., and Zhang, D.-M., "Thermal uv treatment on su-8 polymer for integrated optics," *Optical Materials Express*, vol. 4, no. 3, pp. 509–517, 2014.

Wei, H. and Eilers, H., "Electrical conductivity of thin-film composites containing silver nanoparticles embedded in a dielectric fluoropolymer matrix," *Thin Solid Films*, vol. 517, no. 2, pp. 575–581, 2008.

Wernsman, B., Siergiej, R. R., Link, S. D., Mahorter, R. G., Palmisiano, M. N., Wehrer, R. J., Schultz, R. W., Schmuck, G. P., Messham, R. L., Murray, S., *et al.*, "Greater than 20% radiant heat conversion efficiency of a thermophotovoltaic radiator/module system using reflective spectral control," *Electron Devices, IEEE Transactions on*, vol. 51, no. 3, pp. 512–515, 2004.

Wheeler, M. S., Aitchison, J. S., and Mojahedi, M., "Three-dimensional array of dielectric spheres with an isotropic negative permeability at infrared frequencies," *Physical Review B*, vol. 72, no. 19, p. 193103, 2005.

Wheeler, M. S., "A scattering-based approach to the design, analysis, and experimental verification of magnetic metamaterials made from dielectrics," Ph.D. dissertation, 2010.

White, D. C., Wedlock, B. D., and Blair, J., "Recent advances in thermal energy conversion," in *15th Annual Proceedings, Power Sources Conference*, 1961, pp. 125–132.

Woolf, D., Hensley, J., Cederberg, J., Bethke, D., Grine, A., and Shaner, E., "Heterogeneous metasurface for high temperature selective emission," *Applied Physics Letters*, vol. 105, no. 8, p. 081110, 2014.

Wu, C., Arju, N., Kelp, G., Fan, J. A., Dominguez, J., Gonzales, E., Tutuc, E., Brener, I., and Shvets, G., "Spectrally selective chiral silicon metasurfaces based on infrared fano resonances," *Nature communications*, vol. 5, 2014.

Wu, C., Neuner III, B., John, J., Milder, A., Zollars, B., Savoy, S., and Shvets, G., "Metamaterial-based integrated plasmonic absorber/emitter for solar thermo-photovoltaic systems," *Journal of Optics*, vol. 14, no. 2, p. 024005, 2012.

Wurfel, P. and Ruppel, W., "Upper limit of thermophotovoltaic solar-energy conversion," *Electron Devices, IEEE Transactions on*, vol. 27, no. 4, pp. 745–750, 1980.

Xu, C., Wang, S., Wang, G., Liang, J., Wang, S., Bai, L., Yang, J., and Chen, X., "Temperature dependence of refractive indices for 4h-and 6h-sic," *Journal of Applied Physics*, vol. 115, no. 11, p. 113501, 2014.

Yang, Y., Basu, S., and Wang, L., "Radiation-based near-field thermal rectification with phase transition materials," *Applied Physics Letters*, vol. 103, no. 16, p. 163101, 2013.

Yang, Y., Basu, S., and Wang, L., "Vacuum thermal switch made of phase transition materials considering thin film and substrate effects," *Journal of Quantitative Spectroscopy and Radiative Transfer*, vol. 158, pp. 69–77, 2015.

Yu, N. and Capasso, F., "Flat optics with designer metasurfaces," *Nature materials*, vol. 13, no. 2, pp. 139–150, 2014.

Zhang, J., Tan, K., Hong, G., Yang, L., and Gong, H., "Polymerization optimization of su-8 photoresist and its applications in microfluidic systems and mems," *Journal of Micromechanics and Microengineering*, vol. 11, no. 1, p. 20, 2001.

Zhao, B., Wang, L., Shuai, Y., and Zhang, Z. M., "Thermophotovoltaic emitters based on a two-dimensional grating/thin-film nanostructure," *International Journal of Heat and Mass Transfer*, vol. 67, pp. 637–645, 2013.

Zhao, Q., Zhou, J., Zhang, F., and Lippens, D., "Mie resonance-based dielectric metamaterials," *Materials Today*, vol. 12, no. 12, pp. 60–69, 2009.

Zheludev, N. I. and Kivshar, Y. S., "From metamaterials to metadevices," *Nature materials*, vol. 11, no. 11, pp. 917–924, 2012.

Zheng, Y. and Ghanekar, A., "Radiative energy and momentum transfer for various spherical shapes: A single sphere, a bubble, a spherical shell, and a coated sphere," *Journal of Applied Physics*, vol. 117, no. 6, p. 064314, 2015.

Zheng, Y. and Narayanaswamy, A., "Patch contribution to near-field radiative energy transfer and van der Waals pressure between two half-spaces," *Physical Review A*, vol. 89, no. 2, p. 022512, 2014.

Zhu, B., Wang, Z., Huang, C., Feng, Y., Zhao, J., and Jiang, T., "Polarization insensitive metamaterial absorber with wide incident angle," *Progress In Electromagnetics Research*, vol. 101, pp. 231–239, 2010.

Zhu, L., Otey, C. R., and Fan, S., "Negative differential thermal conductance through vacuum," *Applied Physics Letters*, vol. 100, no. 4, p. 044104, 2012.

Zhu, L., Otey, C. R., and Fan, S., "Ultrahigh-contrast and large-bandwidth thermal rectification in near-field electromagnetic thermal transfer between nanoparticles," *Physical Review B*, vol. 88, no. 18, p. 184301, 2013.